The post-Caledonian tectono-thermal evolution of Western Norway

Åse Hestnes

Thesis for the degree of Philosophiae Doctor (PhD)
University of Bergen, Norway
2023

UNIVERSITY OF BERGEN

The post-Caledonian tectono-thermal evolution of Western Norway

Åse Hestnes

Thesis for the degree of Philosophiae Doctor (PhD)
at the University of Bergen

Date of defense: 19.06.2023

Year: 2023

Title: The post-Caledonian tectono-thermal evolution of Western Norway

Name: Åse Hestnes

Print: Skipnes Kommunikasjon / University of Bergen

Scientific environment

The work presented in this dissertation was carried out at the Department of Earth Science at the University of Bergen (UiB), Norway, between January 2019 and March 2023. The research project was funded by VISTA – a basic research program in collaboration between The Norwegian Academy of Science and Letters, and Equinor [grant number 6274]. Two month of extension where made possible through funding of the Western Norway University of Applied Science. Additional funding was provided by DEEP research school for analysis [project number 249040/F60]. Geochronological analyses were carried out at the Geological Survey of Norway (K-Ar fault gouge dating) by Roelant van der Lelij and Jasmin Schönenberger, and at the Department of Geology, Trinity College Dublin, Irland (U-Pb calcite dating) by Kerstin Drost and David Chew. Thermochronological analysis was carried out at the Department of Earth Science, UiB (apatite fission track analysis), and the Geoscience centre, University of Göttingen, Germany (apatite (U-Th)/He analysis) by István Dunkl and Judit Dunklné-Nagy. DEEP research school funded course participation at the University of Oslo. The work was supervised by Prof. Joachim Jacobs (UiB), Ass. Prof. Deta Gasser (HVL), Ass. Prof. Thomas Scheiber (HVL), Dr. Anna Ksienzyk (NGU), Dr. Tor Sømme (Equinor, UiB), and Prof. Henriette Linge (UiB).

UNIVERSITY OF BERGEN

Western Norway University of Applied Sciences

GEOLOGICAL SURVEY OF NORWAY
- NGU -

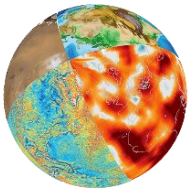

DEEP
Norwegian Research School for Dynamics and Evolution of Earth and Planets

Acknowledgements

There are too many people to thank for their help getting me to this point, but I'm going to do my best.

First and foremost, I would like to thank all my supervisors for giving me the opportunity to embark on this journey and for believing in me and continuously supporting me throughout the past four years. Each of you has contributed with different aspects but I would like to thank all of you for staying positive when I needed it the most. Joachim, I would like to thank you for always having an open door and open ear. The fact that I could always discuss early ideas with you without prejudice has helped me to trust my scientific instincts. I am grateful for that. Knowing you had my back with all the small and big worries has taken a lot of stress of my shoulders and allowed me to focus on what matters most, science. Deta, I look up to you as a person, scientist and friend. You always took time to discuss my research and your critical reflections have helped me sharpen my argumentation and to grow as a researcher. For that I will be forever grateful. You have not only been a supervisor but a long time mentor to me. Thomas, we would probably still be sampling Skåla if it weren't for you collecting most samples while we were trying to catch our breath. Your insights and feedback have lifted this thesis in many ways. Deta and Thomas, I have always enjoyed visiting in Sogndal and I am thankful for you opening your home to me. Anna, Henriette and Tor, I could always count on you for insightful discussions, comments on drafts, and help with figures and in the field. Thank you!

Many thanks to my co-authors. You have contributed in so many ways to the different manuscripts and the work would not have been possible without all of you.

I gratefully acknowledge the support of my funders. Thank you to VISTA for funding my research and professional development.

Several people have helped me along the way. Particular thanks to Istvan, Irina, Andreas, Leif-Erik, Irene and Judit for your help with sample preparation, processing and analyses. You have made even the most tedious lab work enjoyable.

A special thank you to the entire Department of Earth Science for the good work atmosphere; the administration for always making a third floor visit a joy; and Jostein and Bjarte for including me in iEarth and being understanding when my mind kept wandering off to my PhD research.

The time as a PhD and at the Department would certainly not have been the same without the lunch group, especially Karen, Hallgeir, Emilie, Iselin, Thea and Helene for giving me the warmest welcome and the best send-off. Helene, thank you for being a fabulous office mate and never laughing about me complaining about being tired when you only had slept few hours yourself. Hallgeir, thank you for your unwavering support and teaching me fission track analysis, without you this thesis would not have been possible. You were right to tell me at the start that I would come to miss counting fission tracks (although I don't miss dreaming about them).

Embarking on this PhD journey wouldn't have been the same without sharing the experience with my fellow PhDs and postdocs, thank you. Natacha, thank you for all the shared motivational hot chocolates and for pushing me to write. Without you, I would still be stuck on the second manuscript. Matteo, thank you for showing me that procrastination is not all that bad. Linda and Julie, thank you for making conferences fun and for our online writing sessions during and after the lockdowns.

The last years would not have been possible if it wasn't for my friends. Victoria and Rasmus, thank you for more than 10 years of friendship; you have been on this ride with me truly from the start. Thank you also for always having an open door if I needed an escape from the office. Victoria, thank you for so many shared moments, both in and outside the world of science, I am curious of what comes next. Christine, your endless cheering and belief in me did its job! Thank you for being overly positive and singing with me – can't wait for next time. I have had countless of tired Thursdays during the last years thanks to the Wednesday dinner group, I wouldn't have wanted to miss a single one of those evenings though. Thank you for all the shared laughs and bottles of wine, you are the best! Carina, Knut, and David, «verdens beste jenter», I am so grateful for your patients, support, and the push I needed to take breaks during the

last years. In you I can always count on your sympathy, company and distractions. I have missed you and promise I will be back now!

I also want to thank my family, and especially my parents, for encouragement and motivation, and giving me the opportunities to pursue my interests and dreams. You were always interested and knew when to ask (and when not to ask) questions. Mari, not only are you the best flatmate but you are also great at taking care of those around you. I needed you especially during the last year. Thank you for allowing me not to share my feelings.

Finally, I want to thank you, Tom, for your love and support throughout this journey. You are truly "the rock" for me, and can always trust in your help and push to move forward. This journey would certainly not have been as "easy" without you. Even though nothing really went according to the plan during the last year, we made it and I can't wait to finally spend more time together with you!

Åse Hatlnes

Bergen, March, 2023

Summary

The onshore areas of rifted margins are often characterized by high elevation and low-relief landscapes separated from a low laying coastal strip by a distinct escarpment. A lot of our current understanding from these areas is today based on extensive seismic studies and well data information from the offshore realm motivated by the margins high potential as a source for hydrocarbons. The knowledge gain from the onshore regions has often been hampered by the complex basement structural architecture and the often lack of overlaying sedimentary records. In order to fully understand the evolution of a rifted margin, however, our understanding of the tectonic and thermal evolution of onshore areas needs to be improved. The margin of Western Norway is one example of a rifted margin where its formation and development since the Caledonian orogeny has been a long lived debate. The aim of the thesis is to develop a integrated tectonic and thermal model for the evolution of the field area located in the northern part of Western Norway by combining detailed field work on brittle structures, with various geo- and thermochronological methods.

Paper I of this thesis focuses on the brittle structural temporal and spatial evolution of the study region. By combining an extensive field dataset of fracture and fault information with remote sensing analysis and K-Ar fault gouge dating of six faults, the paper gives new insight into the brittle architecture of the region and how it is influenced by ductile precursor structures. Following the Caledonian orogeny, four major stress fields were resolved: 1) NW-SE Silurian compression was followed by Early to Mid-Devonian NW-SE extension. 2) The late Devonian to early Carboniferous was characterized by a dominant strike-slip stress field, with σ1 rotating from N-S to NE-SW from the northern to the southern study area. 3) A minor E-W extensional stress field was possibly related to the Permian-Triassic or the Late Jurassic offshore rift phases. 4) K-Ar fault gouge dating revealed two periods of fault activity in the mid (123-115 Ma) and the late (86-77 Ma) Cretaceous under a WNW-ESE transtensional stress field.

Paper II provides the first ever U-Pb dating of fracture filling calcite from Norway. These data provide information about subtle tectonic events covering both high and low temperature domains, which generally are too cold to be dated by K-Ar fault gouge dating. Based on 15 U-Pb calcite ages, related brittle structural information of the fractures and faults, and stable isotope analysis, four regional tectonic events were deciphered: 1) A Triassic-Jurassic reactivation of the Dalsfjord fault, a fault strand of the Nordfjord-Sogn detachment zone, broadly relates to offshore rift episodes. 2) Late Cretaceous ages (90-80 Ma) of fractures parallel to the Møre-Trøndelag fault complex relate to lithospheric stretching and normal fault reactivation along the fault complex. 3) Late Cretaceous-early Paleocene ages (70-60 Ma) are detected on fractures and faults with various orientations and are related to a domal exhumation following the arrival of the proto-Icelandic mantle plume. 4) Ages younger than 50 Ma, all from fractures and faults with a NE-SW strike, are related to several episodes of fracture dilation during the post-breakup period, indicating a long-lived Cenozoic deformation history.

Paper III presents low-temperature thermochronological data from an elevation transect located in the inner Nordfjord. Here, we show the first multi-sample thermal history model of an elevation transect from the region. The elevation transect reaches 1841 masl, includes 12 samples analysed by Apatite Fission Track (AFT) dating and 4 samples analysed by (U-Th)/He dating, and shows increasing ages with elevation; AFT samples yield ages from 159 ± 11 Ma to 256 ± 21 Ma and apatite (U-Th)/He samples yield ages from 80 ± 4 Ma to 277 ± 15 Ma. By combining the AFT and (U-Th)/He data into a multi-sample thermal history model, we increase the constraints on the model and reduce data noise compared to single-sample models. Testing the model for various thermal cooling histories, the model shows a preferred evolution with fast cooling following the Caledonian orogeny to upper crustal levels (~3 km depth) in the Early-Middle Triassic, slow and steady cooling throughout the Mesozoic until the Late Cretaceous, where the cooling again increases until present day surface temperatures. The multi-sample model also allows for cooling to surface temperatures in the Late Jurassic if followed by Cretaceous reheating and reburial by 1.5-3 km of sediments. This paper highlights that for the inner Nordfjord, at least, the high-elevation low-relief

surfaces most likely formed during the Cenozoic and do not represent a simply uplifted Mesozoic peneplain.

Paper IV provides a new regional dataset of low-temperature thermochronological data from the study area. Samples collected across the region resulted in 29 AFT analyses and 45 single grain apatite (U-Th)/He analyses. Neither the AFT nor the (U-Th)/He samples show a correlation of age and elevation. AFT ages vary from 323 ± 27 to 140 ± 4 Ma and the (U-Th)/He analysis vary from 228 ± 12 to 57 ± 3 Ma. Regionally, the ages are youngest in the inner fjords and along the onshore Møre margin, whereas the oldest ages are found close to the Hornelen Devonian basin at sea level. The ages show large offset over short distances, related to fault offset along reactivated fault strands of the Nordfjord-Sogn detachment zone. The region shows a complex spatial and temporal evolution, where 1) the inner Nordfjord subregion shows slow cooling throughout the Mesozoic and increased cooling by the Late Cretaceous-Cenozoic until present, corresponding to the findings from paper III. 2) The Sognefjord subregion shows a similar general cooling history as the inner Nordfjord, with minor offsets along brittle faults, such as along brittle fault strands of the Nordfjord-Sogn detachment zone, indicating down-to-the-west normal fault reactivation in the Triassic/Jurassic. 3) In the Hornelen basin subregion, large age variations over short distances are related to Late Jurassic-Cretaceous fault offset along steep E-W striking faults. The thermal models reveal that the samples cooled to the upper crust (<8 km) by the Carboniferous-Permian and allow for cooling to surface temperatures in the Late Jurassic followed by Cretaceous reheating. We suggest that local Cretaceous sedimentary basins could have formed in the hanging block of these fault structures. 4) The region north of the Nordfjord shows cooling to the upper crust (<8 km) during the Jurassic and we relate this to footwall uplift from fault reactivation of the Møre-Trøndelag fault complex during Jurassic rifting.

This study shows that Western Norway has undergone a complex tectono-thermal spatial and temporal evolution since the Caledonian orogeny. In conclusion, by using newly available methods within thermochronology and geochronology, and combining them with established methods, we here 1) describe prominent strike-slip fault systems

not been properly described earlier, 2) detect several pulses of tectonic activity in the Cenozoic, 3) produce robust multi-sample thermal models forming a strong basis for regional thermal interpretations, and 4) highlight that cooling along a rifted margin is not continuous and homogenous but vary along strike, controlled by long lived detachment and fault systems.

Sammendrag

En riftet kontinentalmargin viser ofte et karakteristisk landskap som domineres av høye og flate fjell som er separert fra en lavtliggende kyststripe av en tydelig skrent. Mye av vår nåværende forståelse av disse områdene er basert på omfattende seismiske studier og data fra borehull samlet inn fra havbunnen utenskjærs, hvor innsamlingen av data er motivert av kontinentalmargin potensiale som kilde til hydrokarboner. Kunnskapen innhentet på land, derimot, blir ofte begrenset av forløpende komplekse berggrunnstrukturer og mangel på overliggende sedimenter som ville gjort innsikten i tektonisk bevegelse lettere. For å få en god forståelse av en riftet kontinentalmargin må kunnskapen vår om den tektoniske og termiske utviklingen på land forbedres. Vest-Norge er et godt eksempel på en riftet kontinentalmargin. Her har dannelsen og utviklingen siden den Kaledonske fjellkjeden har vært en pågående debatt gjennom mange år. Målet med denne avhandlingen er å utvikle en integrert tektonisk og termisk modell for utviklingen av et feltområde som ligger i de nordlige deler av Vest-Norge. For å få til dette, kombineres detaljerte feltstudier av sprø deformasjonsstrukturer med ulike geokronologiske og termokronologiske metoder.

Artikkel I fokuserer på utviklingen av sprø deformasjonsstrukturer gjennom tid og rom for det valgte studieområdet. Ved å kombinere fjernanalyser av lineamenter med et omfattende datasett som består av feltobservasjoner av sprekker og forkastninger, gir denne artikkelen ny innsikt i forståelsen av sprø deformasjon for regionen og hvordan denne deformasjonen er påvirket av forløpende duktile strukturer. I tillegg gjennomføres K-Ar datering av sleppemateriale fra seks ulike forkastninger. Studien påviser fire forskjellige spenningsfelt som dominerte i tiden etter den Kaledonske fjellkjeden: 1) NV-SØ kompresjon i silur som ble etterfulgt av NV-SØ ekstensjon i tidlig til midt devon. 2) Sen devon og tidlig karbon var karakterisert av et dominerende sidelengs spenningsfelt, hvor σ1 roteres fra N-S i den nordlige delen av studieområdet, til NØ-SV i den sørlige delen. 3) Et mindre utpreget spenningsfelt som viser Ø-V ekstensjon som trolig sammenfaller med riftfaser i perm-trias eller i sen jura. 4) K-Ar datering av sleppemateriale viser to perioder med økt forkastningsaktivitet i midtre (123-115 Ma) og sen (86-77 Ma) kritt under VNV-ØSØ transtensjon.

Artikkel II beskriver resultater fra de første U-Pb dateringer gjennomført på sprekkefyllende kalsitt i Norge. Disse dateringene gir informasjon om subtile tektoniske hendelser som dekker både høye og lave temperaturer, som blant annet er for kalde til å dateres med K-Ar datering av sleppemateriale. I denne studien beskrives det fire regionale tektoniske hendelser ved å kombinere 15 U-Pb kalsittaldre med informasjon fra sprø strukturell deformasjon tilhørende sprekker og forkastninger, samt stabile isotop analyser: 1) Dalsfjord forkastningen, som er en dal av Nordfjord-Sogn skjærsonen, viser reaktivering i trias-jura og som relateres til riftepisoder utenskjærs. 2) Sprekker parallelle med Møre-Trøndelag forkastningskomplekset dateres til sen kritt (90-80 Ma) og kobles til strekking av litosfæren og normal reaktivering langs forkastningskomplekset. 3) Kalsitt fra sprekker som viser varierende orientering er datert til sen kritt – tidlig paleocen alder (70-60 Ma) og relateres til oppløft av en strukturell dom som følge av ankomst av den proto-Islandske manteldiapiren. 4) Kalsitter fra sprekker som viser NØ-SV strøk er datert til ulike aldere yngre enn 50 Ma. Disse alderne kobles til flere episoder av sprekke-utvidelse etter oppbruddfasen av Nord-Atlanteren, noe som indikerer en langvarig kenozoisk deformasjonshistorie.

Artikkel III presenterer lav temperatur termokronologiske data fra et høydeprofil fra indre Nordfjord. Denne studien viser den første termiske modellen som inkluderer flere prøver av et høydeprofil fra regionen. Høyden på profilet er 1841 meter (fjellet Skåla) og inkluderer 12 prøver analysert med apatitt fisjonsspor datering (AFT) og 4 prøver analysert med apatitt (U-Th)/He datering. Prøvene viser økende alder med høyde, hvor AFT prøvene viser aldre fra 159 ± 11 Ma til 256 ± 21 Ma og apatitt (U-Th)/He prøvene viser aldre fra 80 ± 4 Ma til 277 ± 15 Ma. Ved å kombinere flere AFT og (U-Th)/He prøver sammen i en flerprøve termisk modell, begrenser vi modellen og reduserer datastøy sammenlignet med modeller som bare inkluderer en prøve. Når modellen testes for ulike termisk avkjølingshistorier, viser modellen en foretrukket utvikling med rask avkjøling fra den Kaledonske fjellkjeden til øvre nivåer i skorpen (~3 km dypt) i tidlig til midtre trias, etterfulgt av langsom og stødig avkjøling gjennom store deler av mesozoikum til sen kritt, hvor avkjølingen igjen øker til den når dagens temperaturer. Flerprøve-modellen tillater også avkjøling til overflatetemperaturer i sen jura om utviklingen etterfølges av oppvarming i kritt og begravelse av omtrent 1,5-3 km med

sedimenter. Denne artikkelen understreker at for indre Nordfjord ble de høytliggende og flate fjellpartiene sannsynligvis dannet i kenozoikum og representerer ikke et mesozoisk peneplan.

Artikkel IV presenterer et nytt regionalt datasett av lav temperatur termokronologiske data fra studieområdet. Prøver som ble samlet fra hele området resulterte i 29 AFT analyser og 45 apatitt (U-Th)/He analyser av enslige korn. Hverken AFT eller (U-Th)/He aldre viser en korrelasjon mellom alder og høydemeter over havet på prøvelokalitetene. AFT aldere varierer fra 323 ± 27 til 140 ± 4 Ma og (U-Th)/He aldere varierer fra 228 ± 12 til 57 ± 3 Ma. Regionalt sett viser prøver yngre aldre innerst i fjorder og langs Mørekysten, mens de eldre prøvene finnes i nærheten av Hornelen devonbasseng ved havnivå. Prøvene viser stedvis stor spredning i alder over korte avstander, noe som her relateres til sprang langs reaktiverte forkastninger ved Nordfjord-Sogn skjærsonen. Regionen viser en kompleks utvikling i tid og rom, hvor 1) regionen ved indre Nordfjord viser sakte avkjøling gjennom mesozoikum og økt avkjøling fra sen kritt-kenozoikum frem til i dag, som sammenfaller med funn fra artikkel III. 2) Regionen ved Sognefjorden viser liknende avkjølingstrend som indre Nordfjord, men med mindre ned-til-vest normal forkastningsreaktivering i trias/jura langs sprø forkastninger ved kysten som er en del av Nordfjord-Sogn skjærsonen. 3) Regionen rundt Hornelen viser store variasjoner i alder over korte avstander, som relateres til forkastningsaktivitet i sen jura-kritt langs forkastninger med Ø-V strøk. Termiske modeller viser at prøvene ble avkjølt til øvre skorpe (<8 km) fra sen karbon-perm og tillater avkjøling til overflatetemperaturer i sen Jura etterfulgt av oppvarming i kritt. Vi viser at lokale sedimentære bassenger muligens kan ha blitt dannet i hengblokken på disse forkastningsstrukturene i kritt. 4) Møreregionen nord for Nordfjord viser avkjøling til øvre skorpe (<8 km) i jura som kobles til heving av fotvegg under reaktivering i jura av Møre-Trøndelag forkastningskompleks under rifting utenskjærs.

Denne studien viser at Vest-Norge har vært gjennom en kompleks tektonisk og termisk utvikling i tid og rom siden den Kaledoniske fjellkjeden for omtrent 400 millioner år siden. Ved å bruke nye tilgjengelige metoder innen termokronologi og geokronologi,

og ved å kombinere disse med veletablerte metoder, konkluderer vi blant annet med å vise 1) fremtredende system av strøkforkastninger som ikke tidligere er blitt beskrevet, 2) flere subtile perioder med tektonisk aktivitet i kenozoikum, 3) en robust flerprøve termisk modell som danner et sterkt grunnlag for regionale termiske tolkninger, og 4) at avkjøling langs en riftet kontinentalmargin ikke er kontinuerlig og homogen, men varierer langs strøk og er kontrollert av langvarige forkastningssystem.

List of Publications

Publications included in the thesis:

PAPER I

Hestnes, Å., Gasser, D., Scheiber, T., Jacobs, J., van der Lelij, R., Schönenberger, J., and Ksienzyk, A.K. (2022): The brittle evolution of Western Norway – A space-time model based on fault mineralizations, K–Ar fault gouge dating and paleostress analysis: *Journal of Structural Geology*, v. 160, p. 104621, doi: 10.1016/j.jsg.2022.104621.

(published)

Paper II

Hestnes, Å., Drost, K., Sømme, T. O., Gasser, D., Scheiber, T., Linge, H., Chew, D., and Jacobs, J.: Constraining the tectonic evolution of rifted continental margins by U-Pb calcite dating.

(manuscript in review in *Scientific Reports*)

Paper III

Hestnes, Å., Jacobs, J., Gasser, D., Dunkl, I., Ksienzyk, A. K., Scheiber, T., Sirevaag, H., and Ketcham, R.: The thermal evolution of Western Norway based on multi-sample models of an elevation transect: implications for the formation of high-elevation low-relief surfaces.

(manuscript submitted to *Tectonics*)

Paper IV

Hestnes, Å., Jacobs, J., Gasser, D., Ksienzyk, A. K., Dunkl, I., Rydland, L. E., Scheiber, T., Sirevaag, H., and Bauer, F. U. (in prep.): The tectono-thermal evolution of Western Norway – new insights from low-temperature thermochronology.

(manuscript draft)

Contents

1. Introduction

1.1 Rift tectonics in a general setting

Passive continental margins, or **rifted margins**, are well-studied regions across the world due to their importance as a source for hydrocarbon and the understanding of the life cycle of orogens. Characteristic features of rifted margins are typically a low laying coastal strip which is separated from high elevation and low-relief landscape by a prominent escarpment (i.e. east coast of Brazil and Greenland, and the west coast of Norway). The margin represents a zone of rifting and break-up leading to the formation of oceanic domains (Peron-Pinvidic *et al.* 2019). The age and the underlying processes that led to the formation of the high-elevation low-relief surface found along rifted margins around the world is the topic of an ongoing scientific debate (e.g. Braun 2018; da Silva *et al.* 2019; Jess *et al.* 2019; Fonte-Boa *et al.* 2022; Green *et al.* 2022a). The formation and preservation of these surfaces is controlled by several factors, including thermal, surface, and tectonic processes along the onshore regions of a rifted margin.

The **onshore regions** of rifted margins are important to understand because of their controlling role for the entire rift system. However, due to the common lack of sedimentary cover onshore, the tectonic evolution is more difficult to constrain than offshore. Because of hydrocarbon exploration, a lot of information is known from the **offshore regions** of most rift systems. The history of sedimentary basins along continental margins is tightly coupled with the erosional history of the adjacent onshore margin, from which the material for the basin infill is derived. The amount and timing of erosion along onshore margins depends on the interplay between elevated topography and rock exhumation, and erosional agents such as rivers and glaciers. Western Norway is a good example to study such processes.

To understand the post-Caledonian evolution along the rifted margin of Western Norway, studies have focused on different aspects of a rift system; e.g. the interplay between the source to sinks and interpreting onshore causes for the offshore sedimentary sequences (Martinsen *et al.* 1999; Sømme *et al.* 2013a), the relationship

between mantle and crustal dynamics and the topographic signature (Nielsen *et al.* 2009b; Maupin *et al.* 2013; Pedersen *et al.* 2016), the geomorphological signatures in the landscapes (Lidmar-Bergström *et al.* 2013; Egholm *et al.* 2017), and low-temperature thermo-chronological and geochronological methods (Johannessen *et al.* 2013; Ksienzyk *et al.* 2014; Japsen *et al.* 2018; Green *et al.* 2022b). However, there is still a debate on how the post-Caledonian landscape developed through time. Several attempts have been made to explain the interplay between these processes forming the landscape and the evolution of the topography in southern Norway (e.g. Nielsen *et al.* 2009b; Osmundsen *et al.* 2010; Maupin *et al.* 2013; Pedersen *et al.* 2016; Japsen & Chalmers 2022).

The aim of this thesis is to contribute to filling this knowledge gap and help answer the **overarching question**: *What is the tectono-thermal evolution of Western Norway and how can it be explained in terms of rift and other tectonic processes?*

1.2 Aim of thesis

We have separated the overarching research question into the following **specific research questions**:

Q1: How does the onshore fracture and fault systems relate to regional tectonic events?

To detect trends within the fracture and fault systems of the study region, we performed remote sensing analysis combined with acquiring an extensive dataset of ductile and brittle field measurements (**Paper I**). The dataset includes information about surface mineralizations of fault and fracture surfaces, which was used as a first order constraint of the relative age of movement. Additional information about timing of brittle tectonic activity was gained through geochronological methods, such as K-Ar fault gouge dating (**Paper I**) and U-Pb calcite dating (**Paper II**). The knowledge gained is then interpreted in light of known tectonic events of the region.

Q2: Can a denser horizontal and vertical network of low temperature thermochronological data be used to distinguish between slow and steady exhumation versus uplift pulses caused by fault reactivation?

This question was addressed by sampling and analysing a new dataset of low temperature thermochronology, including apatite fission track (AFT) and apatite (U-Th)/He data, from the study area and combining these data with existing data from Western Norway (**Paper IV**). In addition, detailed information about the cooling history could be detected through the sampling and analysis of a near-vertical elevation transect and additional multi-sample thermal modelling (**Paper III**).

Q3: Are the low relief surfaces remnants of old, close-to-sea level paleic surfaces uplifted during the Cenozoic?

To answer this question, we combined the low-temperature thermochronological samples from a near-vertical elevation transect of the inner Nordfjord area with elevation transects from the literature to infer possible timings for the formation of the paleic surfaces (**Paper III**). The multi-sample thermal modelling sets some constraints on the possible age of the low-relief surface at the top of the transect. We could then implement the findings from the study of the elevation transect in the thermal history modelling from the entire region (P**aper IV**).

Q4: How are the evolutions of the North Sea and the Norwegian Sea reflected onshore Norway?

The results from this work are compared with and seen in light of known information from the sedimentary record offshore (**Paper II**) and general tectonic processes along the margin (**Paper I** and **Paper IV**).

1.3 Study area

Our study area is located in the northern part of **Western Norway**, bounded by the Møre-Trøndelag Fault Complex (MTFC) to the north, the Nordfjord-Sogn Detachment (NSD) to the west, and the Sognefjorden in the south (Fig. 1). The study area represents

the onshore transition between the North Sea margin to the west and the Norwegian Sea margin to the northwest. Geologically, the study area is situated within the Western Gneiss Region (WGR) overlain by Caledonian nappes (Fig. 2; section 1.3). In the central part of the study area, the 106 km long Nordfjord stretches from Loen in the innermost part to Bremangerlandet near its opening to the sea (Fig. 1). The flanks of the fjord rise up to 2000 meters above sea level (Fig. 3). We chose this study area for two reasons: (i) due to the **lack of high-resolution data from thermochronology** and (ii) because of its interesting geological location. The region features areas affected by ultra-high pressure metamorphism that stems deep burial during the Caledonian orogeny, orogenic collapse with extensive deformation along major shear zones, and the effects of rifting along two different margins, as described in the following chapter.

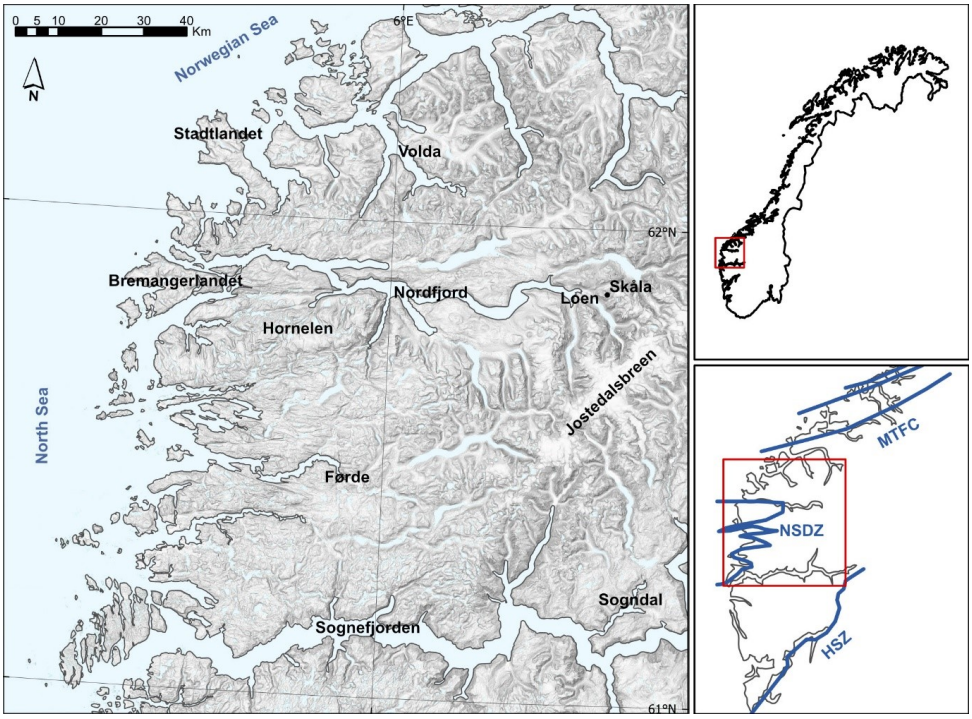

Figure 1. *Slope map of the study area. The two insets show the study area along the western coast of southern Norway and its location related to major tectonic elements like the Møre-Trøndelag Fault Complex (MTFC), the Nordfjord-Sogn Detachment Zone (NSDZ), and the Hardangerfjord Shear Zone (HSZ) marked in dark blue.*

1.4 Geological and tectonic evolution of the study area

The geology of southern Norway is shaped by orogeneses formation and collapse, followed by rift processes that later led to the opening of the North Sea and Norwegian Sea (Fig. 2). During the assembly of Rodinia, the southwestern margin of Baltica was affected by the **Sveconorwegian orogeny**, which lasted from 1.2-0.9 Ga (Bingen *et al.* 2021). Today, it is an ongoing debate whether the Sveconorwegian orogen was the result of a continent-continent collision or an active margin (Slagstad *et al.* 2013, 2022). The following collapse of the orogen led to the opening of the Iapetus ocean in the Neoproterozoic (Robert *et al.* 2021).

The **Caledonian orogeny** started in the early Ordovician, with subduction along both margins of the Iapetus ocean, and the oblique convergence between the continental plates of Baltica and Laurentia led to their collision in the Silurian-Early Devonian (Roberts 2003; Gee *et al.* 2008). Around this time, the Baltican margin was subducted beneath Laurentia to mantle depths resulting in eclogite formation and at the same time nappes were emplaced/thrusted on top of the Baltic shield (Gee 1975). The Lower and Middle nappe series comprise fragments of the pre-collisional continental margin of Baltica, including high grade metasediments. The Upper nappe series is derived from the Iapetus ocean and includes sedimentary and igneous lithologies from ophiolites and island-arcs, whereas the Uppermost nappe series is derived from the Laurentian margin (e.g. Gee 1975; Corfu *et al.* 2014).

During the **collapse of the Caledonides** in the Devonian (~410 Ma), the WGR and the Caledonian nappes experienced shearing, folding, and doming and large parts of the orogen signature got overprinted by extensional fabrics with a top-W to NW direction (Fossen 1992; Dunlap & Fossen 1998; Wiest *et al.* 2021). In southern Norway, the extension was first taken up as backsliding along a low-angle décollement before being localised in extensional shear zones (Fossen 1992). During the backsliding and deformation along shear zones, eclogites got juxtaposed low-grade metamorphic lithologies. Subsequently, Devonian sedimentary basins formed in the hanging wall of regional shear zones (Seranne & Seguret 1987; Osmundsen & Andersen 2001), such

as the Bergen Arc Shear Zone (BASZ; Wennberg 1996), the Hardangerfjord Shear Zone (HSZ; Fossen & Hurich 2005), the Nordfjord-Sogn Detachment zone (NSDZ; e.g. Labrousse *et al.* 2004; Young 2018), the Møre-Trøndelag Fault Complex (MTFC; e.g. Seranne 1992), the Nordfjord Shear Zone (NSZ; e.g. Hacker *et al.* 2010) and the Lom Shear Zone (LSZ; e.g. Wiest *et al.* 2021).

After the Devonian, cooling resulted in **brittle fault movement** overprinting and reactivating the ductile shear zones (Grønlie & Roberts 1989; Fossen 2000; Fossen & Hurich 2005). Brittle faults parallel to the ductile fabric of the BASZ, such as the Fensfjord fault (Fig. 2), have shown repeated episodes of activity in the Mesozoic and probably into the Cenozoic (Wennberg & Milnes 1994; Ksienzyk *et al.* 2014). As part of the low-angle HSZ, brittle faults such as the Lærdal-Gjende fault (LGF) were suggested to have been active during Permian-Triassic and Late Jurassic extensional events (Andersen *et al.* 1999; Fossen & Hurich 2005), while K-Ar fault gouge dating indicates activity in the Jurassic, Cretaceous and Paleogene (Tartaglia *et al.* 2020). The brittle faults of the NSDZ, including the Dalsfjord fault, were active during Permian to Early Triassic, Jurassic and Cretaceous times (Torsvik *et al.* 1992; Eide *et al.* 1997; Braathen *et al.* 2004; Fossen *et al.* 2021). The MTFC shows an extensive faulting history with repeated activity during the Late Devonian, Permian-Triassic, Mid- and Late Jurassic, Cretaceous, and the Cenozoic. Earlier movements show a strike-slip trend whereas the younger, more recent activities show a dip-slip movement towards NW (Redfield *et al.* 2004, 2005a; Osmundsen *et al.* 2006). In addition to the activity along large-scale fault structures, more detailed analyses of brittle faults including K-Ar fault gouge dating have revealed brittle activity across the entire western Norwegian region in the early Carboniferous, Permian, Triassic-Jurassic, Cretaceous and the Paleogene (Ksienzyk *et al.* 2016; Viola *et al.* 2016; Scheiber & Viola 2018; Scheiber *et al.* 2019; Fossen *et al.* 2021; Tartaglia *et al.* 2022).

The onshore brittle activity is linked to the **offshore brittle evolution**, which is described as well-constrained rift phases. For both the North Sea and the Norwegian Sea, Permian-Early Triassic rifting led to the formation of large continental to shallow

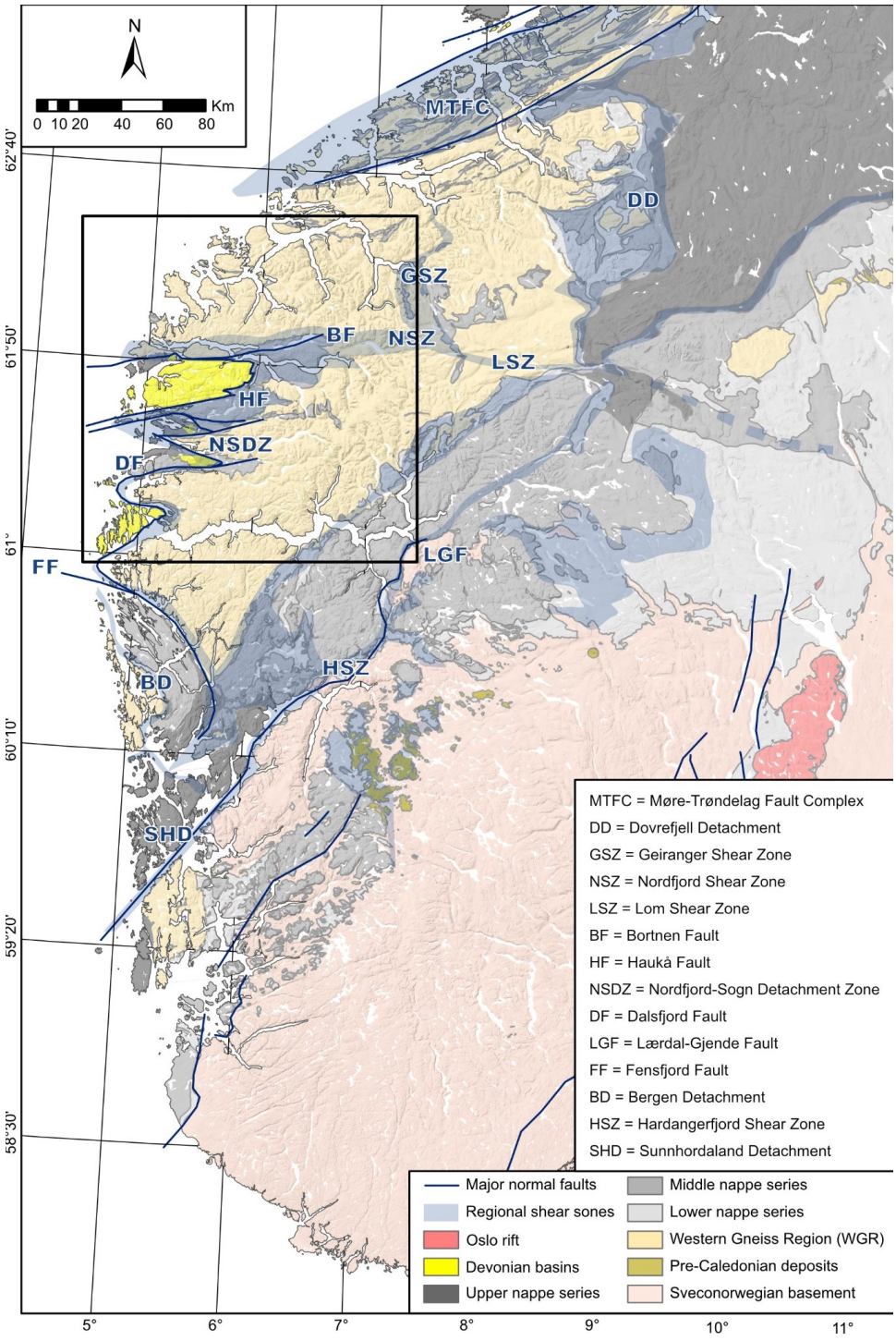

Figure 2. *Simplified tectonic map of southern Norway showing important regional shear and fault zones (from Wiest et al. 2021). The black square marks the study area.*

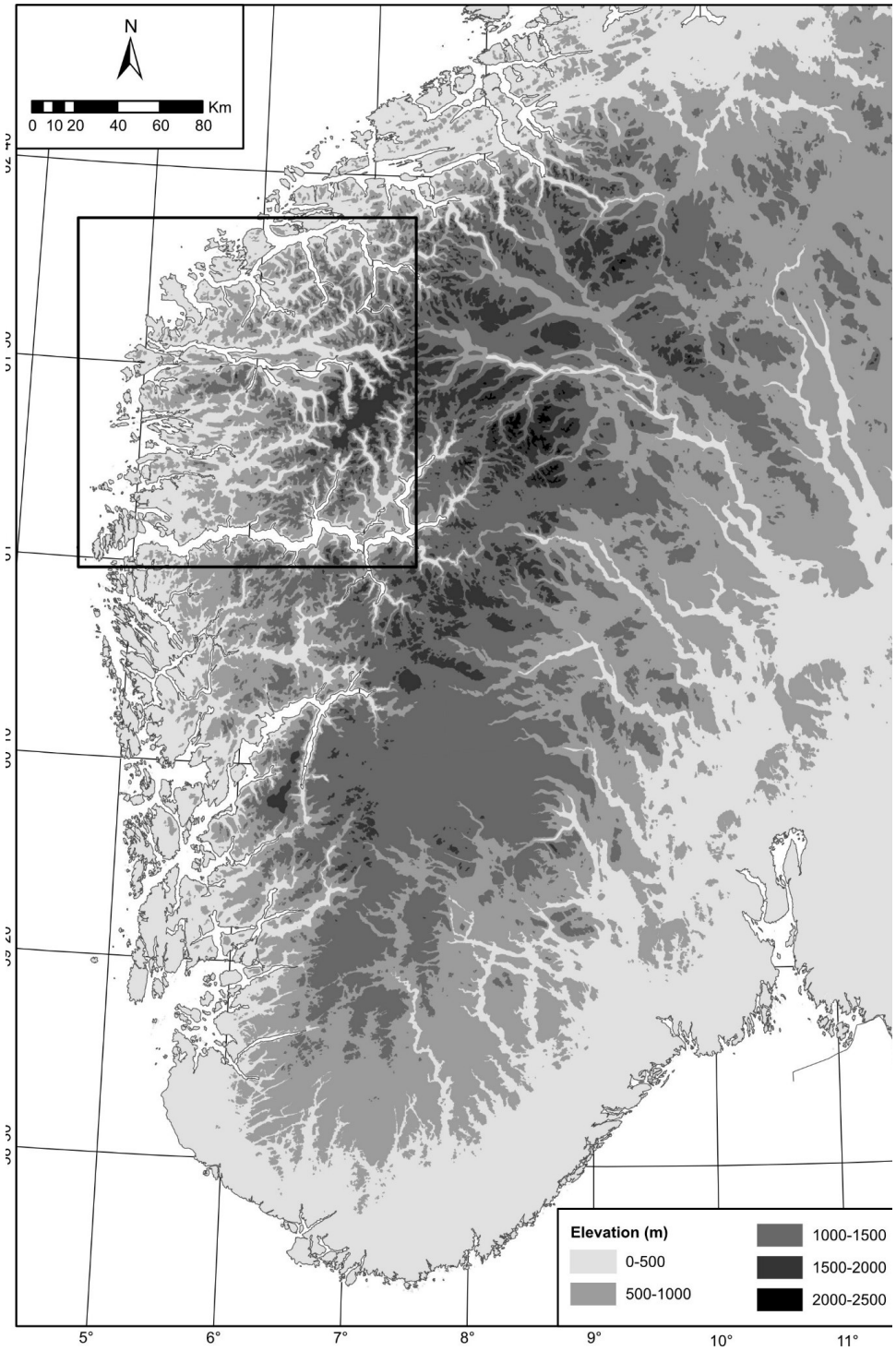

Figure 3. *Elevation map of southern Norway. The black square outlines the study area.*

marine basins (e.g. Viking Graben, Stord Basin; Fig. 8) and volcanic dyke intrusions (e.g. Roberts *et al.* 1995; Fossen & Dunlap 1999). This first rift phase showed E-W extension in the North Sea and a more ENE-WSW extensional trend in the Norwegian Sea (e.g. Færseth 1996). In the North Sea, a second and more localised rift phase in the Late Jurassic-Early Cretaceous lead to the development and fragmentation of sedimentary basins and tilting of fault blocks (e.g. Færseth 1996; Phillips *et al.* 2019). Different modes of extension have been suggested for this rift phase; pure E-W extension (e.g. Bartholomew *et al.* 1993; Reeve *et al.* 2015), NE-SW extension (e.g. Færseth 1996; Færseth *et al.* 1997), or rotation of the extension axis (e.g. Doré *et al.* 1997; Davies *et al.* 2001). In the Norwegian Sea, a similar second Late Jurassic-mid Cretaceous rift phase formed new basins (e.g. Møre Basin; Fig. 8) during a NW-SE extension (e.g. Grunnaleite & Gabrielsen 1995; Theissen-Krah *et al.* 2017). A last rift phase of the Norwegian Sea in the Late Cretaceous- Palaeocene led to the **final break-up** between Greenland and Eurasia approximately 55 million years ago (e.g. Gómez *et al.* 2004; Gaina *et al.* 2017).

1.5 The topographic and tectono-thermal debate in Norway

By the start of the last century, the paleic surfaces of Norway were described as a low relief surface at high altitude and interpreted to have formed at sea level (Reusch 1901). Since then, the processes behind the formation and the age of these surfaces have been scrutinised and debated. The work of Reusch (1901) started by stating:

"*Norges relief er endnu saa lidet forstaaet, at vi ikke har opnaaet en rimerlig begrundet forklaring af, hvorledes oprindelsen til flere af de største træk deri er at opfatte*"

(which approximately translates to "*The relief of Norway is still so poorly understood that we still have not found a reasonable explanation to the formation of many of its largest characteristics*."). In light of the on-going debate, this appears very much true until today, despite the knowledge gain driven by several methodological developments.

Today, the debate of the formation of the Norwegian landscape is centred around **three endmember theories** that have dominated the debate: (1) The "classical" model (Fig. 4a) is similar to the theory proposed by Reusch (1901), that the Caledonian mountain chain was eroded down to sea level during the late Palaeozoic and remained low until late Cenozoic times when fault activity caused the uplift of the base level to present day level (e.g. Redfield *et al.* 2005; Gabrielsen *et al.* 2010a; Osmundsen *et al.* 2010; Sømme *et al.* 2013). According to the "classical" model the paleic surface we find today at high altitude was formed at sea level, and fjords and valleys were later incised by erosion. In recent years, this model has been questioned and (2) a contrasting theory has been proposed that suggests that the Caledonian mountains were never eroded down to a base level, but remained high until the late Cenozoic when climatic changes

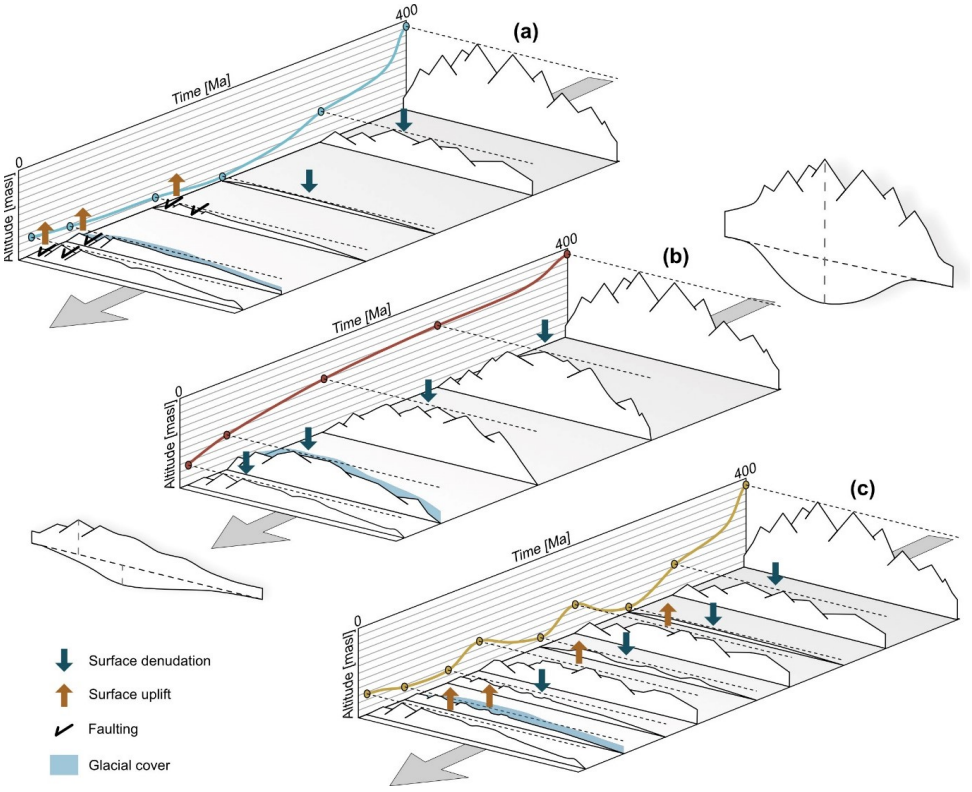

Figure 4. *Simplified schematic sketches of the three end-member theories of landscape evolution of southern Norway.* ***a)*** *Classical model of erosion to base level and later uplift,* ***b)*** *the ICE (Isostasy-Climate-Erosion) model, and* ***c)*** *the repeated peneplain, burial and erosion model. Note that the sketch doesn't show all suggested peneplain formation cycles. The present crustal root is offset from the topographic high (Maupin et al. 2013).*

caused increased erosion down to present day level (Fig. 4b; e.g. Nielsen *et al.* 2009; Pedersen *et al.* 2016). In this case, it is hypothesised that the paleic surface was formed by, for example, a glacial buzz-saw effect during the Quaternary (Egholm *et al.* 2009; Steer *et al.* 2012). Lastly, (3) the third theory of the landscape evolution is based on the interpretation of several generation of peneplains formed through repeated uplift, reburial and erosion from the Permian until the Miocene (Fig. 4c; e.g. Lidmar-Bergström *et al.* 2013; Japsen *et al.* 2018; Green *et al.* 2022). A **peneplain** is here defined as a low-relief surface formed due to erosion down to base level (Phillips 2002; Bonow *et al.* 2007).

The complexity of the debate is reflected in the observations used as arguments for one or the other of the theories. In the following, I will give a brief summary of the debate concerning the south Norwegian landscape and its evolution.

After **the early observations and interpretations** of Reusch (1901), more studies followed, focusing on the morphogenetic idea of peneplains formed at or close to sea level and denudation leading to the present day location at higher elevations (e.g. Strøm 1948). This view of landscape formation was based on the **geographical cycle** introduced by Davis (1899). Those supporting this evolution, interpreted the peneplain to be the result of Tertiary uplift, either as a results of doming or fault activity (Rudberg 1988 and references therein). Strøm (1948) suggested **at least two erosion surfaces/peneplains**, one being elevated in the Miocene and the other in Pliocene and with the Pleistocene glaciation being the cause of the landforms. The same study describes that the sub-Cambrian peneplain was deformed by folding during the Caledonides and broken up by faulting in the Permian and possibly in the Tertiary.

Alternatively to the peneplain theory, it was debated if the stepwise landscape from west to east was a result of so-called **polycyclic Piedmonttreppe** – a landscape consisting of several steps increasing with ~200 m elevation between them where the sub-Cambrian peneplain is the topmost surface (Fig. 5; e.g. Evers 1962). Each Piedmonttreppe is, according to Evers (1962), a result of erosion and denudation under special climatic conditions in pre-glacial times. Landscape formation through

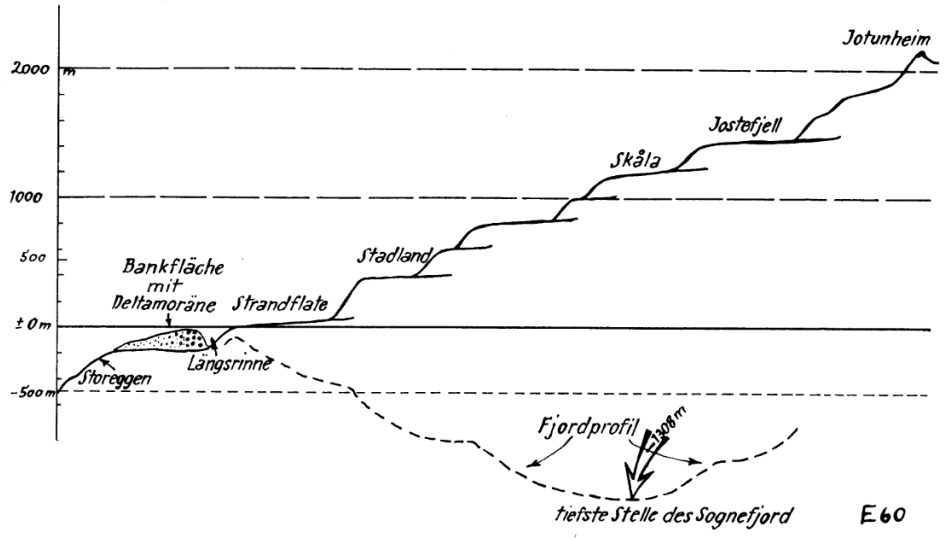

Figure 5. *The landscape of southern Norway described as a series of Piedmonttreppe. This theory was highly disputed. Illustration from Evers (1962).*

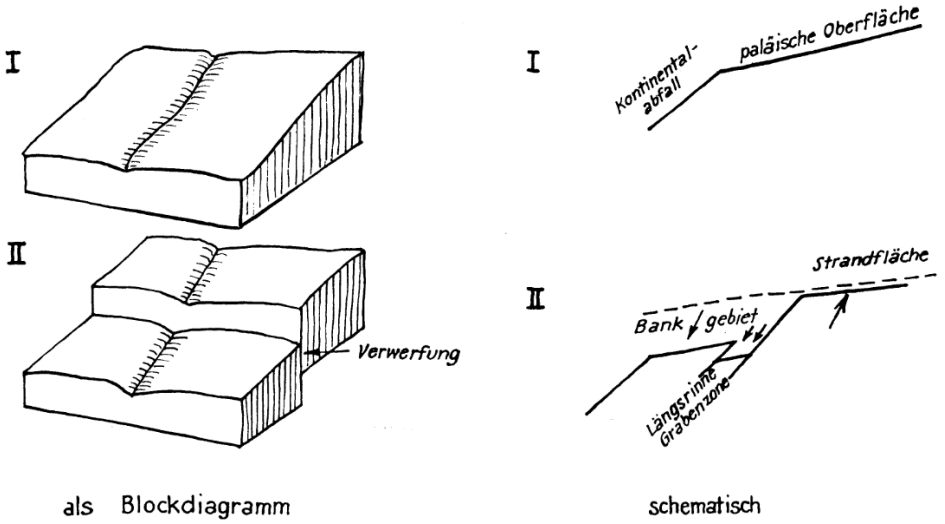

Figure 6. *The formation of low relief surfaces according to Holtedahl (1965). The different low relief surfaces are the result of faulting along the same peneplain, here illustrated with the formation of the strandflat and the bankflat. Illustration from Evers (1962).*

polycyclic piedmonttreppe was highly discussed (e.g. Holtedahl 1965; Rudberg 1965), where Holtedahl (1965) argued that the "steps" of low relief surfaces could have formed through Cenozoic **fault offset** of the same paleic surface (Fig. 6). Another alternative theory was suggested by Gjessing (1967), wherein the paleic landscape, consisting of hills and basins that are connected by passes, was formed by processes **unrelated to the regional base level** during a warmer pre-Quaternary climate. The work of Gjessing (1967), also proposes that the arrangement of paleic surfaces in "steps" was a result of different phases of tectonic uplift.

Geomorphological studies remain an important tool to understand landscape formation. Several generations of landscape formation, each determined by different base levels have been interpreted from stratigraphic landscape analysis (Lidmar-Bergström *et al.* 2007, 2013; Lidmar-Bergström & Bonow 2009). These analyses are based on the relationship between rock cover and peneplains, re-exposed and never covered peneplains, and valley incision into the peneplains. The formation of a **peneplain, or pelagic surface**, should be of (sub)continental extent and would form during fluvial and subaerial erosion close to base level independent of lithologies of different erosive resistance, forming a low relief surface as the ultimate stage of a cycle (Davis 1899; Phillips 2002). Such low relief surfaces are mapped from the study area (Fig. 7), typically showing undulating small surfaces bounded on one or more sides by steep hills (Fig. 7c). It has been argued that it is less likely that such low relief surfaces would be preserved from a base level while being uplifted to great elevations (e.g. Nielsen *et al.* 2009a). Another critique of the stratigraphic landscape analysis is the uncertainty of formation mechanisms of peneplains, which has been much debated (e.g. Egholm *et al.* 2009, 2017; Nielsen *et al.* 2009b, 2010b; Chalmers *et al.* 2010; Hall *et al.* 2013; Japsen *et al.* 2022). It has been proposed that peneplains can form independent of base level, and that the correlation of peneplains across large regions would be challenging due to complex fault patterns and differential uplift that would offset such surfaces (e.g. Calvet *et al.* 2015; Pedersen *et al.* 2018, 2021). For example, models that include ice sheet erosion as a formation mechanism of low relief plateaus/peneplains did predict that the interplay between topography, ice dynamics, and erosion over a million-year timespan, would form low relief surfaces independent of the base level

(Egholm *et al.* 2017). The argument is further supported by the comparison of fjord erosion to relief and offshore sedimentation, which showed a large mismatch between eroded area and sediment accumulation, suggesting considerable erosion of the peneplains away from the fjords (Steer *et al.* 2012). Use of cosmogenic ^{10}Be and ^{26}Al exposure data and regolith sedimentological analysis suggests that slow erosion on the low-relief surfaces was sufficient to smooth the topography over millions of years (Andersen *et al.* 2018b, a). Also, Pedersen *et al.* (2018) inferred ~2 km of topography

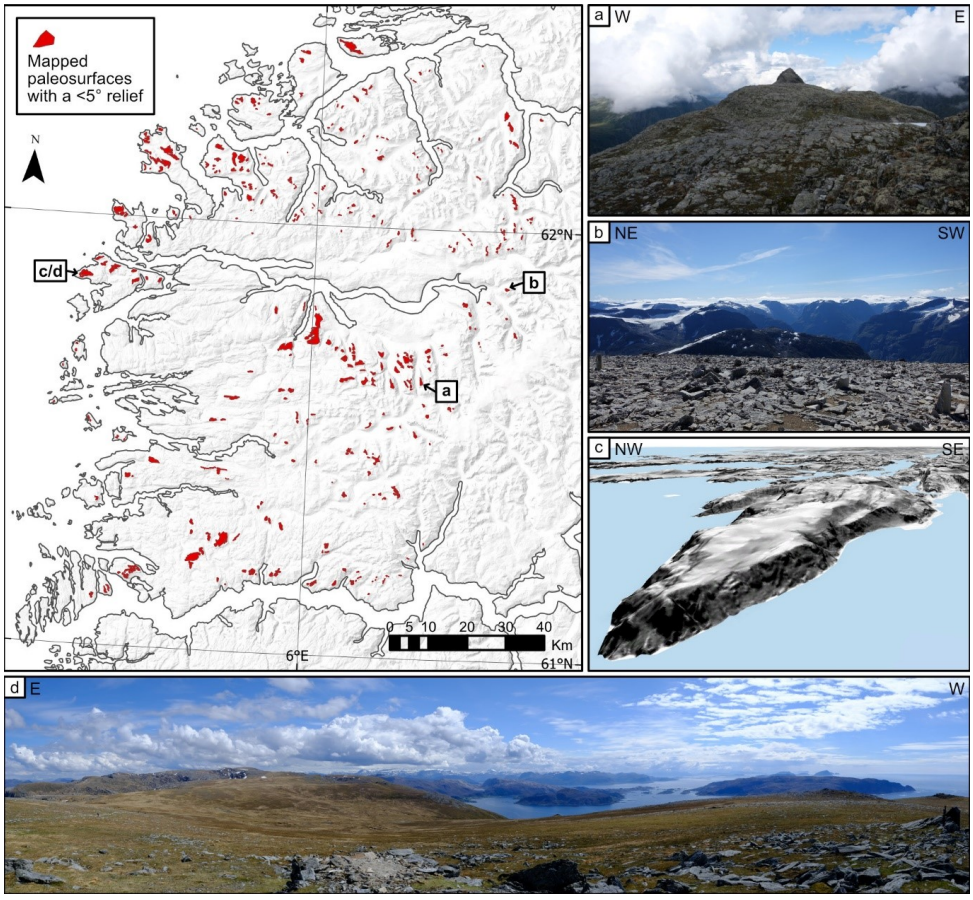

Figure 7. *Overview of mapped paleosurfaces from this study with a relief < 5° (marked in red) within the extent of the study area. Panels to the right and below show impressions of the paleosurface at* ***a)*** *Eggenipa,* ***b)*** *Skåla mountain looking SE and with low relief surfaces visible in the distance, and* ***d)*** *a 180° panorama from Veten facing south. Panel* ***c)*** *shows a 3D-reconstruction of the Veten paleosurface on Bremangerlandet. The location of the different sites shown in the panels are indicated on the map by letters.*

in Southern Norway from Eocene until mid-Pliocene from inverse landscape evolution modelling with no need for repeated episodes of uplift to explain the topographic patterns.

Combining geomorphological studies with **low temperature thermochronology** has been used as a tool before to gain knowledge about cooling and erosion through time. In Norway, the use of Apatite Fission Track (AFT), sometimes combined with Zircon Fission Track and apatite/zircon (U-Th)/He analysis, has been an important tool to interpret erosion and uplift locally and across large spatial scales. The earliest local AFT study revealed fast cooling following the Caledonian collapse until the Permian, continued by slow cooling until a new period of faster cooling starting around the end of the Mesozoic, which lasts until present day (Andriessen 1990). Not long after, the first regional AFT study of southern Norway followed, revealing a similar trend as shown in Andriessen (1990) but with two phases of increased cooling: a first phase during the Triassic-Jurassic forming a Cretaceous-Paleogene peneplain, followed by a second cooling phase in the Paleogene-Neogene as a result of domal uplift (Rohrman *et al.* 1995). The study of Rohrman *et al.* (1995) showed a clear regional trend. The youngest AFT ages were located inland at sea level, whereas the older ages were found in the coastal regions and at high elevations. This trend was further corroborated in the AFT data compiled by Hendriks *et al.* (2007). Work by Leighton (2007), based on AFT and zircon and apatite (U-Th)/He analysis, suggested rapid cooling from the collapse of the Caledonian orogen until the Triassic (1-5 °C km^{-1}), followed by a period of slow cooling from Triassic until the latest Cenozoic (<10 m Ma^{-1}), before a renewed period of fast cooling until present day. Although the timing of the cooling events is similar to those identified by Rohrman *et al.* (1995), Leighton (2007) suggested that the topography of southern Norway was not the result of an uplifted peneplain and major crustal uplift but rather the remnant crustal roots of the Caledonides and a sustained high topography. The view of Leighton (2007), was shared by Nielsen *et al.* (2009b) in their much debated (e.g. Lidmar-Bergström & Bonow 2009; Nielsen *et al.* 2009a) "ICE (isostasy-climate-erosion) hypothesis". Nielsen *et al.* (2009b) combined AFT data with observations from climate, erosion, crustal thickness, and gravity to infer a long-term and slow exhumation of western Scandinavia from the Caledonides until

present with increased Neogene erosion. By combining AFT data and vertical motion in numerical models, Medvedev & Hartz (2015) inferred a late Palaeozoic and Mesozoic erosion rate of <10 m/My and argued that the topographic variations in Scandinavia during this time must have been low. A very contrasting topographic development was proposed by Japsen *et al.* (2018) and Green *et al.* (2022). In their work, AFT data combined with information from stratigraphic landscape analysis from across Norway, Sweden and Finland pointed to repeated episodes of uplift, peneplain formation, and burial in the late Carboniferous, Middle Triassic, Middle Jurassic, middle Cretaceous and the early Miocene. The methods to infer thermal evolution through time that are used by Japsen *et al.* (2018) and Green *et al.* (2022) are subjected to ongoing debate (e.g. Green *et al.* 2019; Jess *et al.* 2019, 2020; Gallagher 2021; Green & Duddy 2021a, b). Even though tectonic processes were mentioned in some of the regional studies, southern Norway was considered more or less one structural block with uniform deformation. This is, however, called into question by the work of Redfield *et al.* (2004, 2005a), Leighton (2007), Johannessen *et al.* (2013), Templeton (2015) and Ksienzyk *et al.* (2014) who all showed major offsets of AFT ages along fault strands and other topographic lineaments. Along the MTFC, reactivation in Late Cretaceous-Tertiary was related to fault block uplift during the late stages of rifting in the Atlantic ocean (Redfield *et al.* 2004, 2005a) and faulting has been shown to play an important part in the development of the coastal Devonian basins (Fig. 2; Templeton 2015). These studies emphasised the importance of considering tectonic activity when inferring a topographic evolution of the region.

Structural geological studies, often combined with geochronological methods, have revealed a close connection between the offshore rift phase evolution and the onshore tectonic processes (Redfield *et al.* 2005b; Fossen *et al.* 2017, 2021). Fault activity has by some been interpreted to be a controlling factor of uplift and topographic development (e.g. Gabrielsen *et al.* 2010a). Based on shifting stress configurations, Gabrielsen *et al.* (2010a) inferred three stages for the tectonomorphological development of Southern Norway; 1) denudation of the Caledonian mountains until the late Permian, 2) tectono-thermal uplift from the Triassic to the Late Cretaceous along major structures such as the Lærdal-Gjende fault zone (Fig. 2), and 3) new tectono-

thermal activity in the Tertiary until present with additional post-glacial rebound. Important for this structural interpretation of landscape evolution is the sub-Cambrian peneplain, which is thought to have covered most of Scandinavia (e.g. Strøm 1948; Gabrielsen *et al.* 2015). The sub-Cambrian peneplain was formed during the early-Cambrian, then covered by marine sediments during the Early Ordovician, and eventually deformed by Caledonian thrusting, offset along post-Caledonian faults, and regionally uplifted (Gabrielsen *et al.* 2015). The use of peneplains and paleic surfaces as a constraint of timing of evolution has been questioned, as described above and by Nielsen *et al.* (2009a, 2010a) and Gabrielsen *et al.* (2010b). Structural data has also been described as the controlling factor of alpine topography, where the Mesozoic and Cenozoic reactivation of rifting form asymmetric ranges in the footwall of normal faults along the MTFC (Fig. 2; Osmundsen *et al.* 2010). It was shown that the topography is related to the taper break along rifted margins, where a sharper taper break would result in higher escarpments (Osmundsen & Redfield 2011).

Along the rifted margin of Norway, a lot of information has been gained from **offshore studies**, especially from the Cenozoic stratigraphic record. In the northern North Sea and the Møre Basin (Fig. 8), five unconformity-bounded stratigraphic mega-sequences can provide information about the spatial and temporal sediment supply; Paleocene-lowermost Eocene, lower Eocene-lowermost Oligocene, lower-upper Oligocene, Miocene-Pliocene and in Pleistocene (Martinsen *et al.* 1999). The unconformities, the off-lapping sedimentation pattern and the varying directions of sediment supply have been interpreted to reflect repeated uplift of onshore Norway (Martinsen *et al.* 1999; Faleide *et al.* 2002; Huuse 2002). The early Paleogene phases of uplift have been related to rift processes, the magmatic influence from the Icelandic plume and/or the final break-up of the Atlantic ocean (e.g. Faleide *et al.* 2002; Huuse 2002; Anell *et al.* 2010). The late Paleogene and the Neogene phases of increased sediment accumulation and uplift have, differently been suggested to be due to climatic variations, especially pronounced during the Eocene-Oligocene climatic transition from “greenhouse” to “icehouse” (Zachos *et al.* 2001; Huuse 2002; Anell *et al.* 2010). It seems to be a common agreement that the Plio-Pleistocene increased sediment accumulation is related to the glacial conditions at that time (Huuse 2002; Anell *et al.* 2010). The

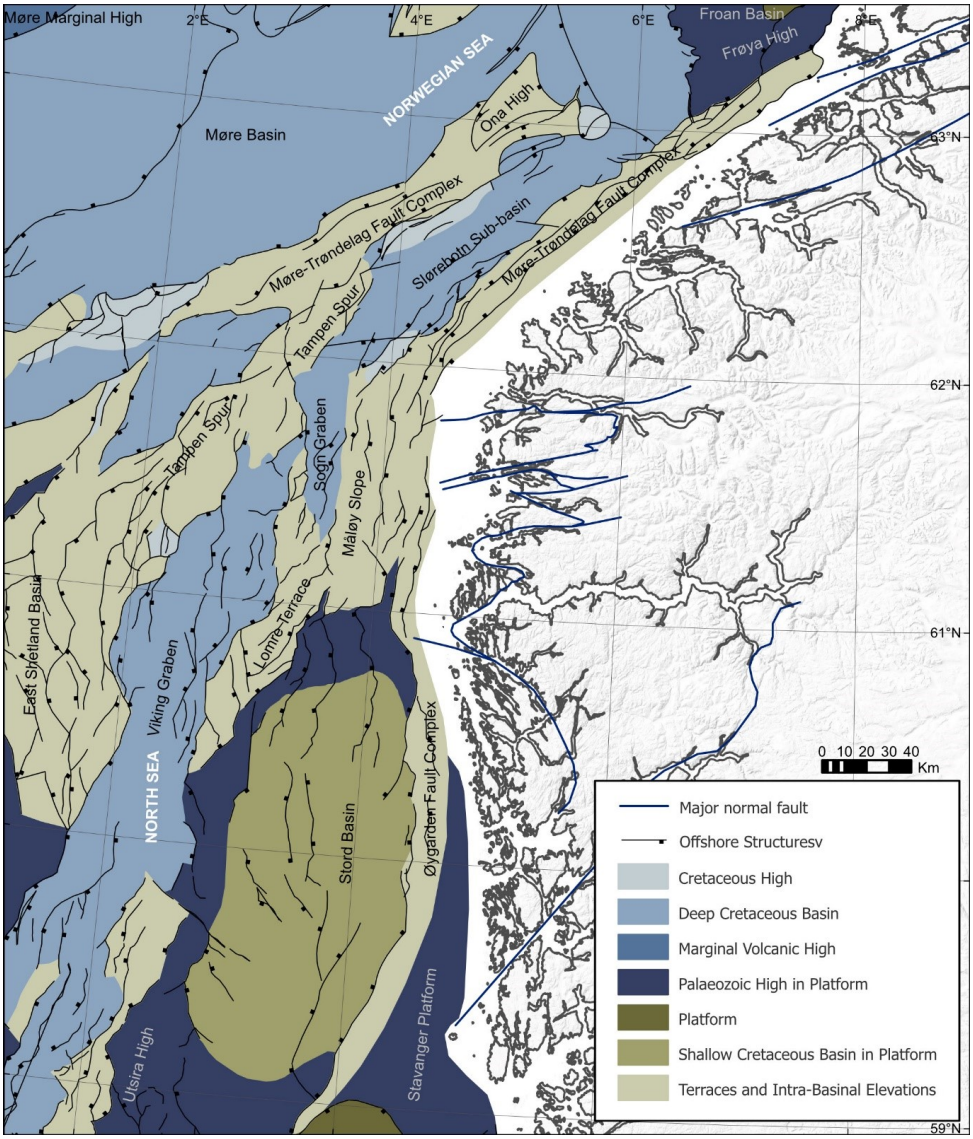

Figure 8. *The main structural elements of the northern North Sea and southern Norwegian Sea. Based on map from the Norwegian Petroleum Directorate* (Blystad *et al.* 1995).

observed sediment volume stored in point-sourced depocenters was used to make inferences about the syndepositional paleo-landscape (Sømme *et al.* 2013a). The Late Jurassic relief with height differences of about 1.6 km was lowered to 0.5 km (or less) by the Late Cretaceous, before a uplift to a ~1.1 km relief in northern parts of southern Norway in the Paleocene. The rejuvenation of the landscape was interpreted to be a

result of tectonic activity along fault systems in the late Jurassic, earliest Paleocene, and earliest Oligocene with minor influence of climatic variations (Sømme *et al.* 2013b, a). In contrast, the inverse models of Pedersen *et al.* (2018) that imply high (~2 km) topography in southern Norway from 54-4 Ma parsimoniously explain the offshore sediment flux without phases of uplift.

The importance of **mantle and lithospheric studies** was increased by recent advances in method developments and data availability. From gravity studies, it is shown that the Southern Norwegian high topography is supported by the mantle (Nielsen *et al.* 2009b). It is also suggested that due to the lack of a pronounced crustal root, the high topography of southern Norway is not compensated by the crust and needs some sort of isostatic support to be sustained (e.g. Maupin *et al.* 2013; Mauerberger *et al.* 2022). Several mechanisms have been suggested, including crustal isostasy, dynamic support, flexural support and lithospheric isostasy (e.g. Maupin *et al.* 2013). The lithospheric mantle below southern Norway shows slow seismic velocities compared to the lithospheric mantle below southern Sweden (Makushkina *et al.* 2019), which has been explained by a thinner subcontinental lithospheric mantle of different composition below southern Norway than below Sweden (Gradmann *et al.* 2013). The different mantle velocities can also indicate a warmer lithosphere below southern Norway, which has been suggested to be due to several reasons, including 1) re-fertilization of the mantle lithosphere and radioactive thermal effects during the Sveconorwegian oceanic subduction (e.g. Slagstad *et al.* 2017), 2) Permian rifting and magmatism , and 3) final break-up of Eurasia and Greenland in the Eocene (~55 Ma) related to the Icelandic plume (e.g. Rohrman *et al.* 1996; Faleide *et al.* 2002; Gabrielsen *et al.* 2010a). By mapping the mantle transition zone below Fennoscandia and showing that the zone is located close to the reference depth, Makushkina *et al.* (2019) argued that the high topography in southern Norway cannot be sustained by influence from the deep mantle. It has been suggested that the lateral velocity variations in the lithosphere below southern Norway and surrounding areas, has been present for at least 300 My (Maupin *et al.* 2013). This was also supported by Pedersen *et al.* (2016), which showed that the topography of southern Norway is supported by a crustal structure. Most recently, dynamic support through edge-driven convection from the lateral plume flow has been

suggested as a mechanism to explain the sustained topography (Mauerberger *et al.* 2022). An alternative explanation based on studies of the P and S wave structures of the upper mantle below southern Norway, suggests that episodic erosion and convective removal from the mantle lithosphere could have triggered episodic uplift during the Mesozoic and Cenozoic (Kolstrup *et al.* 2015).

The above summary of work done on the post-Caledonian evolution of southern Norway shows the complexity of the ongoing debate. In short, a variety of methodological approaches, often combining different methods, have been used to study the topographic and tectono-thermal evolution of southern Norway. The generated explanations are to a varying degree related to, and supported by, geological observations. For example, the formation and existence of the peneplains, the prograding sediment wedges offshore, and the regional trends of AFT data all have been used to support either of the three theories of evolution described above (Fig. 4).

1.6 Methods

The summary above shows that many different approaches and methods have been used to investigate the question of the tectono-thermal and topographic debate of Western Norway, often in combination. To develop a coherent understanding that agrees with known information, it is firstly important to acquire sufficient data. In this study, we aimed to contribute with additional data from an area where few studies so far have focused on the young brittle structures and where low-temperature thermochronological studies were lacking.

Along a rifted margin, the study of brittle structures can help to constrain and relate an area to regional tectonic processes. Within the study area, much work has so far been done related to Caledonian processes and the early phase of orogen collapse (e.g. Hacker 2007; Labrousse *et al.* 2011; Walsh *et al.* 2013; Wiest *et al.* 2021). Few studies have however, focused on the regional colder brittle evolution (exceptions by Braathen 1999, Fossen *et al.* 2017, 2021 and Tartaglia *et al.* 2022), leaving a lack of understanding of how the terrain relates to large and well-known structures, like the

MTFC, NSDS and LGF (Fig. 1). Geochronological methods can help constraining the timing of brittle activity, and in this study we have done the first ever U-Pb dating on calcite from fractures and faults from Western Norway.

Low temperature thermochronology is a suited method to gain information about cooling over time and is a useful proxy for exhumation and erosion. Thermochronological methods such as Ar-Ar analysis on muscovite, biotite or K-feldspar give information about the cooling at temperatures from ~400-200°C at mid-crustal levels (Reiners *et al.* 2017), cosmogenic nuclide dating tells the story of surface rock exposure (Schaefer *et al.* 2022). The low temperature thermochronological methods of AFT and apatite (U-Th)/He data combined will give information about the cooling from ~120-40°C, which represents depths of 6-2 km of the upper crust if we, for example, assume a geothermal gradient of 20°C/km.

1.6.1 Structural analyses

In a first step, I used high-resolution digital elevation models (DEM), built from **remotely sensed elevation data**, to identify lineaments and relevant large-scale structures in the study area. This analysis was carried out in the geographic information system (GIS) software ArcGIS Pro. For a detailed method description, see **Paper I**.

Then, I ground-truthed the remote sensing analysis by **mapping fault and fracture systems in the field**. It was especially important to verify the digitally mapped lineament trends of the region and to make sense of the influence of ductile structures on later brittle tectonics, which is not possible from satellite imagery. Mapping the relationship between fault and fracture orientation, ductile precursor orientation, and the fault and fracture surface mineralisation also helps to understand the spatial and temporal evolution of the fault and fracture systems of the region.

Subsequently, the collected data allowed me to build a **paleostress model** of the region to predict the stress field of which the various faults and fractures are formed. Different fault surface minerals form under different temperatures, for example mica on fault surfaces is a product of high-temperature deformation (Scheiber *et al.* 2016), whereas chlorite, epidote, and quartz form under temperatures between 100 °C and ~400 °C

(Bird & Spieler 2004; Sandström & Tullborg 2009; Schleicher *et al.* 2012). Zeolite, on the other hand, is a product of low-temperature processes of <250 °C (e.g. Weisenberger & Bucher 2010). Therefore, grouping our field data based on region and fault surface mineralization allows us to reconstruct the stress fields under which the various fractures formed. Combing this information with geological information then allows us to draw conclusions about the fault and fracture activity/movement. I used the **software Win-tensor** (Delvaux & Sperner 2003) to extract information about the paleostress field. WinTenor will deduce the local stress tensor of the structural data (Angelier 1979; Lacombe 2012; Simón 2019). More information on this method can be found in **Paper I**.

1.6.2 Geochronology

Even more knowledge about the tectonic evolution is gained when structural data and geochronological methods are combined to extract ages for fault movement and fluid precipitation in fractures and faults. Here, I used two methods that focus on the younger part of the brittle history: K-Ar fault gouge dating and U-Pb calcite dating.

K-Ar fault gouge dating

K-Ar fault gouge dating allows to date several episodes of fault activity and when linked to structural data, the timing of stress orientation can be deduced. The first step of the analysis is to separate the gouge material into five size fractions, each to be analysed individually: 6–10 µm, 2–6 µm, 0.4–2 µm, 0.1–0.4 µm and <0.1 µm. Then, the mineralogical and the crystallographic composition of each fraction is analysed using X-ray diffraction (XRD) and a scanning election microscope (SEM). I describe the K-Ar dating of all five size fractions in more detailed in **Paper I** but see also the supplementary material to **Paper I**.

The results of K-Ar fault gouge analysis need to be carefully considered based on the **gouge mineral composition** and the surrounding host rock. The method is thought to mainly date new grown illite, only stable above certain temperatures. All the K-bearing minerals in the gouge fraction therefore need to be identified to decide whether the mineral represents authigenic mineral growth in the gouge, or not. If the mineral is not

authigenic, then it could, for example, be inherited from the host rock, which then would bias the K-Ar ages and give a wrong estimate for the faulting age (e.g. Zwingmann *et al.* 2010). In addition, the gouge minerals might reflect several phases of faulting, again resulting in a K-Ar age not reflecting a single faulting event (e.g. Torgersen *et al.* 2015; Viola *et al.* 2016).

U-Pb calcite dating

Calcite will precipitate along faults and fractures in the upper crust, and if the calcite contains sufficient amounts of the parent/daughter isotopes of U-Pb, then **U-Pb calcite dating** is a useful tool to determine the age of calcite precipitation. Here, I used U-Pb calcite dating to find better constraints on the younger part of brittle evolution of Western Norway. We analysed the calcite samples for U and Pb isotope concentrations as well as for major elements and trace elements by either a mapping approach or by a spot ablation sampling strategy (see description in **Paper II**, but also Drost *et al.* 2018).

U-Pb calcite dating can often prove challenging, since calcite often lacks sufficient amounts of parent/daughter isotopes and the parent/daughter relationships are easily affected by an open system behaviour (e,g. Roberts *et al.* 2020). From a **tectonic perspective**, the calcite age would provide most information, if the dated mineral is found related to slip lines or slickenfibers on the mineral surface (Roberts & Holdsworth 2022). When such tectonic signatures are lacking, then the stress field under which the fault or fracture was active is much harder to constrain. Additional **stable isotope analysis** provides more information about the source of the fluids and thus the environment under which the calcite was formed (e.g. Roberts *et al.* 2020). Stable isotope analysis is performed as described in **Paper II** and the respective supplementary material.

1.6.3 Low temperature thermochronology

Apatite AFT and apatite (U-Th)/He dating have been used along rifted margins to both understand the dynamic processes (exhumation) along a margin, but also as provenance to get more information about the source-to-sink region. The AFT and apatite (U-Th)/He ages represent cooling through certain temperature ranges. The **partial**

annealing zone (PAZ) for the AFT system ranges from 120–60 °C (Gleadow & Duddy 1981), and for the (U-Th)/He system the **partial retention zone (PRZ)** ranges from 70–35 °C (Farley & Stockli 2002).

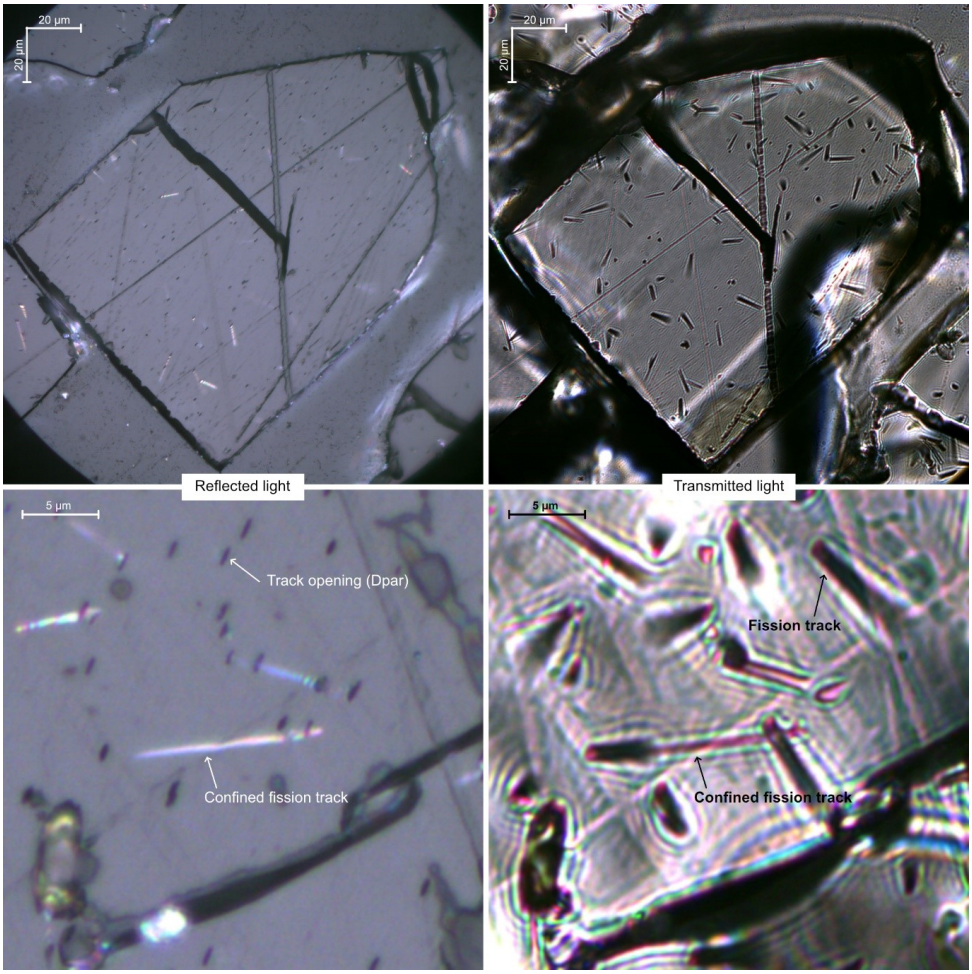

Figure 9. *Apatite grain shown in reflected (left) and transmitted (right) light. The top row shows an apatite grain on 1000x magnification, while the lower row shows a smaller area of an apatite grain on 2000x magnification. In reflected light, the track opening on the polished grain surface becomes clear, where the length of the opening is measured as the parameter Dpar. Also, a confined track is shown. In transmitted light, the fission tracks are visible as black lines.*

Apatite Fission Track dating

AFT dating is wildly used to understand the development along rifted margins. AFT age, together with the confined track length distribution, allows to reconstruct cooling through time (Wildman *et al.* 2019). A **spontaneous fission track** forms when a heavy ^{238}U nuclei sustains a nuclear fission reaction, separating into two lighter nuclei by repulsion and forming a crystal lattice damage trail (Fig. 9; Wagner *et al.* 1992). These spontaneous fission reactions occur at a known rate and therefore, the fission track density will be proportional to the U content of a given grain and the age of that grain (Hurford 2019).

For this study, I have used two methods – the External Detector Method (EDM) and the Laser Ablation-Inductively Coupled Plasma-Mass Spectrometry (LA-ICP-MS) method – to establish the relationship between spontaneous fission track density and the ^{238}U content. Part of the thesis work was to contribute to the **establishment of a new system** to perform both EDM and LA-ICP-MS AFT analysis at the Department of Earth Science at UiB (Fig. 10). I provide a comprehensive method description in **Paper III** and **Paper IV**, including the respective supplementary materials. The sample selection and the mineral separation was identical for the two AFT methods.

In the field, I sampled fresh rock outcrops of various gneisses to avoid weathered surfaces. Whenever possible, I crushed the samples already in the field into small pieces. To crush the rocks, I used a hammer and the same rock as sampled as an anvil to avoid any contamination from other rock sources.

The **crushing and mineral separation** followed a standard procedure. First, I further crushed the rocks using a disk mill until the grain size was <315 µm. Then, I separated the minerals with help of a Wilfley shaking table, Frantz Isodynamic Magnetic Separator, and heavy liquids (LST ~2.9 g/cm^3 and DIM ~3.31 g/cm^3). After the separation procedure was complete, I sieved the samples through a 100 µm mesh, ensuring the grain size of the retained apatites was between 100-315 µm. For the **EDM analysis** (Fig. 10), the AFT age depends on the ratio between the spontaneous (ρ_s) and the induced (ρ_i) track densities, where the induced tracks are a proxy for the ^{235}U

content of the apatite. For the EDM procedure, the grains are first mounted in epoxy and cut into ~1 mm thick slices. The grain mounts are then polished to reveal the centre of the apatite crystals. Etching the mounted apatites with 5 N HNO_3 at 20 ± 1°C for 20 seconds reveals the fission tracks (Gleadow & Lovering 1978).

An external detector, here I used a sheet of muscovite, is attached on the surface of the grain mount. By thermal irradiation in a nuclear reactor, induced tracks will form in the grain mount and on the muscovite external detector. The muscovite detector is then etched with 40% hydrofluoric acid for 20 minutes at 20 ± 1°C to reveal the induced tracks. By counting the ρ_s of crystallographic c-axis parallel grains on the grain mount and the ρ_i of the muscovite external detector, I was then able to determine the ^{238}U content of the apatite grains because the $^{235}U/^{238}U$ relationship is constant in nature (Gallagher *et al.* 1998).

Similar to the EDM, the spontaneous tracks of the apatite grains on the crystallographic c-axis parallel grains are counted for the **LA-ICP-MS analysis** (Fig. 10). However, other than the EDM, the ^{238}U concentration of the individual grain was then measured in the LA-ICP-MS according to the specifications given in paper IV. One clear advantage of the LA-ICP-MS analysis is that it does not require time consuming neutron irradiations. I used NIST612 and Durango standards to frequently calibrate for session variations. Lastly, I calculated the final AFT age based on a session-specific zeta calibration approach as described by Vermeesch (2017).

To complement the EDM and LA-ICP-MS analysis, I measured the horizontal (or close to horizontal) **confined fission track lengths** which allows to conclude about the thermal evolution (Fig. 9). Also, these measurements are a necessary for thermal modelling (Gleadow *et al.* 1986).

Fission tracks are preserved at temperature below the PAZ, quickly annealed (shortened) at temperatures above the PAZ, and gradually annealed within the PAZ temperatures (Gleadow & Duddy 1981). A sample that was rapidly cooled through the PAZ will yield a narrow track length distribution and long track lengths (A, Fig. 11), whereas slow cooling through the PAZ will result in a wider track length distribution

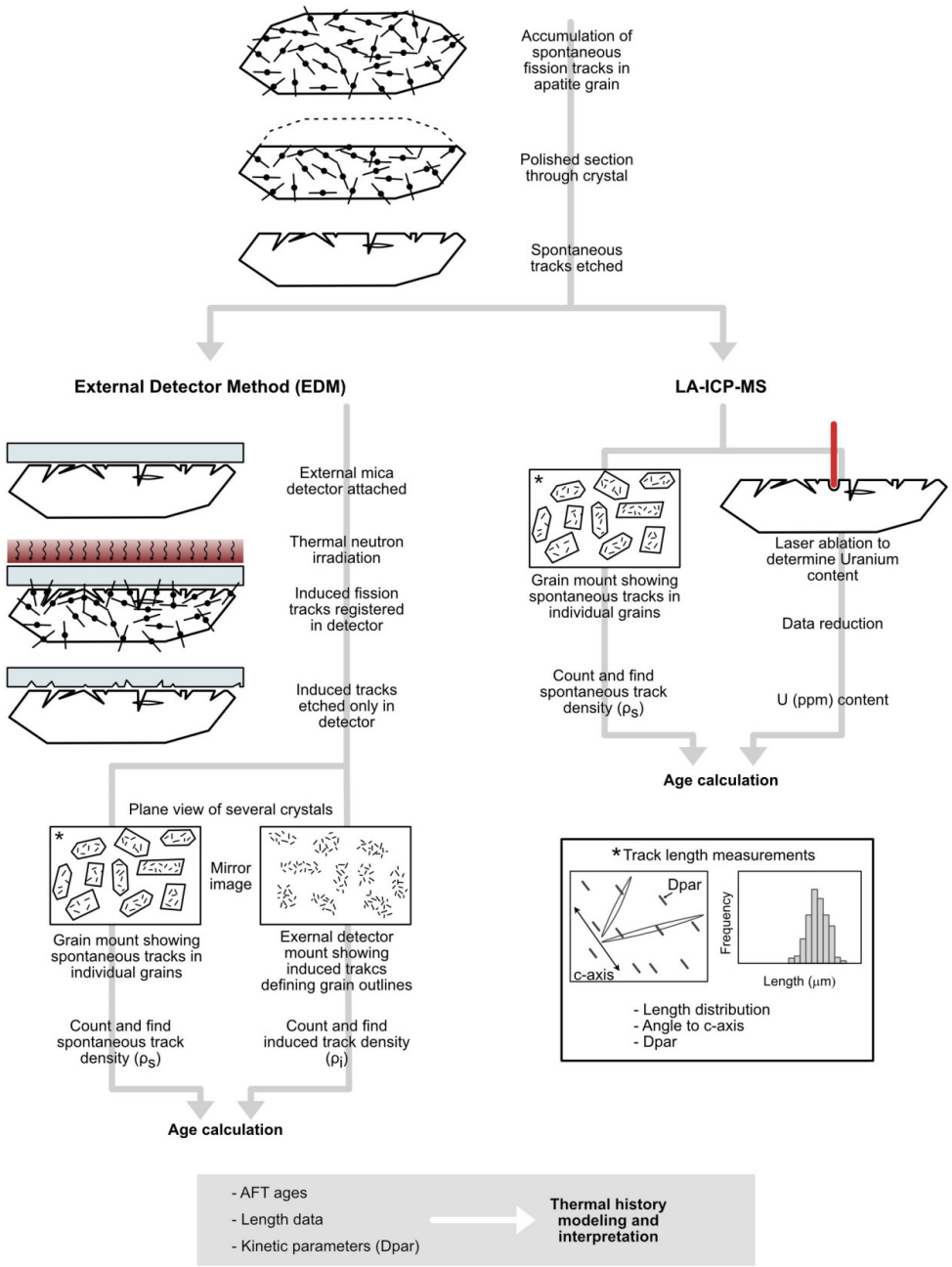

Figure 10. *Stepwise procedure for AFT sample preparation and analysis using both the EDM and the LA-ICP-MS method. Modified from* Gallagher *et al.* (1998) and Kohn *et al.* (2019)*. Note that for both methods, during the counting procedure track lengths and Dpar are also measured (marked * for both methods).*

and shorter track lengths (B, Fig. 11). With more complex cooling histories, e.g. varied cooling through the PAZ (C, Fig. 11) or fast cooling followed by reheating into the PAZ (D, Fig. 11), the track length distributions will reveal less detailed information and may potentially show a bimodal distribution.

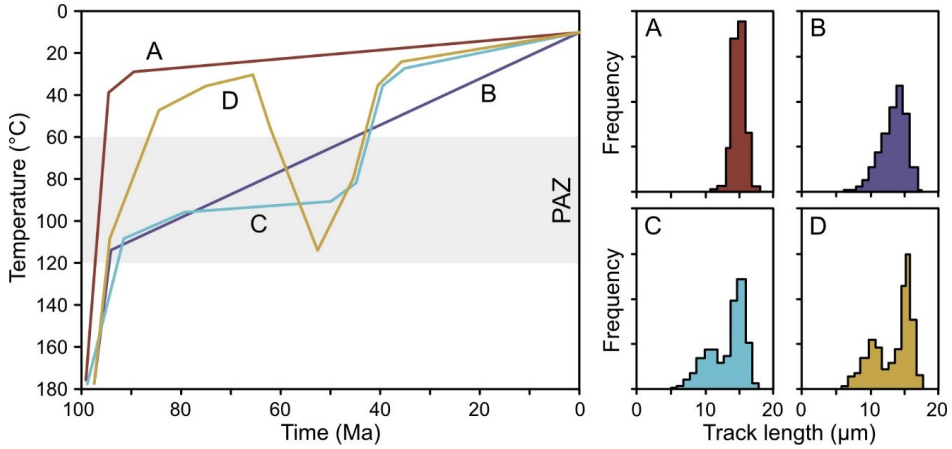

Figure 11. *Modified from* Gleadow & Brown (2000)

Apatite (U-Th)/He dating

(U-Th)/He dating of apatites is another useful technique to reconstruct the cooling history of a sample. The ^{4}He content of an apatite is the results of radioactive decay of ^{238}U, ^{235}U and ^{232}Th (and partially ^{147}Sm) since apatite does not contain any ^{4}He at the time of crystallization (Farley 2002). The ^{4}He particles, also known as alpha (α) particles, are emitted at known rates during the decay of the parent nuclides. The stopping distance of the alpha particles during decay in apatites are approximately 15-20 µm, which is relatively long compared to the apatite grain size. During decay, the α-particle can either be retained within the crystal, be ejected, or be implanted in another apatite crystal, where the amount of retention is dependent on the distance between the parent nuclide and the grain boundary (Farley 2002). An age of cooling can then be calculated by measuring the relationship between parent nuclides (U and Th) and the retained α-particle. During (U-Th)/He age calculations, the effect of α-ejection needs to be corrected for by the F_T-correction (Farley et al. 1996). The

retention of α particles is also dependent on the temperature. At temperatures above the PAZ, α particles will diffuse out of the apatite grains and at temperatures below the PAZ, the α particles will be retained within the crystals (Farley & Stockli 2002).

During (U-Th)/He analysis, 3–5 single apatite grains are normally analysed. It is not uncommon that the **single grains yield different ages**, especially within samples collected from slow cooling cratonic environments (Flowers & Kelley 2011). These variations can be due to several factors, including apatite radiation damage and grain size. The α-decay will cause crystal damage and effective uranium (eU) is used as a proxy for this radiation damage. Higher eU concentrations in an apatite will accumulate more radiation damage, which in turn will reduce the diffusion of ^{4}He potentially resulting in older (U-Th)/He ages (Whipp et al. 2022). Apatites of larger grain size will have a larger He-retentivity than those of smaller grains. This is because larger grains have a greater effective diffusion dimension, meaning less loss of ^{4}He within the PRZ (Flowers & Kelley 2011). The varying single grain (U-Th)/He apatite ages within a sample during slow cooling (1°C Myr^{-1}) will therefore be influenced by a varying closure temperature dependent on the grain size and the eU (Whipp et al. 2022).

Thermal history modelling

For the low temperature thermochronology and thermal history modelling in **Paper III** and **Paper IV**, I have used the **HeFTy software** (v2.1.4.92) (Ketcham et al. 2007b). I applied the annealing model of Ketcham et al. (2007) for the thermal modelling of the AFT data, using the etch pit diameter as the kinetic parameter (Dpar; Donelick et al. 2005) and correcting the track via c-axis projection (Ketcham et al. 2007a). Further, I have used the protocol of Ketcham et al. (2015) to calibrated for operator bias, both for the Dpar and the confined track lengths. To model the apatite (U-Th)/He data, I used the irradiation damage accumulation and annealing model (RDAAM) by Flowers et al. (2009).

The concept when performing inverse thermal modelling with the HeFTy software is to **test for different time-temperature histories** and how compatible the input data is with the different histories. The software will create different t-T paths based on the

input data and the added external constraints. A goodness-of-fit (GOF) value, representing the probability of failure of the null hypothesis, is then calculated for each path. In this study, I used a GOF threshold of ≥ 0.5 and ≥ 0.05 for good and acceptable paths, respectively.

The most recent version of HeFTy (v.2.1.4.92) allows for **multi-sample inverse modelling** of elevation transects, which I used in **Paper III**. During multi-sample modelling, the samples of a transect will be constrained by the samples below and above, resulting in a common cooling history for all samples included. The key advantage is that multi-sample modelling will reduce the risk of overinterpreting the thermal evolution of a region, which has been highlighted as a drawback with single sample models (Gallagher et al. 2005).

2 Synthesis and Outlook

2.1 Summary of the main findings

The four manuscripts of this thesis focus on the post-Caledonian tectono-thermal evolution of Western Norway. In the following, the main findings related to the research questions (section 1.1 and 1.2) will be summarized.

1.1.1 The spatial and temporal evolution of onshore fractures and fault systems

Q1: How does the onshore fracture and fault systems relate to regional tectonic events?

Following the collapse of the Caledonian orogen, Western Norway has undergone a complex tectonic evolution related to deformation along large-scale shear zones and fault complexes and several offshore rift phases. My work has added new knowledge regarding the onshore brittle evolution, and I present a detailed spatial and temporal model for the brittle evolution of the study area. .

From remote sensing analysis and field mapping of brittle structures, the main fault and fractures of the region can be attributed to two conjugate sets with NE-SW and N-S, as well as E-W and NW-SE orientation (**Paper I**). Based on fault and fracture surface mineralizations and paleostress analysis, a complex evolution of the stress field was inferred. (1) Caledonian NW-SE compression was followed by early phases of NW-SE extension in the Early to Mid-Devonian. (2) A large number of fracture and fault surfaces in Western Norway contain mineralizations of epidote, chlorite and quartz, which are related to Late Devonian to early Carboniferous strike-slip stress fields. (3) A limited number of fracture and fault surfaces containing epidote, chlorite and quartz mineralizations are related to E-W extension during the Permian-Early Triassic rifting. (4) WNW-ESE transtension in Cretaceous is supported by K-Ar fault gouge ages, highlighting two main phases of deformation; 123-115 Ma and 86-77 Ma. The study reveals the presence of prominent N-S striking strike-slip faults in the study area, and it is clear that the E-W extension and normal faulting seen in the area south of the study area, has been less important in the region.

K-Ar fault gouge dating is not able to detect fault activity below certain temperatures, limiting the information possible to gain from more recent tectonic activity. By the use of U-Pb calcite dating (**Paper II**), this study shows the possibilities of using this method along rifted margins to gain knowledge about also more subtle low-temperature tectonic events. The obtained U-Pb calcite dataset can be divided into four groups based on fracture orientation and age; 1) calcites dated to ~70-60 Ma are related to the arrival of the proto-Icelandic plume and the consequential dynamic uplift, 2) calcites revealing ages from ~50-0.8 Ma, all sampled along NE-SW striking fractures, reflect post-breakup dilation, 3) calcites dated to 90-80 Ma from the coastal region are related to the reactivation along major ENE-WSE trending fault systems, and 4) the oldest dated calcites of ~208 and 142 Ma are broadly correlated to offshore rift phases.

Also the low-temperature thermochronological dataset helps to detect fault activity and offset along structural lineaments. In this study, a regional dataset of AFT and apatite (U-Th)/He ages yields Carboniferous to Late Cretaceous ages, where the ages in places vary over short distances (**Paper IV**). The dataset indicates that the brittle fault segments related to the NSDZ have been active also through the Mesozoic. The low-temperature thermochronological samples reveal down-to-the-west fault offset along the southern NSDZ in the Triassic/Jurassic and along known brittle structures, such as the Bortnen and Haukå fault (Fig. 2), we detect down-to-the south offset in the Late Jurassic-Early Cretaceous.

1.1.2 The thermal evolution of the study region

Q2: Can a denser horizontal and vertical network of low temperature thermochronological data be used to distinguish between slow and steady exhumation versus uplift pulses caused by fault reactivation?

This study presents a new regional dataset of AFT and apatite (U-Th)/He data, which includes also a near-vertical elevation transect (**Paper III**) and a regional dataset of close-to sea level samples (**Paper IV**). The elevation transect is sampled up the Skåla mountain located in the inner Nordfjord, reaching 1841 meters above sea level, where both the AFT and the (U-Th)/He samples show a trend of increasing age with elevation;

AFT samples yield 159 ± 11 to 256 ± 21 Ma and (U-Th)/He samples yield ages of 80 ± 4 to 277 ± 15 Ma. From a multi-sample model of the elevation transect, we show that the best-fit cooling history for the inner Nordfjord shows high cooling rates from the Caledonian collapse until the Permian. Following the Permian, the region cooled slowly throughout the Mesozoic until the Late Cretaceous, from which the cooling rate increased until reaching surface temperatures. The multi-sample thermal history models do also allow for a cooling to surface levels in the Late Jurassic, on the condition that the region gets reburied in the Cretaceous.

When further studying the regional trends, we can gain more information about the thermal evolution. Apatite samples yield AFT ages from 140 ± 4 to 323 ± 27 Ma and (U-Th)/He ages from 57 ± 3 to 228 ± 12 Ma. The ages in the region show no correlation with elevation and in general, the ages are younger in the inner fjords and in the region north of the Nordfjord. When modelling for a Late Jurassic uplift followed by reheating, the trend reveals that the samples from inner Nordfjord needs to be buried to higher temperatures than the samples from the coast. We concluded that we consider it unlikely that a potential Cretaceous sedimentary cover was thicker inland and do not consider a Late Jurassic cooling to surface temperatures likely for the inner Nordfjord region. The results from this study reveal varying cooling histories across the region, where 1) the inner Nordfjord cooled as described in **Paper III**. 2) The Sognefjorden region shows a similar cooling history but along the coast, offset of low-thermochronology data reveal down-to-the-west faulting during the Triassic/Jurassic along the faults strand of the NSDZ. 3) Fault activity and reactivation is also seen from the region in close proximity, but outside, of the Hornelen Devonian basin. Here, the data reveal early Carboniferous-Permian cooling to the upper crust, followed by cooling until the Late Jurassic to close to surface temperatures. An event of 20-40°C reheating in the Cretaceous was followed by cooling to surface temperatures at the present. 4) Along the Møre margin, north of the Nordfjord, the cooling to the upper crust happens first in the mid-Mesozoic. From the Jurassic until the present, the region generally shows slow and steady cooling, and we relate this evolution to footwall-uplift during rifting along the MTFC and potentially along fault strands of the NSDZ.

1.1.3 The age of low-relief surfaces

Q3: Are the low relief surfaces remnants from old, close-to-sea level paleic surfaces?

The multi sample modelling of the elevation transect of Skåla gives important insight into the cooling evolution of the Inner Nordfjord (**Paper III**). Here, the samples reveal a trend of older ages with elevation, for both AFT and (U-Th)/He data. When testing for various thermal/topographic evolutions, it is clear that combining samples in a multi-model produces a well constrained model where over-interpretations are limited. The multi-sample models show that a Cretaceous peneplain of this region is impossible. Since peneplains should be of (sub)continental extent (e.g. Phillips 2002), **Paper III** shows that such a Cretaceous peneplain did not occur across Southern Norway. Along the coast, offset along major faults and possible reburial has shown that some downfaulted regions might be remnants of old Mesozoic surfaces formed at a base level. The likelihood of these surfaces are, however, poorly constrained and seem to be tectonically bounded and local.

1.1.4 The offshore rift evolution from an onshore perspective

Q4: How are the different tectonic evolutions of the North Sea and the Norwegian Sea reflected onshore Norway?

Two phases of rifting are described from the North Sea, in the Permian-Early Jurassic and in the Late Jurassic-Early Cretaceous respectively (Færseth 1996; Reeve *et al.* 2015; Phillips *et al.* 2019). From the Norwegian Sea, a similar phase of rifting in the Late Jurassic-mid Cretaceous is recognised, ending with the final break-up of the North Atlantic in the latest Cretaceous-Paleocene (Gaina *et al.* 2017; Theissen-Krah *et al.* 2017).

Even though the E-W extensional trend interpreted for the first rift phase in the North Sea is not wide-spread in the study area (**Paper I**), we partially relate the early cooling trend to upper crustal levels of the inner Nordfjord region to this rift phase (**Paper III**).

Further, we relate the cooling along the Møre margin to the second rift phase (**Paper IV**). The results from the thermal models show that this region cooled by the Late

Jurassic to the upper crust and we relate this to tectonic activity during offshore rifting and reactivation of the MTFC and probably the NSDZ. As interpreted from offshore studies, this region is interpreted to have shown increased Late Jurassic topography (Sømme *et al.* 2013a; Bauck *et al.* 2021) and our findings show that this region must be seen in light of tectonic activity during the Late Jurassic-mid Cretaceous rift phase.

Towards the end of the late Cretaceous, we see a period of increasing fault activity (**Paper I**). The thermal models reveal a shift for the inner Nordfjord in the Late Cretaceous-Cenozoic to increased cooling rates which we relate to large-scale tectonic events (**Paper III**). From U-Pb dating of fracture filling calcite, this study makes a correlation between subtle tectonic pulses onshore with the offshore sedimentary stratigraphy, particularly highlighting the relationship between a regional period of what seems to be domal uplift and relating it to the arrival of the Icelandic plume (**Paper II**).

2.2 Future work

A key product of this thesis is the extensive structural measurement dataset which I have compiled. The dataset includes new geochronological data for the ages of fault and fracture activity, calcite stable isotope data, and a regional dataset of AFT and (U-Th)/He ages. Thus, this dataset provides a solid base for future work along the passive margin of Western Norway.

One interesting avenue for future research would be to expand the work on **correlating onshore data with the sedimentary stratigraphy offshore**. This work could focus on the sedimentary drainage systems offshore that can be studied from high quality seismic surveys and connect these data with the low temperature thermochronological data onshore to expand the knowledge of the onshore-offshore relationship. Specifically, it would be interesting to see if specific offsets in the thermochronological dataset can be directly correlated to drainage networks of the time. Is there a direct link or is there a slowness in the system?

This thesis, together with other studies, also makes an important contribution to the data basis needed to develop and further improve **numerical modelling tools** to aid the interpretation of landscape evolution. For example, the thermochronological data presented in this thesis could be implemented into software like *Pecube* (Braun 2003) to study the heat transport under uplift and surface erosion. Additionally, modelling software, like *Fastscape* (Bovy 2021), could provide important knowledge to better understand the evolution of rifted margins.

My work has also highlighted the benefit of sampling **elevation transects** for low temperature thermochronological studies. Now being able to combine the data in a multi-sample thermal evolution models, elevation transects provide better constraints on the thermochronological data and reduce the risk of over-interpretating the data. For further work, several, as vertical as possible, elevations transects could be sampled and modelled in multi-sample models in the region to decipher a more holistic uplift history, preferably also from the coastal regions due to the likely higher influence from rift tectonics.

It is a general problem of Western Norway that the uranium concentration of the apatite grains is zoned, which could affect the α ejection correction factor and the rate of diffusion loss (Farley *et al.* 2011). Hence, for future analysis of apatite (U-Th)/He analysis, the **degree of U zonation** and the effect of the (U-Th)/He should be tested by grain abrasion or by polishing the chosen grains to investigate the degree of zonation prior to analysis.

It is clear that low temperature thermochronology is insufficient to pick up on details in a complex low-temperature tectonic evolution, which is shown by the dataset of K-Ar fault gouge and U-Pb calcite ages presented in this thesis. It is, therefore, important to build on this work, i.e. expand the dataset by collecting more samples, especially for a new method like **U-Pb calcite dating**. A combination of **clumped isotope analysis** and the analysis of fluid inclusions, in addition to REE analysis, would be a good approach to gain valuable new insights into the fluid composition, formation temperature, and the mineral formation (Roberts *et al.* 2020).

The mapping of low-relief and high-elevation surfaces in this study (Fig. 7) has shown that these surfaces are abundant and spread across the region. Further detailed **geomorphological landscape analysis** of the study area could by potentially useful to study the geometry and the elevation of low-relief surfaces. By trying to link these even tighter to low-temperature thermochronological data, we could gain more knowledge of the formation of these surfaces.

References cited

Andersen, J.L., Egholm, D.L., et al. 2018a. Pleistocene Evolution of a Scandinavian Plateau Landscape. *Journal of Geophysical Research: Earth Surface*, **0**, 1–18, https://doi.org/10.1029/2018JF004670.

Andersen, J.L., Egholm, D.L., et al. 2018b. Widespread erosion on high plateaus during recent glaciations in Scandinavia. *Nature Communications*, **9**, https://doi.org/10.1016/0377-8401(93)90006-6.

Andersen, T.B., Torsvik, T.H., Eide, E.A.E.A., Osmundsen, P.T. & Faleide, J.I. 1999. Permian and Mesozoic extensional faulting within the Caledonides of central south Norway. *Journal of the Geological Society, London*, **156**, 1073–1080, https://doi.org/10.1144/gsjgs.156.6.1073.

Andriessen, P.A.M. 1990. Anomalous fission track apatite ages of the Precambrian basement in the Hunnedalen region, south-western Norway. *International Journal of Radiation Applications and Instrumentation. Part D. Nuclear Tracks and Radiation Measurements*, **17**, 285–291, https://doi.org/10.1016/1359-0189(90)90048-3.

Anell, I., Thybo, H. & Stratford, W. 2010. Relating Cenozoic North Sea sediments to topography in southern Norway: The interplay between tectonics and climate. *Earth and Planetary Science Letters*, **300**, 19–32, https://doi.org/10.1016/j.epsl.2010.09.009.

Angelier, J. 1979. Determination of the mean principal directions of stresses for a given fault population. *Tectonophysics*, **56**, https://doi.org/10.1016/0040-1951(79)90081-7.

Bartholomew, I.D., Peters, J.M. & Powell, C.M. 1993. Regional structural evolution of the North Sea: Oblique slip and the reactivation of basement lineaments. *Petroleum Geology Conference Proceedings*, **4**, 1109–1122, https://doi.org/10.1144/0041109.

Bauck, M.S., Faleide, J.I. & Fossen, H. 2021. Late Jurassic to Late Cretaceous canyons on the Måløy Slope: Source to sink fingerprints on the northernmost North Sea rift margin, Norway. *Norwegian Journal of Geology*, 1–30, https://doi.org/10.17850/njg101-3-1.

Bingen, B., Viola, G., Möller, C., Vander Auwera, J., Laurent, A. & Yi, K. 2021. The Sveconorwegian orogeny. *Gondwana Research*, **90**, 273–313, https://doi.org/10.1016/j.gr.2020.10.014.

Bird, D.K. & Spieler, A.R. 2004. Epidote in geothermal systems. *Reviews in Mineralogy and Geochemistry*, **56**, 235–300, https://doi.org/10.2138/gsrmg.56.1.235.

Blystad, P., Brekke, H., Færseth, R.B., Larsen, B.T., Skogseid, J. & Tørudbakken, B. 1995. Structural elements of the Norwegian continental shelf. Part 2: The Norwegian Sea region. *NPD-Bulletin*, **8**.

Bonow, J.M., Lidmar-Bergström, K., Japsen, P., Chalmers, J.A. & Green, P.F. 2007. Elevated erosion surfaces in central West Greenland and southern Norway: Their significance in integrated studies of passive margin development. *Norsk Geologisk Tidsskrift*, **87**, 197–206.

Bovy, B. 2021. fastscape-lem/fastscape: Release v0.1.0beta3, https://doi.org/10.5281/ZENODO.4435110.

Braathen, A. 1999. Kinematics of post-Caledonian polyphase brittle faulting in the Sunnfjord region, western Norway. *Tectonophysics*, **302**, 99–121, https://doi.org/10.1016/S0040-1951(98)00281-9.

Braathen, A., Osmundsen, P.T. & Gabrielsen, R.H. 2004. Dynamic development of fault rocks in a crustal-scale detachment: An example from western Norway. *Tectonics*, **23**, 1–21, https://doi.org/10.1029/2003TC001558.

Braun, J. 2003. Pecube: A new finite-element code to solve the 3D heat transport equation including the effects of a time-varying, finite amplitude surface topography. *Computers and Geosciences*, **29**, 787–794, https://doi.org/10.1016/S0098-3004(03)00052-9.

Braun, J. 2018. A review of numerical modeling studies of passive margin escarpments leading to a new analytical expression for the rate of escarpment migration velocity. *Gondwana Research*, **53**, 209–224, https://doi.org/10.1016/j.gr.2017.04.012.

Calvet, M., Gunnell, Y. & Farines, B. 2015. Flat-topped mountain ranges: Their global distribution and value for understanding the evolution of mountain topography. *Geomorphology*, **241**, 255–291, https://doi.org/10.1016/j.geomorph.2015.04.015.

Chalmers, J.A., Green, P., Japsen, P. & Rasmussen, E.S. 2010. The Scandinavian mountains have not persisted since the Caledonian orogeny. A comment on Nielsen et al. (2009a). *Journal of Geodynamics*, **50**, 94–101, https://doi.org/10.1016/j.jog.2010.02.001.

Corfu, F., Andersen, T.B. & Gasser, D. 2014. The Scandinavian Caledonides: main features, conceptual advances and critical questions. *Geological Society, London, Special Publications*, **390**, 9–43, https://doi.org/10.1144/SP390.25.

da Silva, B.V., Hackspacher, P.C., et al. 2019. Evolution of the Southwestern Angolan Margin: episodic burial and exhumation is more realistic than long-term denudation. *International Journal of Earth Sciences*, **108**, 89–113, https://doi.org/10.1007/s00531-018-1644-4.

Davies, R.J., Turner, J.D. & Underhill, J.R. 2001. Sequential dip-slip fault movement during rifting: A new model for the evolution of the Jurassic trilete North sea rift system. *Petroleum Geoscience*, **7**, 371–388, https://doi.org/10.1144/petgeo.7.4.371.

Davis, W.M. 1899. The Geographical cycle. *Climate Geomorphology*, **14**, 481–504.

Delvaux, D. & Sperner, B. 2003. New aspects of tectonic stress inversion with reference to the TENSOR program. *Geological Society Special Publication*, **212**, 75–100, https://doi.org/10.1144/GSL.SP.2003.212.01.06.

Donelick, R.A., O'Sullivan, P.B. & Ketcham, R.A. 2005. Apatite fission-track analysis. *Reviews in Mineralogy and Geochemistry*, **58**, 49–94, https://doi.org/10.2138/rmg.2005.58.3.

Doré, A.G., Lundin, E.R., Fichler, C. & Olesen, O. 1997. Patterns of basement structure and reactivation along the NE Atlantic margin. *Journal of the Geological Society*, **154**, 85–92, https://doi.org/10.1144/gsjgs.154.1.0085.

Drost, K., Chew, D., Petrus, J.A., Scholze, F., Woodhead, J.D., Schneider, J.W. & Harper, D.A.T. 2018. An Image Mapping Approach to U-Pb LA-ICP-MS Carbonate Dating and Applications to Direct Dating of Carbonate Sedimentation. *Geochemistry, Geophysics, Geosystems*, **19**, 4631–4648, https://doi.org/10.1029/2018GC007850.

Dunlap, W.J. & Fossen, H. 1998. Early Paleozoic orogenic collapse, tectonic stability, and late Paleozoic continental rifting revealed through thermochronology of K-felsdspars, souther Norway. *Tectonics*, **17**, 604–620, https://doi.org/10.1029/98TC01603.

Egholm, D.L., Nielsen, S.B., Pedersen, V.K. & Lesemann, J.E. 2009. Glacial effects limiting mountain height. *Nature*, **460**, 884–887, https://doi.org/10.1038/nature08263.

Egholm, D.L., Jansen, J.D., et al. 2017. Formation of plateau landscapes on glaciated continental margins. *Nature Geoscience*, **10**, 592–597, https://doi.org/10.1038/ngeo2980.

Eide, E.A., Torsvik, T.H. & Andersen, T.B. 1997. Absolute dating of brittle fault movements: Late Permian and late Jurassic extensional fault breccias in western Norway. *Terra Nova*, **9**, 135–139, https://doi.org/10.1046/j.1365-3121.1997.d01-21.x.

Evers, W. 1962. The Problem of Coastal Genesis, with Special Reference to the 'Strandflat,' the 'Banks,' or 'Grounds,' and 'Deep Channels' of the Norwegian and Greenland Coasts. *The Journal of Geology*, **70**, 621–630, https://doi.org/10.1086/626858.

Færseth, R.B. 1996. Interaction of permo-triassic and jurassic extensional fault-blocks during the development of the northern North Sea. *Journal of the Geological Society*, **153**, 931–944, https://doi.org/10.1144/gsjgs.153.6.0931.

Færseth, R.B., Knudsen, B.E., Liljedahl, T., Midbøe, P.S. & Søderstrøm, B. 1997. Oblique rifting and sequential faulting in the Jurassic development of the northern North Sea. *Journal of Structural Geology*, **19**, 1285–1302, https://doi.org/10.1016/s0191-8141(97)00045-x.

Faleide, J.I., Kyrkjebø, R., Kjennerud, T., Gabrielsen, R.H., Jordt, H., Fanavoll, S. & Bjerke, M.D. 2002. Tectonic impact on sedimentary processes during Cenozoic evolution of the northern North Sea and surrounding areas. *Geological Society, London, Special Publications*, **196**, 235–269, https://doi.org/10.1144/GSL.SP.2002.196.01.14.

Farley, K.A. 2002. (U-Th)/He dating: Techniques, calibrations, and applications. *Reviews in Mineralogy and Geochemistry*, **47**, 819–844, https://doi.org/10.2138/rmg.2002.47.18.

Farley, K.A. & Stockli, D.F. 2002. (U-Th)/He Dating of Phosphates: Apatite, Monazite, and Xenotime. *Reviews in Mineralogy and Geochemistry*, **48**, 559–577, https://doi.org/10.2138/rmg.2002.48.15.

Farley, K.A., Wolf, R.A. & Silver, L.T. 1996. The effects of long alpha-stopping distances on (U-Th)/He ages. *Geochimica et Cosmochimica Acta*, **60**, 4223–4229, https://doi.org/10.1016/S0016-7037(96)00193-7.

Farley, K.A., Shuster, D.L. & Ketcham, R.A. 2011. U and Th zonation in apatite observed by laser ablation ICPMS, and implications for the (U-Th)/He system. *Geochimica et Cosmochimica Acta*, **75**, 4515–4530, https://doi.org/10.1016/j.gca.2011.05.020.

Flowers, R.M. & Kelley, S.A. 2011. Interpreting data dispersion and ‘ inverted’ dates in apatite (U-Th)/He and fission-track datasets: An example from the US midcontinent. *Geochimica et Cosmochimica Acta*, **75**, 5169–5186, https://doi.org/10.1016/j.gca.2011.06.016.

Flowers, R.M., Ketcham, R.A., Shuster, D.L. & Farley, K.A. 2009. Apatite (U-Th)/He thermochronometry using a radiation damage accumulation and annealing model. *Geochimica et Cosmochimica Acta*, **73**, 2347–2365, https://doi.org/10.1016/j.gca.2009.01.015.

Fonte-Boa, T.M.R., Peifer, D., Fonseca, A. & Novo, T.A. 2022. The southeast Brazilian rifted continental margin is not a single, continuous upwarp: Variations in morphology and denudation patterns along the continental drainage divide. *Earth-Science Reviews*, **231**, 104091, https://doi.org/10.1016/j.earscirev.2022.104091.

Fossen, H. 1992. The role of extensional tectonics in the Caledonides of south Norway. *Journal of Structural Geology*, **14**, 1033–1046, https://doi.org/10.1016/0191-8141(92)90034-T.

Fossen, H. 2000. Extensional tectonics in the Caledonides: Synorogenic or postorogenic. *Tectonics*, **19**, 213–224, https://doi.org/10.1029/1999TC900066.

Fossen, H. & Dunlap, W.J. 1999. On the age and tectonic significance of Permo-Triassic dikes in the Bergen-Sunnhordland region, southwestern Norway. *Norsk Geologisk Tidsskrift*, **79**, 169–177, https://doi.org/10.1080/002919699433807.

Fossen, H. & Hurich, C.A. 2005. The Hardangerfjord Shear Zone in SW Norway and the North Sea: A large-scale low-angle shear zone in the Caledonian crust. *Journal of the Geological Society*, **162**, 675–687, https://doi.org/10.1144/0016-764904-136.

Fossen, H., Khani, H.F., Faleide, J.I., Ksienzyk, A.K. & Dunlap, W.J. 2017. Post-Caledonian extension in the West Norway–northern North Sea region: the role of structural inheritance. *Geological Society, London, Special Publications*, **439**, 465–486, https://doi.org/10.1144/SP439.6.

Fossen, H., Ksienzyk, A.K., Rotevatn, A., Bauck, M.S. & Wemmer, K. 2021. From widespread faulting to localised rifting: Evidence from K-Ar fault gouge dates from the Norwegian North Sea rift shoulder. *Basin Research*, bre.12541, https://doi.org/10.1111/bre.12541.

Gabrielsen, R.H., Faleide, J.I., Pascal, C., Braathen, A., Nystuen, J.P., Etzelmuller, B. & O’Donnell, S. 2010a. Latest Caledonian to Present tectonomorphological development of southern Norway. *Marine and Petroleum Geology*, **27**, 709–723, https://doi.org/10.1016/j.marpetgeo.2009.06.004.

Gabrielsen, R.H., Faleide, J.I., Pascal, C., Braathen, A., Nystuen, J.P., Etzelmuller, B. & O’Donnell, S. 2010b. Reply to discussion of Gabrielsen et al. (2010) by Nielsen et al. (this volume): Latest Caledonian to present tectonomorphological development of southern Norway. *Marine and Petroleum Geology*, **27**, 1290–1295, https://doi.org/10.1016/j.marpetgeo.2010.02.003.

Gabrielsen, R.H., Nystuen, J.P., Jarsve, E.M. & Lundmark, A.M. 2015. The Sub-Cambrian

Peneplain in southern Norway: Its geological significance and its implications for post-Caledonian faulting, uplift and denudation. *Journal of the Geological Society*, **172**, 777–791, https://doi.org/10.1144/jgs2014-154.

Gaina, C., Nasuti, A., Kimbell, G.S. & Blischke, A. 2017. Break-up and seafloor spreading domains in the NE Atlantic. *Geological Society, London, Special Publications*, **447**, 393–417, https://doi.org/10.1144/SP447.12.

Gallagher, K. 2021. Comment on "Discussion: Extracting thermal history from low temperature thermochronology/A comment on the recent exchanges between Vermeesch and Tian and Gallagher and Ketcham", by Paul Green and Ian Duddy, Earth Science Reviews, https://doi.org/10.1016/j. *Earth-Science Reviews*, **216**, 103549, https://doi.org/10.1016/j.earscirev.2021.103549.

Gallagher, K., Brown, R. & Johnson, C. 1998. Fission track analysis and its applications to geological problems. *Annual Review of Earth and Planetary Sciences*, **26**, 519–572, https://doi.org/10.1146/annurev.earth.26.1.519.

Gallagher, K., Stephenson, J., Brown, R., Holmes, C. & Fitzgerald, P. 2005. Low temperature thermochronology and modeling strategies for multiple samples 1: Vertical profiles. *Earth and Planetary Science Letters*, **237**, 193–208, https://doi.org/10.1016/j.epsl.2005.06.025.

Gee, D.G. 1975. A tectonic model for the central part of the Scandinavian Caledonides. *Amer. J. Sci.*, **275-A**, 468–515.

Gee, D.G., Fossen, H., Henriksen, N. & Higgins, A.K. 2008. From the early Paleozoic platforms of Baltica and Laurentia to the Caledonide orogen of Scandinavia and Greenland. *Episodes*, **31**, 44–51.

Gjessing, J. 1967. Norway's Paleic Surface. *Norsk Geografisk Tidsskrift*, **21**, 69–132, https://doi.org/10.1080/00291956708621854.

Gleadow, A.J. & Brown, R.W. 2000. Fission-track thermochronology and the long-term denudational response to tectonics. *In*: *M.J. Summerfield (Ed) Geomorphology and Global Tectonics*. New York, Wiley, 57–75.

Gleadow, A.J.W. & Duddy, I.R. 1981. A natural long-term track annealing experiment for apatite. *Nuclear Tracks*, **5**, 169–174, https://doi.org/10.1016/0191-278X(81)90039-1.

Gleadow, A.J.W. & Lovering, J.F. 1978. Fission track geochronology of King Island, Bass Strait, Australia: Relationship to continental rifting. *Earth and Planetary Science Letters*, **37**, 429–437, https://doi.org/10.1016/0012-821X(78)90058-4.

Gleadow, A.J.W.W., Duddy, I.R., Green, P.F. & Hegarty, K.A. 1986. Fission track lengths in the apatite annealing zone and the interpretation of mixed ages. *Earth and Planetary Science Letters*, **78**, 245–254, https://doi.org/10.1016/0012-821X(86)90065-8.

Gómez, M., Vergés, J., Fernàndez, M., Torne, M., Ayala, C., Wheeler, W. & Karpuz, R. 2004. Extensional geometry of the Mid Norwegian Margin before Early Tertiary continental breakup. *Marine and Petroleum Geology*, **21**, 177–194, https://doi.org/10.1016/j.marpetgeo.2003.11.017.

Gradmann, S., Ebbing, J. & Fullea, J. 2013. Integrated geophysical modelling of a lateral transition zone in the lithospheric mantle under Norway and Sweden. *Geophysical Journal International*, **194**, 1359–1374, https://doi.org/10.1093/gji/ggt213.

Green, P. & Duddy, I. 2021a. Discussion: Extracting thermal history from low temperature thermochronology. A comment on recent exchanges between Vermeesch and Tian and Gallagher and Ketcham. *Earth-Science Reviews*, **216**, 103197, https://doi.org/10.1016/j.earscirev.2020.103197.

Green, P. & Duddy, I. 2021b. Reply to Comment on "Discussion: Extracting thermal history from low temperature thermochronology/ A comment on the recent exchanges between Vermeesch and Tian and Gallagher and Ketcham", by Paul Green and Ian Duddy, Earth Science Reviews https://doi.org/. *Earth-Science Reviews*, **216**, 103550, https://doi.org/10.1016/j.earscirev.2021.103550.

Green, P., Duddy, I. & Japsen, P. 2022a. Episodic kilometre-scale burial and exhumation and the importance of missing section. *Earth-Science Reviews*, **234**, 104226, https://doi.org/10.1016/j.earscirev.2022.104226.

Green, P.F., Japsen, P., Bonow, J.M., Chalmers, J.A. & Duddy, I.R. 2019. Thermal history solutions from thermochronology must be governed by geological relationships: a comment on Jess et al. (2019). *Geomorphology*, 106848, https://doi.org/https://doi.org/10.1016/j.geomorph.2019.106848.

Green, P.F., Japsen, P., Bonow, J.M., Chalmers, J.A., Duddy, I.R. & Kukkonen, I.T. 2022b. The post-Caledonian thermo-tectonic evolution of Fennoscandia. *Gondwana Research*, **107**, 201–234, https://doi.org/10.1016/j.gr.2022.03.007.

Grønlie, A. & Roberts, D. 1989. Resurgent strike-slip duplex development along the Hitra-Snåsa and Verran Faults, Møre-trøndelag fault zone, Central Norway. *Journal of Structural Geology*, **11**, 295–305, https://doi.org/10.1016/0191-8141(89)90069-2.

Grunnaleite, I. & Gabrielsen, R.H. 1995. Structure of the Møre basin, mid-Norway continental margin. *Tectonophysics*, **252**, 221–251, https://doi.org/10.1016/0040-1951(95)00095-X.

Hacker, B.R. 2007. Ascent of the ultrahigh-pressure Western Gneiss region, Norway. *Special Paper of the Geological Society of America*, **419**, 171.

Hacker, B.R., Andersen, T.B., Johnston, S., Kylander-Clark, A.R.C.C., Peterman, E.M., Walsh, E.O. & Young, D. 2010. High-temperature deformation during continental-margin subduction & exhumation: The ultrahigh-pressure Western Gneiss Region of Norway. *Tectonophysics*, **480**, 149–171, https://doi.org/10.1016/j.tecto.2009.08.012.

Hall, A.M., Ebert, K., Kleman, J., Nesje, A. & Ottesen, D. 2013. Selective glacial erosion on the Norwegian passive margin. *Geology*, **41**, 1203–1206, https://doi.org/10.1130/G34806.1.

Hendriks, B.W.H.H., Andriessen, P.A.M.M., et al. 2007. A fission track data compilation for Fennoscandia. *Norsk Geologisk Tidsskrift*, **87**, 143–155.

Holtedahl, O. 1965. The South-Norwegian Piedmonttreppe of W. Evers. *Norsk Geografisk Tidsskrift*, **20**, 74–84, https://doi.org/10.1080/00291956508551831.

Hurford, A.J. 2019. An Historical Perspective on Fission-Track Thermochronology. *In*: Malusà, M. G. & Fitzgerald, P. G. (eds) *Fission-Track Thermochronology and Its Application to Geology*. Springer International Publishing, 3–23., https://doi.org/10.1007/978-3-319-89421-8_1.

Huuse, M. 2002. Cenozoic uplift and denudation of southern Norway: Insights from the North Sea Basin. *Geological Society Special Publication*, **196**, 209–233, https://doi.org/10.1144/GSL.SP.2002.196.01.13.

Japsen, P. & Chalmers, J.A. 2022. The Norwegian mountains: the result of multiple episodes of uplift and subsidence. *Geology Today*, **38**, 13–19, https://doi.org/10.1111/gto.12377.

Japsen, P., Green, P.F., Chalmers, J.A. & Bonow, J.M. 2018. Mountains of southernmost Norway: uplifted Miocene peneplains and re-exposed Mesozoic surfaces. *Journal of the Geological Society*, **175**, 721–741, https://doi.org/10.1144/jgs2017-157.

Japsen, P., Green, P.F. & Chalmers, J.A. 2022. Widespread glacial erosion on the Scandinavian passive margin. *Geology Forum Comment*, **50**, 546–546, https://doi.org/10.1130/G49865C.1.

Jess, S., Stephenson, R., Roberts, D.H. & Brown, R. 2019. Differential erosion of a Mesozoic rift flank: Establishing the source of topography across Karrat, central West Greenland. *Geomorphology*, **334**, 138–150, https://doi.org/10.1016/j.geomorph.2019.02.026.

Jess, S., Stephenson, R., Roberts, D.H. & Brown, R. 2020. Reply to: Thermal history solutions from thermochronology must be governed by geological relationships: A comment on Jess et al. (2019). *Geomorphology*, **360**, 106971, https://doi.org/10.1016/j.geomorph.2019.106971.

Johannessen, K.C., Kohlmann, F., Ksienzyk, A.K., Dunkl, I. & Jacobs, J. 2013. Tectonic evolution of the SW Norwegian passive margin based on low-temperature thermochronology from the innermost Hardangerfjord area. *Norsk Geologisk Tidsskrift*, **93**, 243–260, https://doi.org/10.1111/jmi.12023.

Ketcham, R.A., Carter, A., Donelick, R.A., Barbarand, J. & Hurford, A.J. 2007a. Improved measurement of fission-track annealing in apatite using c-axis projection. *American Mineralogist*, **92**, 789–798, https://doi.org/10.2138/am.2007.2280.

Ketcham, R.A., Carter, A., Donelick, R.A., Barbarand, J. & Hurford, A.J. 2007b. Improved modeling of fission-track annealing in apatite. *American Mineralogist*, **92**, 799–810, https://doi.org/10.2138/am.2007.2281.

Ketcham, R.A., Carter, A. & Hurford, A.J. 2015. Inter-laboratory comparison of fission track confined length and etch figure measurements in apatite. *American Mineralogist*, **100**, 1452–1468, https://doi.org/10.2138/am-2015-5167.

Kohn, B., Chung, L. & Gleadow, A. 2019. Fission-Track Analysis: Field Collection, Sample Preparation and Data Acquisition. *In*: Malusà, M. G. & Fitzgerald, P. G. (eds) *Fission-Track Thermochronology and Its Application to Geology*. Springer International Publishing, 25–48., https://doi.org/10.1007/978-3-319-89421-8_2.

Kolstrup, M.L., Hung, S.H. & Maupin, V. 2015. Multiscale, finite-frequency P and S

tomography of the upper mantle in the southwestern Fennoscandian Shield. *Geophysical Journal International*, **202**, 190–218, https://doi.org/10.1093/gji/ggv130.

Ksienzyk, A.K., Dunkl, I., Jacobs, J., Fossen, H. & Kohlmann, F. 2014. From orogen to passive margin: constraints from fission track and (U–Th)/He analyses on Mesozoic uplift and fault reactivation in SW Norway. *Geological Society, London, Special Publications*, **390**, 679–702, https://doi.org/10.1144/SP390.27.

Ksienzyk, A.K., Wemmer, K., et al. 2016. Post-caledonian brittle deformation in the Bergen area, West Norway: Results from K–Ar illite fault gouge dating. *Norsk Geologisk Tidsskrift*, **96**, 275–299, https://doi.org/10.17850/njg96-3-06.

Labrousse, L., Jolivet, L., Andersen, T.B., Agard, P., Hébert, R., Maluski, H. & Schärer, U. 2004. Pressure-temperature-time deformation history of the exhumation of ultra-high pressure rocks in the Western Gneiss Region, Norway. *Special Paper of the Geological Society of America*, **380**, 155–183, https://doi.org/10.1130/0-8137-2380-9.155.

Labrousse, L., Prouteau, G. & Ganzhorn, A.-C. 2011. Continental exhumation triggered by partial melting at ultrahigh pressure. *Geology*, **39**, 1171–1174, https://doi.org/10.1130/G32316.1.

Lacombe, O. 2012. Do fault slip data inversions actually yield ‘ paleostresses’ that can be compared with contemporary stresses? A critical discussion. *Comptes Rendus - Geoscience*, **344**, 159–173, https://doi.org/10.1016/j.crte.2012.01.006.

Leighton, C.A. 2007. *The Thermotectonic Development of Southern Norway: Constraints from Low-Temperature Thermochronology*. Imperial College London, South Kensington, London.

Lidmar-Bergström, K. & Bonow, J.M. 2009. Hypotheses and observations on the origin of the landscape of southern Norway-A comment regarding the isostasy-climate-erosion hypothesis by Nielsen et al. 2008. *Journal of Geodynamics*, **48**, 95–100, https://doi.org/10.1016/j.jog.2009.06.003.

Lidmar-Bergström, K., Näslund, J.O., Ebert, K., Neubeck, T. & Bonow, J.M. 2007. Cenozoic landscape development on the passive margin of northern Scandinavia. *Norsk Geologisk Tidsskrift*, **87**, 181–196, https://doi.org/10.1016/j.forsciint.2016.01.009.

Lidmar-Bergström, K., Bonow, J.M. & Japsen, P. 2013. Stratigraphic Landscape Analysis and geomorphological paradigms: Scandinavia as an example of Phanerozoic uplift and subsidence. *Global and Planetary Change*, **100**, 153–171, https://doi.org/10.1016/j.gloplacha.2012.10.015.

Makushkina, A., Tauzin, B., Tkalčić, H. & Thybo, H. 2019. The Mantle Transition Zone in Fennoscandia: Enigmatic High Topography Without Deep Mantle Thermal Anomaly. *Geophysical Research Letters*, **46**, 3652–3662, https://doi.org/10.1029/2018GL081742.

Martinsen, O.J., Bøen, F., Charnock, M.A., Mangerud, G. & Nøttvedt, A. 1999. Cenozoic development of the Norwegian margin 60–64°N: sequences and sedimentary response to variable basin physiography and tectonic setting. *Geological Society, London, Petroleum Geology Conference series*, **5**, 293–304, https://doi.org/10.1144/0050293.

Mauerberger, A., Sadeghisorkhani, H., Maupin, V., Gudmundsson, Ó. & Tilmann, F. 2022. A shear-wave velocity model for the Scandinavian lithosphere from Rayleigh waves and ambient noise - Implications for the origin of the topography of the Scandes mountain range. *Tectonophysics*, **838**, 229507, https://doi.org/10.1016/j.tecto.2022.229507.

Maupin, V., Agostini, A., et al. 2013. The deep structure of the Scandes and its relation to tectonic history and present-day topography. *Tectonophysics*, **602**, 15–37, https://doi.org/10.1016/j.tecto.2013.03.010.

Medvedev, S. & Hartz, E.H. 2015. Evolution of topography of post-Devonian Scandinavia: Effects and rates of erosion. *Geomorphology*, **231**, 229–245, https://doi.org/10.1016/j.geomorph.2014.12.010.

Nielsen, S.B., Gallagher, K., Egholm, D.L., Clausen, O.R. & Summerfield, M. 2009a. Reply to comment regarding the ICE-hypothesis. *Journal of Geodynamics*, **48**, 101–106, https://doi.org/10.1016/j.jog.2009.06.004.

Nielsen, S.B., Gallagher, K., et al. 2009b. The evolution of western Scandinavian topography: A review of Neogene uplift versus the ICE (isostasy-climate-erosion) hypothesis. *Journal of Geodynamics*, **47**, 72–95, https://doi.org/10.1016/j.jog.2008.09.001.

Nielsen, S.B., Clausen, O.R., et al. 2010a. Discussion of Gabrielsen et al. (2010): Latest Caledonian to Present tectonomorphological development of southern Norway. *Marine and Petroleum Geology*, **27**, 1285–1289, https://doi.org/10.1016/j.marpetgeo.2010.02.004.

Nielsen, S.B., Clausen, O.R., et al. 2010b. The ICE hypothesis stands: How the dogma of late Cenozoic tectonic uplift can no longer be sustained in the light of data and physical laws. *Journal of Geodynamics*, **50**, 102–111, https://doi.org/10.1016/j.jog.2010.02.002.

Osmundsen, P.T. & Andersen, T.B. 2001. The middle Devonian basins of western Norway: Sedimentary response to large-scale transtensional tectonics? *Tectonophysics*, **332**, 51–68, https://doi.org/10.1016/S0040-1951(00)00249-3.

Osmundsen, P.T. & Redfield, T.F. 2011. Crustal taper and topography at passive continental margins. *Terra Nova*, **23**, 349–361, https://doi.org/10.1111/j.1365-3121.2011.01014.x.

Osmundsen, P.T.T., Eide, E.A.A., et al. 2006. Kinematics of the Høybakken detachment zone and the Møre–Trøndelag Fault Complex, central Norway. *Journal of the Geological Society*, **163**, 303–318, https://doi.org/10.1144/0016-764904-129.

Osmundsen, P.T.T., Redfield, T.F.F., et al. 2010. Fault-controlled alpine topography in Norway. *Journal of the Geological Society*, **167**, 83–98, https://doi.org/10.1144/0016-76492009-019.

Pedersen, V.K., Huismans, R.S. & Moucha, R. 2016. Isostatic and dynamic support of high topography on a North Atlantic passive margin. *Earth and Planetary Science Letters*, **446**, 1–9, https://doi.org/10.1016/j.epsl.2016.04.019.

Pedersen, V.K., Braun, J. & Huismans, R.S. 2018. Eocene to mid-Pliocene landscape evolution in Scandinavia inferred from offshore sediment volumes and pre-glacial topography using inverse modelling. *Geomorphology*, **303**, 467–485,

https://doi.org/10.1016/j.geomorph.2017.11.025.

Pedersen, V.K., Knutsen, Å.R., Pallisgaard-Olesen, G., Andersen, J.L., Moucha, R. & Huismans, R.S. 2021. Widespread glacial erosion on the Scandinavian passive margin. *Geology*, **49**, 1004–1008, https://doi.org/10.1130/G48836.1.

Peron-Pinvidic, G., Manatschal, G., et al. 2019. Rifted Margins: State of the Art and Future Challenges. *Frontiers in Earth Science*, **7**, 1–8, https://doi.org/10.3389/feart.2019.00218.

Phillips, J.D. 2002. Erosion, isostatic response, and the missing peneplains. *Geomorphology*, **45**, 225–241, https://doi.org/10.1016/S0169-555X(01)00156-8.

Phillips, T.B., Fazlikhani, H., et al. 2019. The Influence of Structural Inheritance and Multiphase Extension on Rift Development, the NorthernNorth Sea. *Tectonics*, **38**, 4099–4126, https://doi.org/10.1029/2019TC005756.

Redfield, T.F., Torsvik, T.H., Andriessen, P.A.M.M. & Gabrielsen, R.H. 2004. Mesozoic and Cenozoic tectonics of the Møre Trøndelag Fault Complex, central Norway: Constraints from new apatite fission track data. *Physics and Chemistry of the Earth*, **29**, 673–682, https://doi.org/10.1016/j.pce.2004.03.005.

Redfield, T.F., Braathen, A., Gabrielsen, R.H., Osmundsen, P.T., Torsvik, T.H. & Andriessen, P.A.M.M. 2005a. Late Mesozoic to Early Cenozoic components of vertical separation across the Møre-Trøndelag Fault Complex, Norway. *Tectonophysics*, **395**, 233–249, https://doi.org/10.1016/j.tecto.2004.09.012.

Redfield, T.F.F., Osmundsen, P.T.T. & Hendriks, B.W.H.W.H. 2005b. The role of fault reactivation and growth in the uplift of western Fennoscandia. *Journal of the Geological Society*, **162**, 1013–1030, https://doi.org/10.1144/0016-764904-149.

Reeve, M.T., Bell, R.E., Duffy, O.B., Jackson, C.A.L. & Sansom, E. 2015. The growth of non-colinear normal fault systems; What can we learn from 3D seismic reflection data? *Journal of Structural Geology*, **70**, 141–155, https://doi.org/10.1016/j.jsg.2014.11.007.

Reiners, P.W., Carlson, R.W., Renne, P.R., Cooper, K.M., Granger, D.E., McLean, N.M. & Schoene, B. 2017. *Geochronology and Thermochronology*. Chichester, UK, John Wiley & Sons, Ltd, https://doi.org/10.1002/9781118455876.

Reusch, H. 1901. Nogle bidrag til forstaaelsen af , hvorledes Norges dale og fjelde er blevne til. *Norges Geologiske Undersøkelse*, **32**, 124–217.

Robert, B., Domeier, M. & Jakob, J. 2021. On the origins of the Iapetus ocean. *Earth-Science Reviews*, **221**, 103791, https://doi.org/10.1016/j.earscirev.2021.103791.

Roberts, A.M., Yielding, G., Kusznir, N.J., Walker, I.M. & Dorn- Lopez, D. 1995. Quantitative analysis of Triassic extension in the northern Viking Graben. *Journal - Geological Society (London)*, **152**, 15–26, https://doi.org/10.1144/gsjgs.152.1.0015.

Roberts, D. 2003. The Scandinavian Caledonides: Event chronology, palaeogeographic settings and likely modern analogues. *Tectonophysics*, **365**, 283–299, https://doi.org/10.1016/S0040-1951(03)00026-X.

Roberts, N.M.W. & Holdsworth, R.E. 2022. Timescales of faulting through calcite geochronology: A review. *Journal of Structural Geology*, **158**, 104578, https://doi.org/10.1016/j.jsg.2022.104578.

Roberts, N.M.W., Drost, K., et al. 2020. Laser ablation inductively coupled plasma mass spectrometry (LA-ICP-MS) U–Pb carbonate geochronology: strategies, progress, and limitations. *Geochronology*, **2**, 33–61, https://doi.org/10.5194/gchron-2-33-2020.

Rohrman, M., van der Beek, P., Andriessen, P. & Cloetingh, S. 1995. Meso-Cenozoic morphotectonic evolution of southern Norway: Neogene domal uplift inferred from apatite fission track thermochronology. *Tectonics*, **14**, 704–718, https://doi.org/10.1029/95TC00088.

Rohrman, M., Andriessen, P. & Van Der Beek, P. 1996. The relationship between basin and margin thermal evolution assessed by fission track thermochronology: An application to offshore southern Norway. *Basin Research*, **8**, 45–63, https://doi.org/10.1111/j.1365-2117.1996.tb00114.x.

Rudberg, S. 1965. Reconstruction of Polycyclical Relief in Scandinavia: A discussion in connection with the theories of w. evers on the relief development of southern norway. *Norsk Geografisk Tidsskrift - Norwegian Journal of Geography*, **20**, 65–73, https://doi.org/10.1080/00291956508551830.

Rudberg, S. 1988. Gross morphology of Fennoskandia - six complementary ways of explanation. *Geografiska Annaler, Series A*, **70 A**, 135–167, https://doi.org/10.1080/04353676.1988.11880244.

Sandström, B. & Tullborg, E.L. 2009. Episodic fluid migration in the Fennoscandian Shield recorded by stable isotopes, rare earth elements and fluid inclusions in fracture minerals at Forsmark, Sweden. *Chemical Geology*, **266**, 126–142, https://doi.org/10.1016/j.chemgeo.2009.04.019.

Schaefer, J.M., Codilean, A.T., Willenbring, J.K., Lu, Z.-T., Keisling, B., Fülöp, R.-H. & Val, P. 2022. Cosmogenic nuclide techniques. *Nature Reviews Methods Primers*, **2**, 18, https://doi.org/10.1038/s43586-022-00096-9.

Scheiber, T. & Viola, G. 2018. Complex Bedrock Fracture Patterns: A Multipronged Approach to Resolve Their Evolution in Space and Time. *Tectonics*, **37**, 1030–1062, https://doi.org/10.1002/2017TC004763.

Scheiber, T., Viola, G., Wilkinson, C.M., Ganerød, M., Skår, Ø. & Gasser, D. 2016. Direct40Ar/39Ar dating of Late Ordovician and Silurian brittle faulting in the southwestern Norwegian Caledonides. *Terra Nova*, **28**, 374–382, https://doi.org/10.1111/ter.12230.

Scheiber, T., Viola, G., Lelij, R. Van Der, Margreth, A. & Schönenberger, J. 2019. Microstructurally-constrained versus bulk fault gouge K - Ar dating. *Journal of Structural Geology*, **127**, 103868, https://doi.org/10.1016/j.jsg.2019.103868.

Schleicher, A.M., van der Pluijm, B.A. & Warr, L.N. 2012. Chlorite-smectite clay minerals and fault behavior: New evidence from the San Andreas Fault Observatory at Depth (SAFOD) core. *Lithosphere*, **4**, 209–220, https://doi.org/10.1130/L158.1.

Seranne, M. 1992. Late Palaeozoic kinematics of the More-Trondelag fault zone and adjacent areas, central Norway. *Norsk Geologisk Tidsskrift*, **72**, 141–158.

Seranne, M. & Seguret, M. 1987. The Devonian basins of western Norway: tectonics and kinematics of an extending crust. *Geological Society, London, Special Publications*, **28**, 537–548, https://doi.org/10.1144/GSL.SP.1987.028.01.35.

Simón, J.L. 2019. Forty years of paleostress analysis: has it attained maturity? *Journal of Structural Geology*, **125**, 124–133, https://doi.org/10.1016/j.jsg.2018.02.011.

Slagstad, T., Roberts, N.M.W., Marker, M., Røhr, T.S. & Schiellerup, H. 2013. A non-collisional, accretionary Sveconorwegian orogen. *Terra Nova*, **25**, 30–37, https://doi.org/10.1111/ter.12001.

Slagstad, T., Roberts, N.M.W. & Kulakov, E. 2017. Linking orogenesis across a supercontinent; the Grenvillian and Sveconorwegian margins on Rodinia. *Gondwana Research*, **44**, 109–115, https://doi.org/10.1016/j.gr.2016.12.007.

Slagstad, T., Kulakov, E. V., Anderson, M.W., Saalmann, K., Kirkland, C.L., Henderson, I.H.C. & Ganerød, M. 2022. Was Baltica part of Rodinia? *Terra Nova*, 1–7, https://doi.org/10.1111/ter.12640.

Sømme, T.O., Martinsen, O.J. & Lunt, I. 2013a. Linking offshore stratigraphy to onshore paleotopography: The Late Jurassic-Paleocene evolution of the south Norwegian margin. *Bulletin of the Geological Society of America*, **125**, 1164–1186, https://doi.org/10.1130/B30747.1.

Sømme, T.O., Helland-Hansen, W. & Martinsen, O.J. 2013b. Quantitative aspects of stratigraphic onshoreoffshore relationships along the western margin of southern Norway: Implications for Late Mesozoic and Cenozoic topographic evolution. *Norsk Geologisk Tidsskrift*, **93**, 261–276.

Steer, P., Huismans, R.S., Valla, P.G., Gac, S. & Herman, F. 2012. Bimodal plio-quaternary glacial erosion of fjords and low-relief surfaces in Scandinavia. *Nature Geoscience*, **5**, 635–639, https://doi.org/10.1038/ngeo1549.

Strøm, K.M. 1948. The Geomorphology of Norway. *The Geographical Journal*, **112**, 19, https://doi.org/10.2307/1789153.

Tartaglia, G., Viola, G., van der Lelij, R., Scheiber, T., Ceccato, A. & Schönenberger, J. 2020. "Brittle structural facies" analysis: A diagnostic method to unravel and date multiple slip events of long-lived faults. *Earth and Planetary Science Letters*, **545**, 116420, https://doi.org/10.1016/j.epsl.2020.116420.

Tartaglia, G., Ceccato, A., Scheiber, T., van der Lelij, R., Schönenberger, J. & Viola, G. 2022. Time-constrained multiphase brittle tectonic evolution of the onshore mid-Norwegian passive margin. *GSA Bulletin*, https://doi.org/10.1130/B36312.1.

Templeton, J.A. 2015. Structural Evolution of the Hornelen Basin (Devonian, Norway) from Detrital Thermochronology.

Theissen-Krah, S., Zastrozhnov, D., Abdelmalak, M.M., Schmid, D.W., Faleide, J.I. &

Gernigon, L. 2017. Tectonic evolution and extension at the Møre Margin – Offshore mid-Norway. *Tectonophysics*, **721**, 227–238, https://doi.org/10.1016/j.tecto.2017.09.009.

Torgersen, E., Viola, G., Zwingmann, H. & Harris, C. 2015. Structural and temporal evolution of a reactivated brittle-ductile fault - Part II: Timing of fault initiation and reactivation by K-Ar dating of synkinematic illite/muscovite. *Earth and Planetary Science Letters*, **410**, 212–224, https://doi.org/10.1016/j.epsl.2014.09.051.

Torsvik, T.H., Sturt, B.A., Swensson, E., Andersen, T.B. & Dewey, J.F. 1992. Palaeomagnetic dating of fault rocks: evidence for Permian and Mesozoic movements and brittle deformation along the extensional Dalsfjord Fault, western Norway. *Geophysical Journal International*, **109**, 565–580, https://doi.org/10.1111/j.1365-246X.1992.tb00118.x.

Vermeesch, P. 2017. Statistics for fission track thermochronology. 1–19.

Viola, G., Scheiber, T., Fredin, O., Zwingmann, H., Margreth, A. & Knies, J. 2016. Deconvoluting complex structural histories archived in brittle fault zones. *Nature Communications*, **7**, 1–10, https://doi.org/10.1038/ncomms13448.

Wagner, G.A., Van den Haute, P., et al. 1992. *Fission-Track Dating*. Dordrecht, Springer Netherlands, https://doi.org/10.1007/978-94-011-2478-2.

Walsh, E.O., Hacker, B.R., Gans, P.B., Wong, M.S. & Andersen, T.B. 2013. Crustal exhumation of the Western Gneiss Region UHP terrane, Norway: 40Ar/39Ar thermochronology and fault-slip analysis. *Tectonophysics*, **608**, 1159–1179, https://doi.org/10.1016/j.tecto.2013.06.030.

Weisenberger, T. & Bucher, K. 2010. Zeolites in fissures of granites and gneisses of the Central Alps. *Journal of Metamorphic Geology*, **28**, 825–847, https://doi.org/10.1111/j.1525-1314.2010.00895.x.

Wennberg, O.P. 1996. Superimposed fabrics due to reversal of shear sense: An example from the Bergen Arc Shear Zone, western Norway. *Journal of Structural Geology*, **18**, 871–879, https://doi.org/10.1016/0191-8141(96)00014-4.

Wennberg, O.P. & Milnes, A.G. 1994. Interpretation of kinematic indicators along the northeastern margin of the Bergen Arc system: a preliminary field study. *Norsk Geologisk Tidsskrift*, **74**, 166–173.

Whipp, D.M., Kellett, D.A., Coutand, I. & Ketcham, R.A. 2022. Short communication: Modeling competing effects of cooling rate, grain size, and radiation damage in low-temperature thermochronometers. *Geochronology*, **4**, 143–152, https://doi.org/10.5194/gchron-4-143-2022.

Wiest, J.D., Jacobs, J., Fossen, H., Ganerød, M. & Osmundsen, P.T. 2021. Segmentation of the Caledonian orogenic infrastructure and exhumation of the Western Gneiss Region during transtensional collapse. *Journal of the Geological Society*, **178**, jgs2020-199, https://doi.org/10.1144/jgs2020-199.

Wildman, M., Cogné, N. & Beucher, R. 2019. Fission-Track Thermochronology Applied to the Evolution of Passive Continental Margins. *In*: Malusà, M. G. & Fitzgerald, P. G. (eds)

Fission-Track Thermochronology and Its Application to Geology. 351–371., https://doi.org/10.1007/978-3-319-89421-8_20.

Young, D.J. 2018. Structure of the (ultra)high-pressure Western Gneiss Region, Norway: Imbrication during Caledonian continental margin subduction. *Bulletin of the Geological Society of America*, **130**, 926–940, https://doi.org/10.1130/B31764.1.

Zachos, J., Pagani, H., Sloan, L., Thomas, E. & Billups, K. 2001. Trends, rhythms, and aberrations in global climate 65 Ma to present. *Science*, **292**, 686–693, https://doi.org/10.1126/science.1059412.

Zwingmann, H., Mancktelow, N., Antognini, M. & Lucchini, R. 2010. Dating of shallow faults: New constraints from the AlpTransit tunnel site (Switzerland). *Geology*, **38**, 487–490, https://doi.org/10.1130/G30785.1.

Paper I

Hestnes, Å., Gasser, D., Scheiber, T., Jacobs, J., van der Lelij, R., Schönenberger, J., and Ksienzyk, A.K**.**, 2022: The brittle evolution of Western Norway – A space-time model based on fault mineralizations, K–Ar fault gouge dating and paleostress analysis

(published in *Journal of Structural Geology*)

Journal of Structural Geology 160 (2022) 104621

Contents lists available at ScienceDirect

Journal of Structural Geology

journal homepage: www.elsevier.com/locate/jsg

The brittle evolution of Western Norway – A space-time model based on fault mineralizations, K–Ar fault gouge dating and paleostress analysis

Åse Hestnes [a,*], Deta Gasser [b,c], Thomas Scheiber [b], Joachim Jacobs [a], Roelant van der Lelij [c], Jasmin Schönenberger [c], Anna K. Ksienzyk [c]

[a] Department of Earth Science, University of Bergen, PB 7803, 5020, Bergen, Norway
[b] Department of Environmental Sciences, Western Norway University of Applied Sciences, Røyrgata 6, 6856, Sogndal, Norway
[c] Geological Survey of Norway, PB 6315, 7491, Trondheim, Norway

ARTICLE INFO

Keywords:
K-Ar fault gouge geochronology
Brittle deformation
Fault mineralization
Paleostress analysis
Western Norway

ABSTRACT

Basement fracture and fault patterns on passive continental margins control the onshore landscape and offshore distribution of sediment packages and fluid pathways. In this study, we decipher the spatial-temporal evolution of brittle faults and fractures in the northern section of the passive margin of Western Norway by combining field observations of fault mineralizations and K–Ar fault gouge dating with different paleostress approaches, resulting in the following model: (1) High-T fault mineralizations indicate Silurian NW-SE compression followed by NW-SE extension in the Early to Mid-Devonian. (2) Epidote, chlorite and quartz fault mineralizations indicate a dominant strike-slip stress field in the Late Devonian to early Carboniferous. (3) E-W extensional stress fields which could be related to Permo-Triassic or Late Jurassic rifting are not prominent in our data set. (4) K–Ar fault gouge ages indicate two extensive faulting events under a WNW-ESE transtensional stress regime with related precipitation of zeolite and calcite in the mid (123-115 Ma) and late (86-77 Ma) Cretaceous. Our results show that the brittle architecture of the study area is dominated by reactivation of ductile precursors and newly formed strike-slip faults, which is different from the dip-slip dominated brittle architecture of the southern section of the West Norway margin.

1. Introduction

Fractures and faults are common geological features in the upper crust. Onshore, fractures and faults represent zones of weakness with generally high erodibility, controlling the location of important landscape features such as valleys and fjords. Offshore, similar structures offset sedimentary packages, impacting the permeability and fluid and gas pathways, which have implications for hydrocarbon exploration and CO_2 storage projects. Understanding the formation and evolution of fault and fracture patterns in space and time is therefore an important task when we try to resolve the evolution of landscapes or to understand the pathways of fluids and gasses.

Western Norway has long been an important site for the study of rift processes and source to sink relationships along passive continental margins. The region is one key area where basement fault and fracture patterns both influence the onshore landscape and impact the distribution of sedimentary packages offshore (Redfield et al., 2005; Fossen et al., 2017, 2021; Scheiber and Viola, 2018). Deciphering the spatial and temporal evolution of complex fault and fracture patterns in metamorphic basement is challenging, and one needs to address the issues that follows: (a) the role of ductile structural precursors (e.g. Walsh et al., 2013; Skyttä & Torvela, 2018), (b) the role of reactivation of fault systems under changing stress fields (Redfield et al., 2005; Scheiber and Viola, 2018) and (c) complexities in interpreting K–Ar fault gouge data. The latter requires a good understanding of the thermal evolution of the study area and the complexity of fault zone architecture (Viola et al., 2016; Scheiber and Viola, 2018; Tartaglia et al., 2020).

In this study, we aim to unravel the spatial and temporal evolution of fault and fracture patterns in a so-far little-studied key area of Western Norway: the transitional area between the N–S trending North Sea margin in the south and the NE–SW trending Møre margin in the north (Fig. 1). We combine remote sensing lineament analysis with ductile foliation trace mapping to investigate the significance of ductile precursors for the subsequent brittle evolution. We then present an extensive field data set from brittle faults and fractures, highlighting the presence of both newly formed structures and structures reactivating

* Corresponding author.
E-mail address: ase.hestnes@uib.no (Å. Hestnes).

https://doi.org/10.1016/j.jsg.2022.104621
Received 17 December 2021; Received in revised form 8 May 2022; Accepted 10 May 2022
Available online 13 May 2022

older, ductile precursors. Observations of fault and fracture mineralizations help to constrain the relative timing of faulting activity, and K–Ar fault gouge data provide absolute age constraints on faulting. By applying different approaches of paleostress analysis to our dataset, we then suggest a spatial-temporal model for the brittle evolution of our study area. We show that the area is dominated by strike-slip kinematics and that prominent phases of rifting offshore are less prominent in the onshore realm.

2. Geological setting

The bedrock in the study area consists of the following elements (Fig. 1): 1) Proterozoic gneisses of the Western Gneiss Region (WGR) (e.g. Røhr et al., 2004, 2013; Corfu et al., 2014; Wiest et al., 2021), 2) Proterozoic and Paleozoic ortho- and paragneisses of the Caledonian nappes (e.g. Furnes et al. 1990; Corfu and Andersen 2002), and 3) Devonian sedimentary rocks (e.g. Osmundsen and Andersen 2001). The bedrock is highly influenced by the Caledonian orogeny with the subduction of parts of the WGR to ultra-high pressure depths in the Devonian (e.g. Hacker et al. 2003, 2010; Kylander-Clark et al. 2007), translation of the nappes during the collisional phase (e.g. Roberts and Sturt 1980; Hacker and Gans 2005; Corfu et al. 2014), subsequent extensional collapse (e.g. Fossen 1992, 2010; Krabbendam and Dewey, 1998) and the associated formation of the Devonian basins (e.g. Seranne and Seguret 1987; Osmundsen et al. 1998; Braathen et al. 2004).

2.1. Ductile precursor structures

The WGR and the overlying Caledonian nappes experienced extensive shearing, folding and doming during the collapse of the Caledonian orogen, starting at about 410 Ma and leading to the formation of the main ductile precursor structures in the study area (e.g. Fossen and Dunlap, 1998; Wiest et al., 2021). Several Devonian shear zones separate the orogenic root of the WGR from the overlying Caledonian nappes and the Devonian basins. The large-scale, corrugated detachment system of the Nordfjord-Sogn Detachment Zone (NSDZ; e.g. Labrousse et al., 2004; Young, 2018) connects with the Bergen Arc Shear Zone (BASZ) (e.g. Wennberg 1996) to the south (Fig. 1a). The Møre-Trøndelag Fault Complex (MTFC, Seranne, 1992), the Nordfjord Shear Zone (NSZ, Hacker et al., 2010) and the Lom Shear Zone (LSZ, Wiest et al. 2021) all

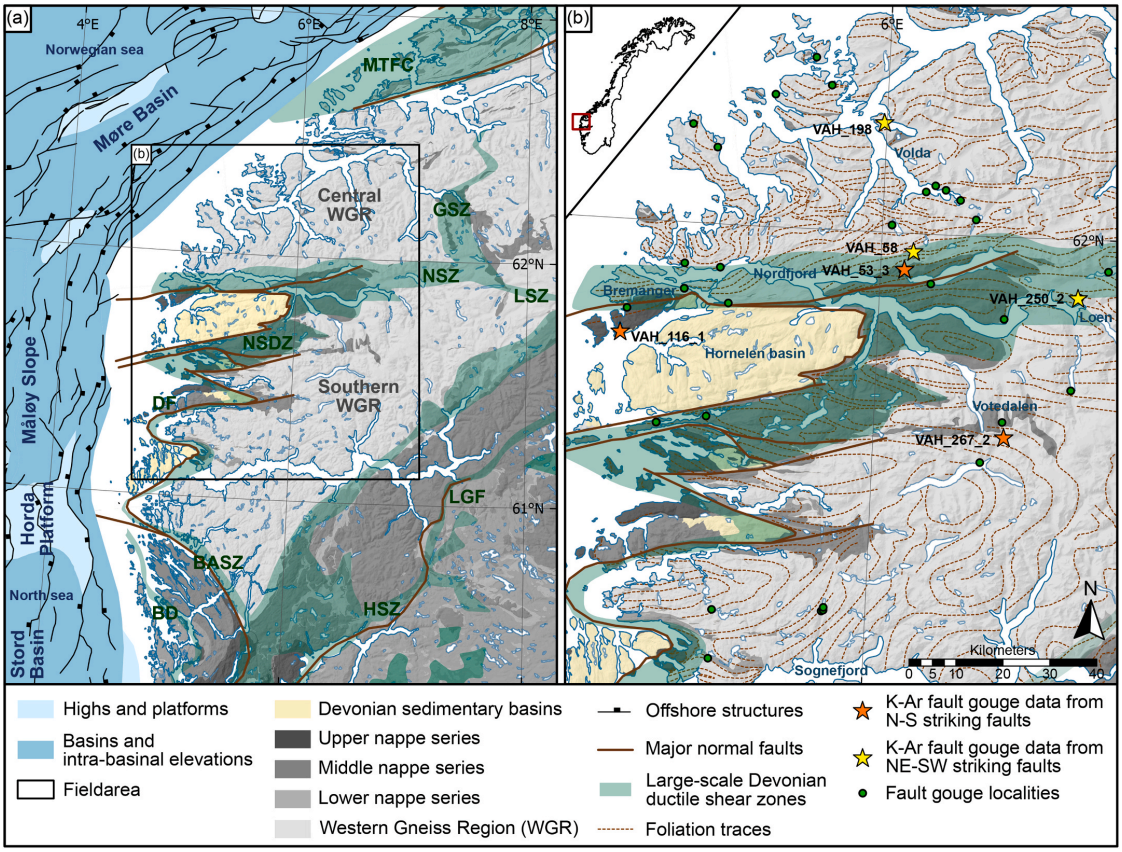

Fig. 1. (a) Simplified tectonic map of Western Norway showing offshore structures and onshore major shear zones (transparent green areas) and major faults (brown solid lines). BD= Bergen Detachment; BASZ=Bergen Arcs Shear Zone; DF = Dalsfjord Fault; GSZ = Geiranger Shear Zone; HSZ=Hardangerfjord Shear Zone; LGF = Lærdal-Gjende Fault; LSZ = Lom Shear Zone; MTFC = Møre-Trøndelag Fault Complex; NSDZ=Nordfjord-Sogn Detachment Zone; NSZ=Nordfjord Shear Zone. The black square indicates the study area. White offshore and coastal areas indicate basement highs. Map modified from Wiest et al. (2021). (b) Tectonic map of the study area. Red square on inset of Norway indicates the location of the study area. Stars indicate the location of dated K–Ar fault gouge samples (orange stars = N–S striking faults, yellow stars = NE-SW striking faults). Green dots indicate the location of sampled fault gouges that were not analysed in this study. Foliation traces modified from Wiest et al. (2021). (For interpretation of the references to colour in this figure legend, the reader is referred to the Web version of this article.)

show mostly ductile sinistral kinematics and acted as strike-slip transfer zones during transtensional collapse (Krabbendam and Dewey, 1998; Osmundsen and Andersen, 2001; Wiest et al., 2021). These structures are reflected in the regional foliation trends. Foliation trace mapping based on published foliation measurements shows E–W to NE–SW-striking foliations north of and along the Nordfjord, and E–W to NW–SE-striking foliations south of the Nordfjord, with several domes developed in the WGR (Figs. 2 and 3a; Wiest et al., 2021). The foliation is dominantly flat to gently dipping, but steeper dips occur as well (Supplementary 1).

2.2. Brittle faulting

From the Devonian onwards, the ductile structural pattern has been overprinted by repeated episodes of brittle faulting (Gabrielsen et al., 2002; Fossen et al., 2017, 2021; Ksienzyk et al., 2016; Scheiber and Viola, 2018), including the brittle reactivation of major ductile shear zones. North of the study area, the MTFC has shown repeated brittle activity in the Late Devonian, Permo-Triassic, Mid- and Late Jurassic, Cretaceous, and Cenozoic (Redfield et al., 2004, 2005; Osmundsen et al., 2006). Similar repeated activity has been documented from other regional faults: the Nordfjord-Sogn Detachment fault in the Permian and Jurassic-Cretaceous (Braathen et al., 2004), the Dalsfjord fault (DF) in Late Permian-Early Triassic, Jurassic, and Cretaceous times (Torsvik et al., 1992; Eide et al., 1994; Fossen et al., 2021), and the Lærdal-Gjende fault (LGF) in Permian, Late Jurassic-Early Cretaceous and the Paleocene (Andersen et al., 1999; Fossen et al., 2017; Tartaglia et al., 2020). Detailed analyses of minor fault zones and fracture patterns, mainly south of our study area, revealed early Carboniferous, Permian, Triassic-Jurassic, Cretaceous and Paleogene episodes of brittle faulting (Ksienzyk et al., 2014, 2016; Viola et al., 2016; Scheiber and Viola, 2018; Scheiber et al., 2019; Fossen et al., 2021).

2.3. Brittle evolution offshore

The onshore fault activity relates to two well-constrained phases of rifting in the North Sea (Steel and Ryseth, 1990; Roberts et al., 1995; Færseth, 1996): 1) rift phase 1 during the Permian and Early Triassic affecting a wide area and showing general E–W extension, and 2) the more localized rift phase 2 during the Late Jurassic and Early Cretaceous of which the extension direction is controversial. Several suggestions have been made for the latter, including E–W extension (Bartholomew et al., 1993; Reeve et al., 2015), NE–SW extension (Færseth, 1996; Færseth et al., 1997), or one or two phases of rotation throughout the rift phase (Doré et al., 1997; Davies et al., 2001). Similar phases of rifting have also been suggested for the Møre Margin in the Norwegian Sea (Talwani and Eldholm, 1972; Grunnaleite and Gabrielsen, 1995; Gómez et al., 2004; Theissen-Krah et al., 2017): 1) a first rift phase is constrained to early Permian-Early Triassic with a ENE-WSW extension direction, 2) a major NW–SE directed rift phase in Late Jurassic and Early Cretaceous, suggested to have ended by mid-Cretaceous, and 3) a last stretching event in Late Cretaceous and Palaeocene leading to the final break-up between Greenland and Eurasia in the Eocene. In this study, we aim at deciphering the structural evolution of the onshore transition zone between the North Sea and the Norwegian Sea rift systems.

3. Methods

3.1. Remote sensing

We conducted foliation trace analysis and lineament mapping in ArcGIS to acquire an overview of the structural architecture of the region. We used foliation traces drawn by Wiest et al. (2021), which were manually interpolated between field measurements of foliations stored in the 1:50 000 and 1:250 000 bedrock map database of the Geological Survey of Norway (NGU). Manual extraction of lineaments is a qualitative method where the results depend on the operator, what map sources are used, and the scale used for mapping (Scheiber et al., 2015). Manual extraction of lineaments was conducted by the first author on digital elevation models (DEMs) and on vertical derivatives of the topography which is a map source not sensitive to illumination direction and was made in Seequent Oasis Montaj (Supplementary 2). Orthophotos were used to study specific lineaments in more detail and, in some cases, hillshaded DEMs were used for further analysis.

A conservative approach was applied where only distinct linear topographic bedrock features that clearly represent the expression of brittle bedrock structures were included in the lineament map (see Supplementary 2). Lineament mapping was performed at three different scales (1:300 000, 1:200 000 and 1:100 000) and is presented as a synthesis map with lineaments from all scales (Fig. 2).

3.2. Structural field work

Our foliation trace and lineament analysis served as a base for choosing areas for fieldwork. In the field, we systematically collected fault and fracture data, including orientation, slip line orientation, fault rock type, fracture surface mineralization, sense of slip, geometric relation to the local foliation, and if present, signs of reactivation. For the sense of slip, we attributed each fault-slip measurement with a value based on confidence and preservation (C – certain, P – probable, S – supposed, X – unknown). We also collected fault gouge samples for K–Ar geochronology.

3.3. K–Ar fault gouge dating

The K–Ar fault gouge analyses including separation into grain size fractions, XRD characterization and K–Ar dating were carried out at the Geological Survey of Norway and a detailed method description is provided in the supplementary material (Supplementary 3). The samples were separated into five grain size fractions before dating: 6–10 μm, 2–6 μm, 0.4–2 μm, 0.1–0.4 μm and <0.1 μm. The mineralogical composition of each fraction was determined by X-ray diffraction (XRD). The XRD patterns were also inspected in terms of possible illite polytypes that may represent different generations of illite (Grathoff and Moore, 1996).

To study the mineralogical and crystallographic properties of the fault gouge samples, we used scanning electron microscopy (SEM) at the Elmilab, University of Bergen. The gouge samples were first encapsulated in epoxy and surfaces were polished. Backscatter electron imaging (BSE) was done using a Zeiss Supra 55 VP. Element mapping and energy dispersive X-ray analysis (EDX) was done by using a Thermo Fisher X-ray detector and the Pathfinder software. Only the fractions of 2–6 μm and 6–10 μm were studied under the SEM. The other fractions were too fine grained and did not reveal any useful information.

3.4. Paleostress analysis

Observations of a brittle fault's plane and slip line orientation together with kinematic information can be used to deduce a local stress tensor under which the fault has formed (Angelier, 1979; Lacombe, 2012; Simón, 2019). When performing paleostress analysis, the measured kinematic data are inverted into a single reduced stress tensor. The stress tensor provides information about the orientation of the principal stress axes ($\sigma_1 \geq \sigma_2 \geq \sigma_3$) and the stress ratio R. R indicates the relative magnitude of the principal stresses and is defined as $(\sigma_2 - \sigma_3)/(\sigma_1 - \sigma_3)$ (Angelier, 1984).

To perform paleostress analysis, we used the program WinTensor by Delvaux and Sperner (2003). The dataset was divided into local stations based on location size and number of included fault and fracture measurements. In Win Tensor, we did the following procedure: First, we applied the Right Dihedron method, which finds the best fit stress tensor for a given number of field measurements and which removes outliers.

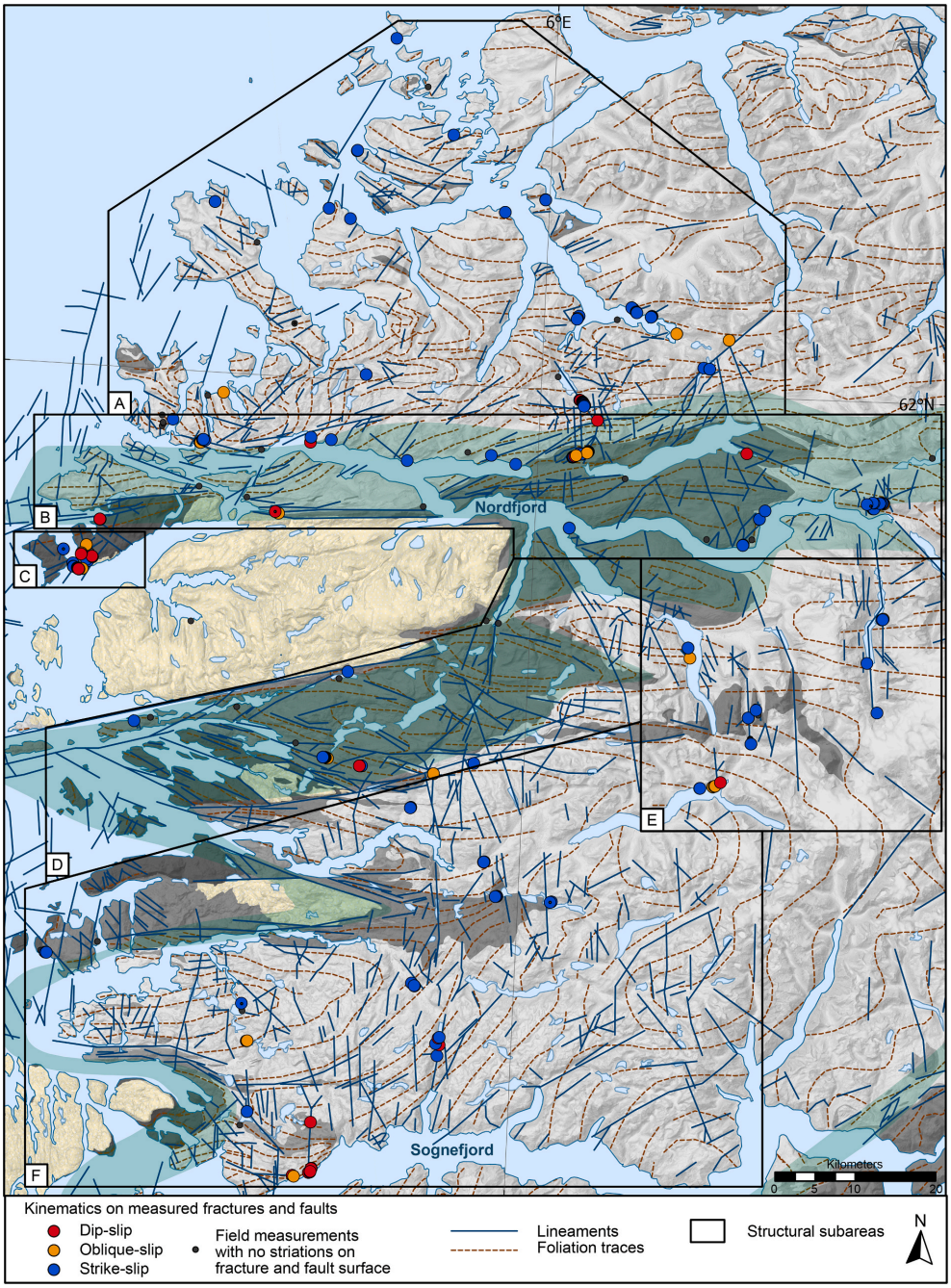

Fig. 2. Map with foliation traces (stippled brown lines, modified from Wiest et al. 2021) and manually extracted lineaments (blue lines). Lineaments represent a compilation extracted from DEMs and the vertical derivatives of the topography at three different scales (1:300 000, 1:200 000 and 1:100 000). Based on overall structural characteristics, the study area is divided into six subareas indicated by black boxes labelled A-F. Coloured circles indicate orientation of the observed lineation along brittle faults (red = dip-slip; orange = oblique slip; blue = strike-slip), whereas black dots correspond to localities where no kinematic indicators were observed. A total of 620 field localities are included. (For interpretation of the references to colour in this figure legend, the reader is referred to the Web version of this article.)

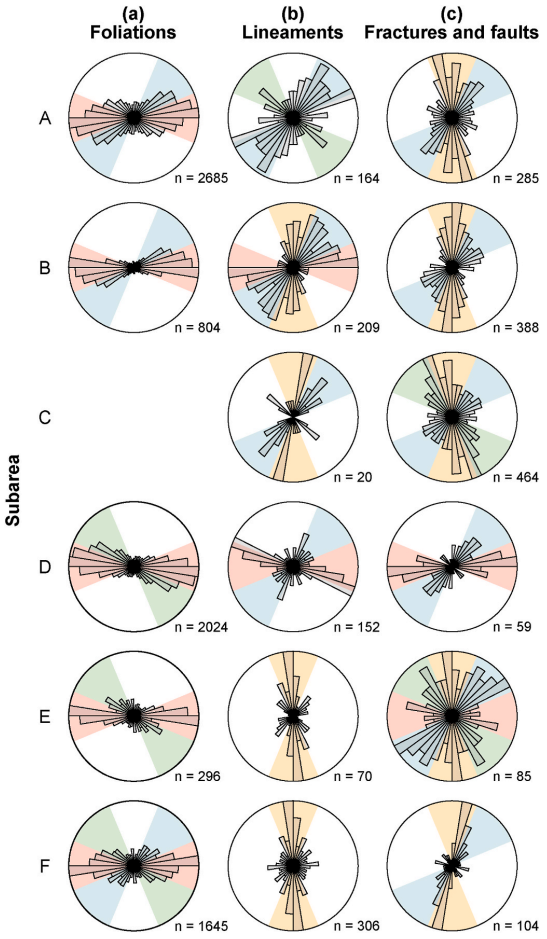

Fig. 3. Strike orientation of structural data from subareas A-F (Fig. 2) shown as number weighted rose plots (bin size 40). (a) Foliation measurements from the structural database of NGU. (b) Lineament trends. (c) Fractures and faults measured in the field, also those not containing observed surface mineralizations. Background colours shows the main groups of strike orientation for each plot (yellow = N–S; blue = NE-SW; pink = E-W; green = NW-SE). Subarea C represents the Bremanger Granitoid Complex which lacks ductile foliation. (For interpretation of the references to colour in this figure legend, the reader is referred to the Web version of this article.)

The selected stress tensor was further analysed with the Rotational Optimization method, where the stress tensor is iteratively adjusted to the data set. During this step, fault planes containing slip lineations but lacking information about sense of movement were also included. For each subset, measurements exceeding an alpha misfit angle of 17° were rejected as suggested by Simón (2019). Alpha is the angle between the measured slip line and the theoretical slip direction according to the resolved shear stress on the plane. To evaluate the resulting stress field, we used the modified stress index regime R' (Delvaux and Sperner, 2003). R′ is a numerical parameter ranging from 0 to 3: extensional stress regime (σ_1 vertical) when R' = R; strike-slip stress regime (σ_2 vertical) when R' = 2 – R; and compressional stress regime (σ_3 vertical) when R' = 2 + R (Delvaux and Sperner, 2003). The following five categories of stress tensors are used (after Mattila and Viola (2014)): pure extension, R' = 0–0.75, transtension, R' = 0.75–1.25, pure strike-slip, R' = 1.25–1.75, transpression, R' = 1.75–2.25, and pure compression, R' = 2.25–3.

Following the first order paleostress analysis at the local stations, we perform significance tests for the individual local stress tensors according to Orife and Lisle (2006). We arrange the test results according to amount of included fracture and fault measurements and the average alpha value. Further, we categorize the individual measurements of each station by fault surface mineralization and redo the paleostress analysis. The resulting local stress tensors are again tested according to Orife and Lisle (2006), a procedure suggested by Simón (2019).

4. Results

Based on the large-scale ductile architecture of the study area, we divide the study area into six subareas (Fig. 2): subarea A encompasses the area north of the NSDZ and NSZ; subarea B comprises the area along Nordfjord including the NSZ and parts of the NSDZ; subarea C represents the Bremanger Granitoid Complex dated to 440 ± 5 Ma (Hansen et al., 2002), which does not contain a ductile precursor foliation due to its high structural position within the Caledonian nappe stack; subarea D comprises the NSDZ south and east of the Hornelen Devonian basin; subarea E encompasses the most inland parts of the study area dominated by N–S trending valley systems; and subarea F includes the southernmost part of the field area east of the NSDZ and north of the Sognefjord.

4.1. Lineament mapping

Fig. 2 shows the lineaments identified within the different subareas. Three main lineament orientation trends are visible (Fig. 3b): 1) N–S (yellow in Fig. 3), 2) NE–SW (blue in Fig. 3) and 3) E–W (red in Fig. 3). In subarea A, the NE–SW trend dominates, whereas in subareas B and D, the E–W trend dominates, following mainly the trend of the ductile foliation. In subareas C, E and F, the N–S trend dominates, clearly cutting the trend of the main foliation (Fig. 3a and b).

4.2. Field observations

We collected structural data from brittle faults and fractures at 620 field localities, representing 1385 individual fault and fracture surfaces with fault mineralizations and 452 slip lines on fault planes (Fig. 2, Supplementary 4). In general, the three main orientation trends identified from lineament mapping are also present in the field measurements within each subarea, except for the E–W trend in subarea B, which is missing in the field data (Fig. 3b and c). The E–W lineament trend in subarea B is therefore more likely an effect of the pervasive E–W ductile foliation trend (Fig. 3a). In addition, the field measurements show that N–S striking faults and fractures are more pronounced throughout the study area than what the lineament mapping shows, except for subarea D, where this trend is missing in the field data as well (Fig. 3b and c). The NW–SE striking fractures and faults are minor in all subareas (green in Fig. 3).

At each location, we studied the relationship between the orientation of brittle faults and fractures and the local foliation. In subareas A, B and F, the NE–SW fractures strike generally parallel to subparallel to the local foliation, whereas in subareas D and E, the E–W brittle structures strike parallel to subparallel to the foliation. In general, the dip of the foliation is moderate to shallow, which is different from the steep dip of the fractures and faults (Supplementary 1). The N–S striking faults and fractures cut the local foliation throughout the study area.

The dip of the measured faults and fractures is generally steep (Fig. 4 and Supplementary 1). The slip line trends vary throughout the study area, depending on the strike of the corresponding faults, with a generally shallow plunge (Fig. 4). Slip line orientations show predominantly strike-slip kinematic indicators, with 248 strike-slip dominated

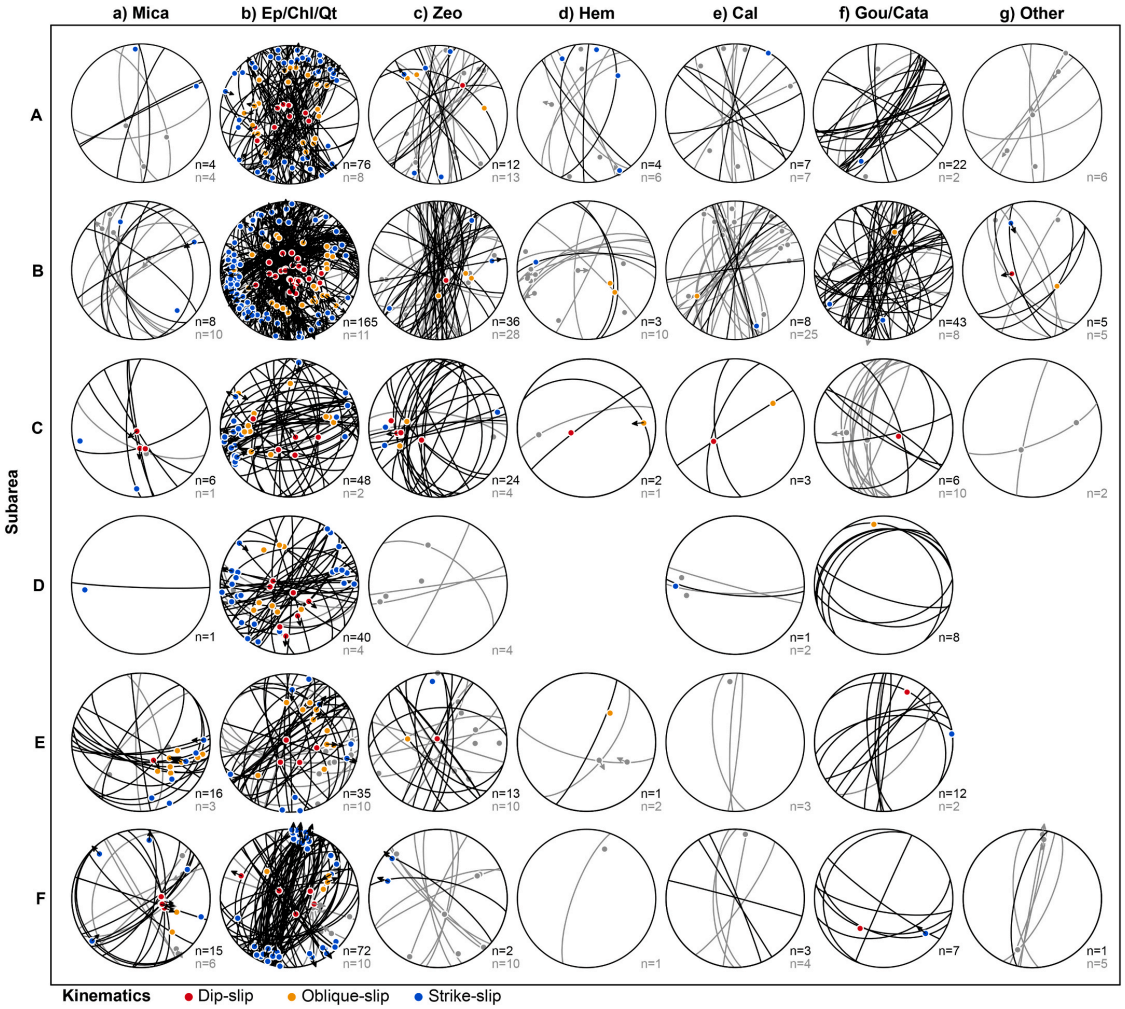

Fig. 4. Stereoplots of all measured fracture and fault surfaces with mineral coatings and/or cataclasite/gouge from the study area. A-F correspond to subareas from Fig. 2. The measurements are grouped according to their mineral coating and/or whether they are associated with cataclasite/gouge. Ep = epidote; Chl = chlorite; Qt = quartz; Zeo = zeolite; Hem = hematite; Cal = calcite; Gou = gouge; Cata = cataclasite. Black and coloured (red = dip-slip dominated kinematic indicators (dip 90-60°); orange = oblique-slip dominated kinematic indicators (dip 60-30°); blue = strike-slip dominated kinematic indicators (dip 30-0°)) measurements indicate surfaces dominated by the main mineral within each category, whereas grey measurements represent surfaces where the mineral of the category is a minor constituent; these grey surfaces appear as well within the plot of the dominating mineralization. (For interpretation of the references to colour in this figure legend, the reader is referred to the Web version of this article.)

faults, 125 oblique-slip faults and 79 dip-slip dominated faults observed (Fig. 2).

Based on observed fault and fracture mineralizations, we assigned our field measurements to seven different groups, sorted according to inferred high-to low-temperature mineralizations (Figs. 4 and 5): 1) Discrete fracture surfaces characterized by aligned muscovite/biotite and/or stretched quartz, feldspar and hornblende (stretched host rock, SHR) were mostly observed in subareas B, E and F (Figs. 4a and 5a). The stretching of these minerals must have happened under relatively high-temperature and thus semi-ductile conditions. These surfaces are, in places, covered by epidote, chlorite and/or quartz mineralizations (Fig. 5b). SHR surfaces have variable dip angles and they have been found both cutting and being parallel to the foliation with variable strike orientation (Fig. 4a). The observed kinematic indicators are mainly dextral or sinistral strike-slip to oblique-slip. 2) Surfaces with epidote, chlorite and/or quartz are the most common mineralizations in all subareas (Figs. 4b and 5c). These surfaces do not show clear orientation trends. Steeply dipping surfaces showing slip lines with shallow plunge and strike-slip movements seem to be more abundant. Some of these surfaces contain two generations of slip lines (Fig. 5d). 3) Surfaces with zeolite mineralizations occur throughout the study area (Fig. 4c). The zeolite mineralizations vary in colour from white to pink to orange and occur as euhedral radial crystals or as striated fibres (Fig. 5e–g). Zeolite often occurs on top of epidote and chlorite mineralizations and is the apparent younger mineral (Fig. 5e). The zeolite surfaces are commonly steeply dipping and generally strike N–S or NE–SW to E–W, and when

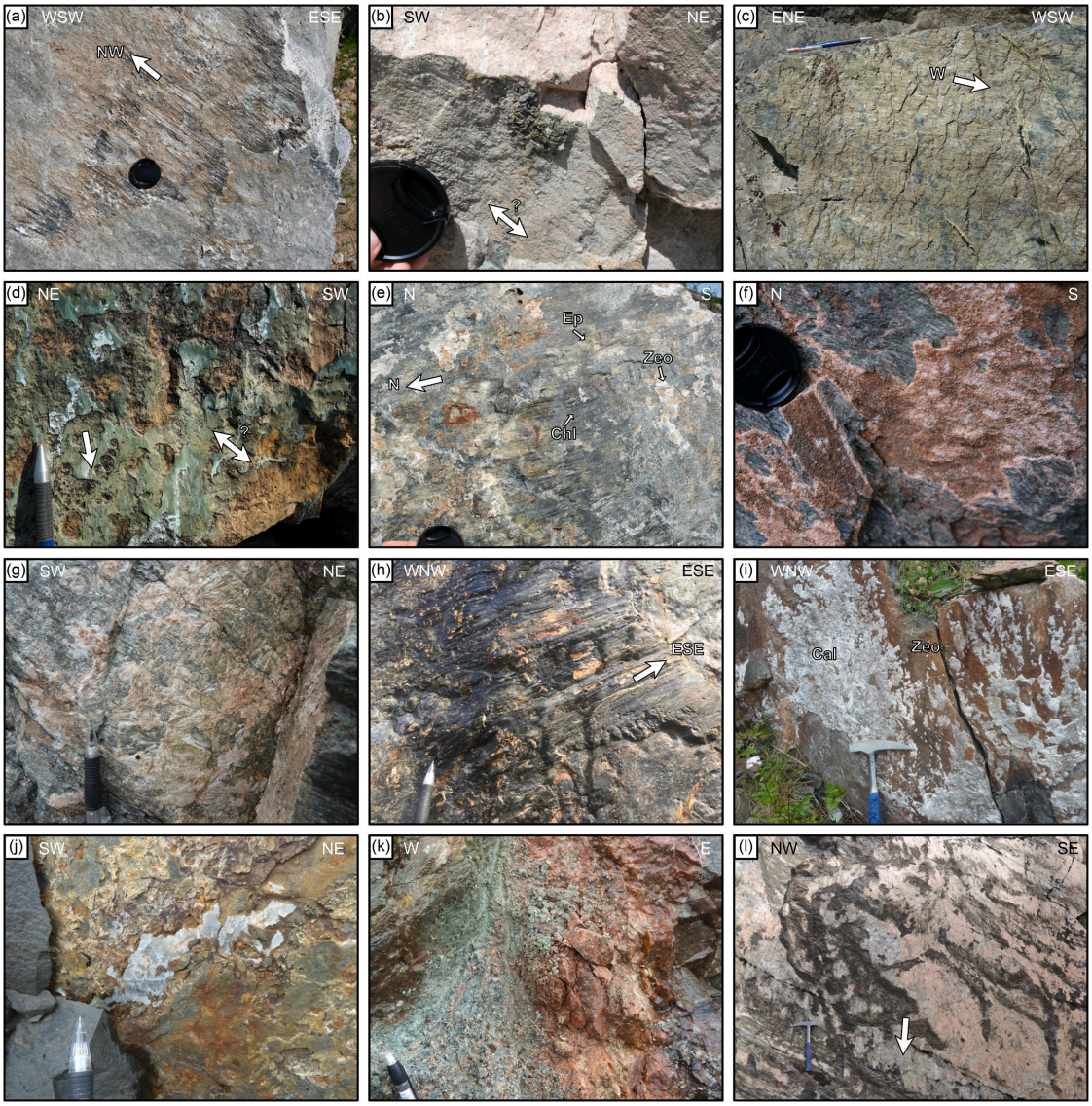

Fig. 5. (a) Semi-ductile strained fault surface with stretched amphibole and muscovite mineralization (all coordinates of localities here and in the following UTM 32N: 364324/6828098). Arrow indicates sinistral shear. (b) Semi-ductile strained fault surface with stretched feldspar and quartz rods and with chlorite, epidote, and quartz crystals on top (364340/6828103). Arrow indicates shear, direction unknown. (c) Epidote and chlorite mineralization with slickensides (347502/6869635). Arrow indicates dextral shear. (d) Fault in serpentinite showing two generations of slickensides on epidote- and chlorite-coated surface (321049/6879673). Shear sense of older slip line is unknown. Arrow indicates normal shear on younger slickenside. (e) Striated fracture surface with chlorite and minor epidote (384313/6863612). Arrow indicates sinistral shear. Patches of white zeolite on top, also showing sinistral shear. (f) Pink-orange zeolite crystals on the fracture surface, no slip line developed (368751/6836728). (g) Pale pink radial zeolite crystals on fracture surface (368751/6836728). (h) Striated hematite- and chlorite-coated surface (280996/6807453). Arrow indicates dextral shear. (i) Fracture surface coated with zeolite (orange to pink) and calcite (white) (324866/6921786). Zeolite is found both below the calcite and in small patches above the calcite. (j) Fracture in the Kalvåg Melange on Bremangerlandet with white calcite (283257/6857875). (k) Zoned cataclasite (385183/6863538). Dark green – chlorite; light green – epidote; white – quartz and patches of calcite; pink; altered host rock and zeolite. (l) Fracture in peridotite coated with pale orange talc (316692/6871528). Arrow indicates normal shear. (For interpretation of the references to colour in this figure legend, the reader is referred to the Web version of this article.)

found alone, they rarely show any slip lines (Fig. 4c). 4) Surfaces with hematite are more common in the northern field area and are commonly found together with dark green chlorite (Figs. 4d and 5h). These surfaces have similar orientations and sense of shear as the surfaces with epidote, chlorite and/or quartz (grey, Fig. 4d). 5) Surfaces with calcite (Fig. 5i–j) are most common in subarea B (Fig. 4e). The calcite appears as thin mineral coatings or as bigger crystals, and both alone on surfaces or together with any of the above-mentioned mineralizations. If occurring together with other mineralizations, calcite is normally found on top and seems to be the younger mineral (Fig. 5i). We rarely observed slip lines on calcite, and no kinematic indicators were observed (Fig. 4e). 6) Faults containing cataclasite and/or uncohesive fault rock such as breccia and gouge occur throughout the study area, with most observations in subarea B (Figs. 4f, 5k and 6). These faults show variable orientations with shallow to steep dips. Slip lines and kinematic indicators were rarely observed on the fault surfaces in direct contact with the gouge. If observed, it was commonly seen on other surface minerals and is plotted in the corresponding mineral stereoplot in Fig. 4 and only shown in grey for Fig. 4f. The observed cataclasites represent 5–80 cm thick zones of crushed host rock containing minerals like chlorite, epidote, K-feldspar, and zeolite (Fig. 5k). 7) A smaller group of faults contains other minerals like talc, K-feldspar or pyrite (Figs. 4 and 5l).

4.3. K–Ar gouge dating

In total, 56 gouges from 43 different faults were sampled (Fig. 1b). We collected gouges from all the three main fracture orientation trends observed (Figs. 3c and 4f). Six samples from the two most dominant gouge-bearing fault sets were selected for K–Ar gouge dating (i.e., N–S and NE–SW trending, representing the trend of the North Sea and Møre margins, respectively). For both the N–S and NE–SW trending fault sets, we chose to analyse three samples representing the coastal, central and inland region of the study area, respectively (Fig. 1b). Detailed results from XRD analyses are shown in Supplementary 5.

4.3.1. N–S striking faults

4.3.1.1. VAH_116_1. Sample VAH_116_1 is from a W-dipping fault in the unfoliated Bremanger granodiorite that is exposed within a quarry (Figs. 1b and 6a). The main fault plane dips moderately towards the W (263/39, dip azimuth/dip) and contains slip lines oriented 263-45 (plunge direction-plunge) associated with normal (W-down) dip-slip kinematic indicators. Slickensides were observed on striated white zeolite on the fault plane. The sharp fault scarp can be followed for about 150 m, and the width of the exposed fault core is ca. 1–1.5 m (Fig. 6a). At the sample locality, the fault core consists of fault breccia with variable clast sizes, layers of gouge as well as layers of coarse-grained orange zeolite crystals. We sampled a ca. 3–6 cm thick gouge layer close to the hanging wall (Fig. 6a). The three larger grain size fractions contain smectite, quartz, K-feldspar, chlorite, illite/muscovite and plagioclase (Fig. 7a). BSE imaging of the coarsest fraction shows smectite replacing K-feldspar crystals (Fig. 7a). The two finest grain size fractions of the sampled gouge consist of smectite with possible traces of illite/muscovite. Palygorskite may also be present as inferred from its characteristic peak at 10.4 Å (Supplementary 6). The K–Ar dates show a slightly convex-upward age spectrum ranging from 155 ± 2 Ma for the coarsest fraction (6–10 μm) to 115 ± 2 Ma for the finest fraction (<0.1 μm) (Table 1, Fig. 8a).

4.3.1.2. VAH_53_3. Sample VAH_53_3 is from a fault zone located along Rv651 north of Nordfjord (Figs. 1b and 6b). The host rock is a banded gneiss with a foliation oriented 128/56. The fault itself measures 075/85 with slip lines oriented 159-15. The fault shows strike-slip movement through slip lines on calcite but kinematic indicators were not observed. The fault consists of one 10–40 cm wide fault strand containing gouge and clasts of host rock and calcite. All grain size fractions are poorly crystalline as shown by broad diffractions peaks with low intensities. The two coarser fractions of the sampled gouge contain mainly smectite with subordinate K-feldspar, chlorite and minor quartz, whereas the three finest grain size fractions are entirely dominated by smectite (Table 1; Fig. 7b). The finest fraction is monomineralic. BSE imaging of the coarsest fraction shows K-feldspar with smectite replacement textures (Fig. 7b). The K–Ar dates show an inclined age spectrum with dates ranging from 124 ± 2 Ma for the coarsest fraction (6–10 μm) to 86 ± 2 Ma for the finest fraction (<0.1 μm) (Table 1, Fig. 8a). The three coarsest fractions overlap within their uncertainties with a mean age of 123 ± 2 Ma.

4.3.1.3. VAH_267_2. Sample VAH_267_2 is from a fault zone located along E39 at the southern end of Votedalen (Figs. 1b and 6c). The monzonitic host rock has a foliation oriented 125/30. The entire outcrop is cross-cut by subvertical fractures coated with pink zeolite crystals and, in some places, calcite minerals in the centre (Fig. 6c, insert). There are two zones of fault breccia, where one also contains gouge. The orientation of the gouge-bearing zone is 261/65 with a slip line of 355-13. The fault shows strike-slip movement on striated pink zeolite but kinematic indicators were not observed. The brecciated zone also contains epidote. Only four grain-size fractions could be extracted from the gouge sample (Table 1, Fig. 7c). The three coarser fractions of the sampled gouge contain smectite, illite/muscovite, plagioclase, zeolite, pyroxene, quartz, chlorite, and minor rutile, whereas the finest grain size fraction is monomineralic and consists entirely of smectite (Table 1, Fig. 7c). From XRD, the two coarsest fractions contain the 2M1 illite polytype (Supplementary 6). The K–Ar dates show an inclined age spectrum ranging from 240 ± 3 Ma for the coarsest fraction (6–10 μm) to 158 ± 4 Ma for the finest fraction (0.1–0.4 μm) (Table 1, Fig. 8a).

4.3.2. NE–SW striking faults

4.3.2.1. VAH_198. Sample VAH_198 is from a fault zone located along road 653 close to Volda (Figs. 1b and 6d). The host rock is a dioritic gneiss with a foliation oriented 071/47. The fault is located close to a lens of amphibolitic gneiss. The fault zone is approximately 2 m wide and consists of five fault branches, where two of these contain gouge and are separated by fractured host rock (Fig. 6d). The sampled fault has an orientation of 122/80 and a slip line of 204-25. The fault shows strike-slip movement on striated K-feldspar, but no sense of shear was observed. The coarser fractions of the sampled gouge contain biotite, smectite, K-feldspar, chlorite, plagioclase, zeolite and traces of amphibole, whereas the finest grain size fraction consists of biotite, chlorite and smectite (Fig. 7d). Biotite was identified with XRD according to its 5 Å/10 Å peak proportion (Supplementary 6). The presence of biotite is also supported by chemical data from ICP-OES analyses which show high concentrations of both Fe and Mg in contrast to Al. The smectite content decreases with decreasing grain size fraction, whereas biotite content increases (Fig. 7d). BSE imaging from the coarsest fraction shows fractured K-feldspar decomposing along its rims (Table 1, Fig. 7d). The K–Ar dates show a slight convex-upward age spectrum ranging from 194 ± 2 Ma for the coarsest fraction (6–10 μm) to 180 ± 2 Ma for the finest fraction (<0.1 μm) (Table 1, Fig. 8b).

4.3.2.2. VAH_58. Sample VAH_58 is from a fault zone located along road Rv651 north of Nordfjord close to a major NE–SW trending lineament crossing the valley (Figs. 1b and 2). The host rock is a banded gneiss with a foliation of 134/61. The fault zone is about 1 m wide and exhibits two slip planes containing incohesive fault rock and having sharp boundaries to the host rock (Fig. 6e). The orientation of the sampled fault is 122/55 with a slip line of 122-55. The fault shows dip-slip movement on striated K-feldspar, but kinematic indicators were not observed. The fault zone shows K-feldspar mineralization on the fault

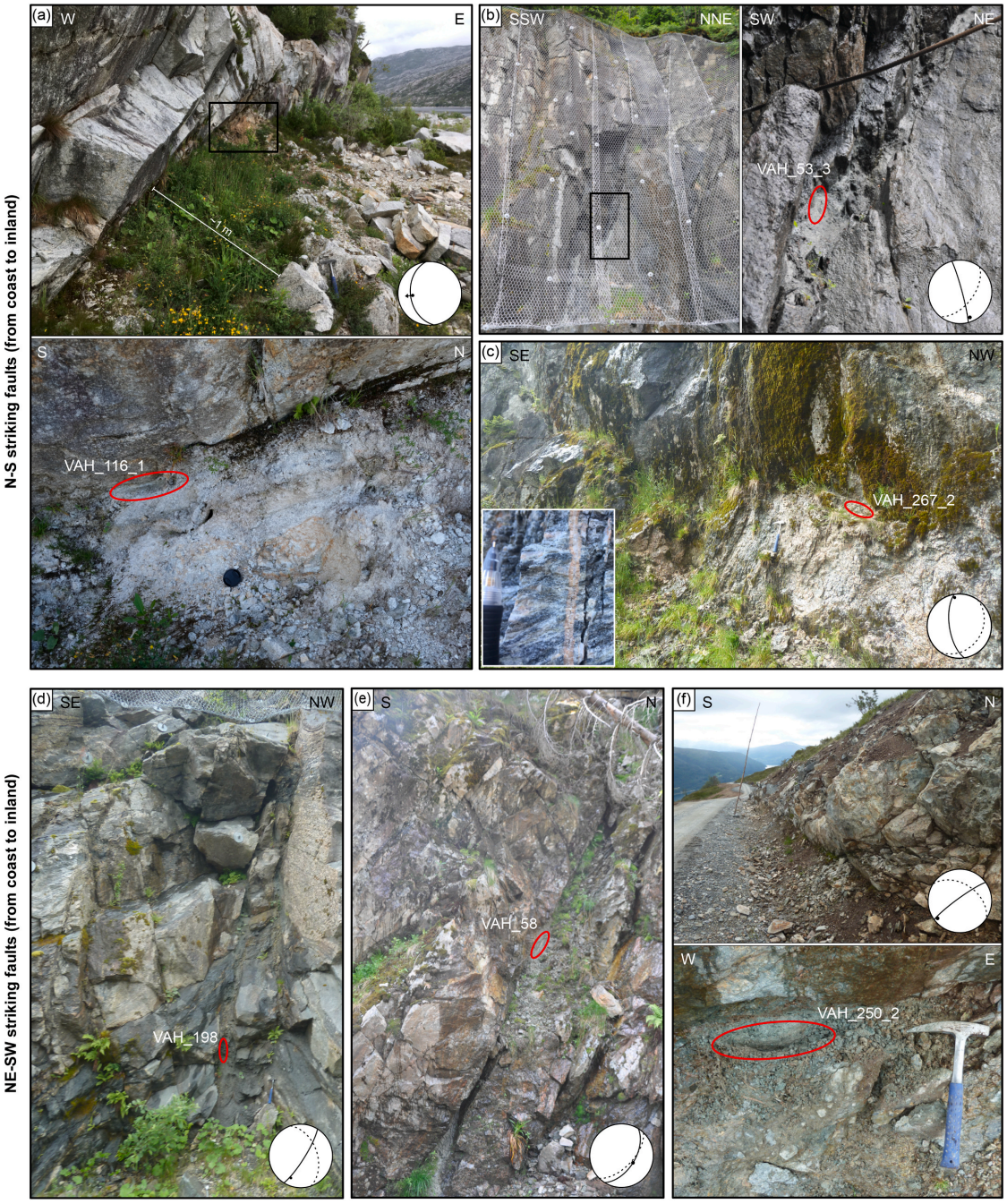

Fig. 6. Field photographs of dated (a–c) N–S striking faults and (d–f) NE-SW striking faults. The red circle marks the sample locality for K–Ar fault gouge dating. Stereoplots show structural measurements for each fault (stippled black great circle = foliation at sample location; black great circle = fault plane; black dot = slip line measured on host rock on the boundary to the sampled gouges; black arrow = observed kinematic indicators). (For interpretation of the references to colour in this figure legend, the reader is referred to the Web version of this article.)

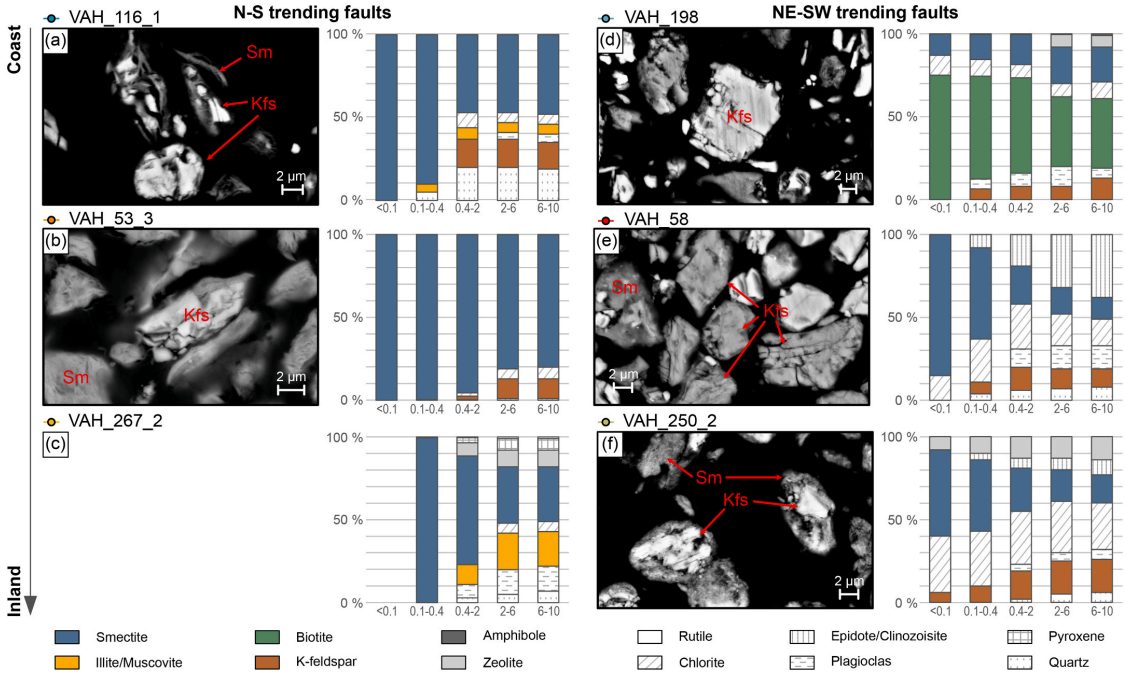

Fig. 7. XRD data from the dated gouge samples (cf. Supplementary 5 and 6) and corresponding BSE photographs of the 6–10 µm fractions. Minerals are indicated in red (Kfs = K-feldspar; Sm = smectite). (For interpretation of the references to colour in this figure legend, the reader is referred to the Web version of this article.)

surface. The coarser fractions of the sampled gouge contain epidote/clinozoisite, chlorite, smectite, plagioclase, K-feldspar and quartz, whereas the finest fraction consists mainly of smectite, with minor chlorite (Fig. 6e). BSE imagining from the coarsest fraction shows fractured and cracked K-feldspars (Fig. 6e). The K–Ar dates show an inclined age spectrum ranging from 191 ± 2 Ma for the coarsest fraction (6–10 µm) to 77 ± 1 Ma for the finest fraction (<0.1 µm) (Table 1, Fig. 8b).

4.3.2.3. VAH_250_2. Sample VAH_250_2 is from a fault zone exposed along the construction road to the top of the Loen skylift at the innermost Nordfjord (Fig. 1b). The host rock is a monzonitic augen gneiss with a foliation oriented 033/46. A 5–6 m long fault scarp is exposed along the road (Fig. 6f). The fault measures 336/60 and the slip line is 261-19. The fault shows strike-slip movement on a fault surface containing striated chlorite, quartz and white to orange zeolite, but kinematic indicators were not observed. The fault plane bends off from an about 2 m wide zone of cataclastic rock containing clasts of the host rock, epidote, chlorite, zeolite, K-feldspar, and calcite in a matrix of epidote, chlorite, zeolite, K-feldspar and quartz (Fig. 5k). The sampled gouge layer is 10–15 cm thick and is partly covered with superficial deposits (Fig. 6f). The coarser fractions of the sampled gouge contain chlorite, K-feldspar, smectite, zeolite, epidote/clinozoisite, plagioclase and quartz, whereas the finest grain size fraction consists of smectite, chlorite, zeolite and K-feldspar (Fig. 7f). BSE imaging of the coarsest fraction shows K-feldspar being replaced by smectite (Fig. 7f). The K–Ar dates show an inclined age spectrum ranging from 241 ± 3 Ma for the coarsest fraction (6–10 µm) to 129 ± 3 Ma for the finest fraction (<0.1 µm) (Table 1, Fig. 8b).

5. Interpretation

5.1. Interpretation of K–Ar fault gouge age spectra

In recent studies, the "Age Attractor Model" (Torgersen et al. 2015a; Viola et al. 2016) has been used to explain how an inclined age spectrum (K–Ar age vs. grain size fraction) defines a mixing curve between two end-members; the coarsest grain size fraction representing inherited host rock or early grown K-bearing minerals, and the finest grain size fraction representing K-bearing minerals formed under the last detectable faulting/fluid alteration event. The amount of authigenic K-bearing mineral phases increases with decreasing grain size and the finest fraction (here <0.1 µm) is generally interpreted to represent the last event of faulting (Torgersen et al., 2015a; Viola et al., 2016; Tartaglia et al., 2020). This model serves as a useful first-order interpretation, but several additional complexities have to be addressed when interpreting K–Ar age spectra as described in the following.

Firstly, all different K-bearing mineral phases which contribute to the age have to be identified, with possibly several inherited and several authigenic phases. Secondly, the effect of inherited K-bearing minerals from the host rock has to be estimated (e.g. Zwingmann et al. 2010), and thirdly, the possibility for fault reactivation and the generation of more than one phase of authigenic K-bearing minerals has to be taken into account (Torgersen et al., 2015a; Viola et al., 2016; Fossen et al., 2021).

5.1.1. K-bearing mineral phases

Our mineralogical dataset shows that the following K-bearing minerals can contribute to the K–Ar dates: K-feldspar (up to 20 wt% in some fractions), biotite (up to 65 wt% in some fractions), illite/muscovite (up to 22 wt% in some fractions), smectite (up to 100 wt% in some fractions), and zeolite (up to 14 wt% in some fractions). Biotite, illite/muscovite and K-feldspar have known average K-contents of 9 wt%, 6/

Table 1
Results from K–Ar fault gouge geochronology.

Sample	Sample locality (UTM 32)		Dip direction/ dip	Grain size fraction (μm)	^{40}Ar*				K			Age data	
	Easting	Northing			Mass mg	Mol/g	σ (%)	^{40}Ar* %	Mass mg	wt %	σ (%)	Age (Ma)	± σ (Ma)
VAH_53_3	347717	6869820	075/85	<0.1	2.284	6.254E-11	1.45	14.4	49.9	0.408	1.53	86.3	1.8
				0.1–0.4	2.302	9.577E-11	1.06	18.6	50.3	0.537	1.48	100.1	1.8
				0.4–2	1.624	2.028E-10	0.80	34.7	50.8	0.927	1.38	121.9	1.9
				2–6	2.084	2.679E-10	0.45	50.5	50.8	1.202	1.33	124.1	1.7
				6–10	1.622	2.818E-10	0.54	52.7	51.5	1.265	1.32	124.1	1.7
VAH_58	349682	6873671	122/55	<0.1	2.436	9.175E-11	0.92	28.2	50.2	0.672	1.44	77.1	1.3
				0.1–0.4	2.552	2.309E-10	0.42	57.9	50.4	1.208	1.33	107.0	1.5
				0.4–2	2.498	5.253E-10	0.31	85.6	51.5	1.857	1.25	156.1	1.9
				2–6	1.834	5.261E-10	0.37	90.0	51.4	1.605	1.28	179.7	2.3
				6–10	2.692	4.987E-10	0.30	91.5	49.7	1.427	1.31	191.1	2.4
VAH_116_1	286379	6856537	277/53	<0.1	1.082	1.832E-10	1.10	41.0	50.2	0.886	1.39	115.5	2.0
				0.1–0.4	2.504	4.845E-10	0.31	60.0	50.0	1.807	1.26	148.3	1.9
				0.4–2	1.978	7.797E-10	0.32	72.0	50.5	2.532	1.20	169.3	2.0
				2–6	1.196	7.407E-10	0.45	70.5	51.4	2.697	1.18	151.8	1.8
				6–10	1.686	7.139E-10	0.36	68.6	50.4	2.551	1.20	154.6	1.9
VAH_198	343457	6901544	122/80	<0.1	1.316	1.467E-09	0.39	72.0	50.2	4.458	1.10	180.4	2.0
				0.1–0.4	1.368	1.809E-09	0.37	77.6	50.1	4.595	1.09	213.9	2.3
				0.4–2	1.034	1.744E-09	0.46	77.6	50.3	4.318	1.10	219.0	2.5
				2–6	1.314	1.549E-09	0.39	77.4	50.7	4.197	1.11	201.2	2.2
				6–10	1.886	1.522E-09	0.31	77.9	49.7	4.278	1.11	194.3	2.1
VAH_250_2	385184	6863534	322/67	<0.1	1.548	1.002E-10	1.35	65.5	51.1	0.432	1.52	128.9	2.5
				0.1–0.4	2.182	2.400E-10	0.47	83.3	50.9	0.812	1.40	162.8	2.3
				0.4–2	1.144	6.577E-10	0.48	94.2	50.7	1.894	1.25	189.9	2.4
				2–6	1.796	9.386E-10	0.33	96.7	50.8	2.204	1.22	230.2	2.7
				6–10	1.588	9.876E-10	0.35	96.9	52.0	2.207	1.22	241.2	2.9
VAH_267_2	369092	6833464	261/65	<0.1									
				0.1–0.4	1.574	8.296E-11	1.57	60.6	35.9	0.290	1.66	157.9	3.5
				0.4–2	2.008	2.601E-10	0.47	81.0	52.3	0.662	1.43	213.4	3.0
				2–6	0.986	5.212E-10	0.59	89.0	50.4	1.221	1.33	230.7	3.2
				6–10	1.082	6.271E-10	0.51	89.3	50.5	1.410	1.31	239.9	3.1

10 wt% and 14 wt%, respectively (Barthelmy, 2014). Smectite and zeolite are generally considered not to contain K in their crystal structure (Howie et al., 1992). It is, however, common to find smectite intercalated with illite due to smectite illitization (Altaner and Ylagan, 1997), which can be difficult to identify with XRD analysis at low concentrations (Bense et al., 2014; Viola et al., 2016; Scheiber et al., 2019). For fractions consisting entirely of smectite, but giving a well-defined K–Ar date, we therefore assume that the K-content in these fractions can be assigned to illite interlayers in smectite.

5.1.2. The effect of inheritance

The gneisses of the WGR commonly contain K-feldspar, and this mineral is therefore an obvious candidate for inheritance in our samples. Dunlap and Fossen (1998) and Walsh et al. (2013) showed that the K-feldspar in the WGR cooled through ~400 °C at 400–330 Ma and through ~200 °C at 330–230 Ma. If a fraction consists solely of inherited K-feldspar, the K–Ar date should be the age at closure temperature (200–400 °C, Reiners et al. (2017)). Alternatively, K-feldspar might be an authigenic growth phase depending on fluid geochemistry and PT

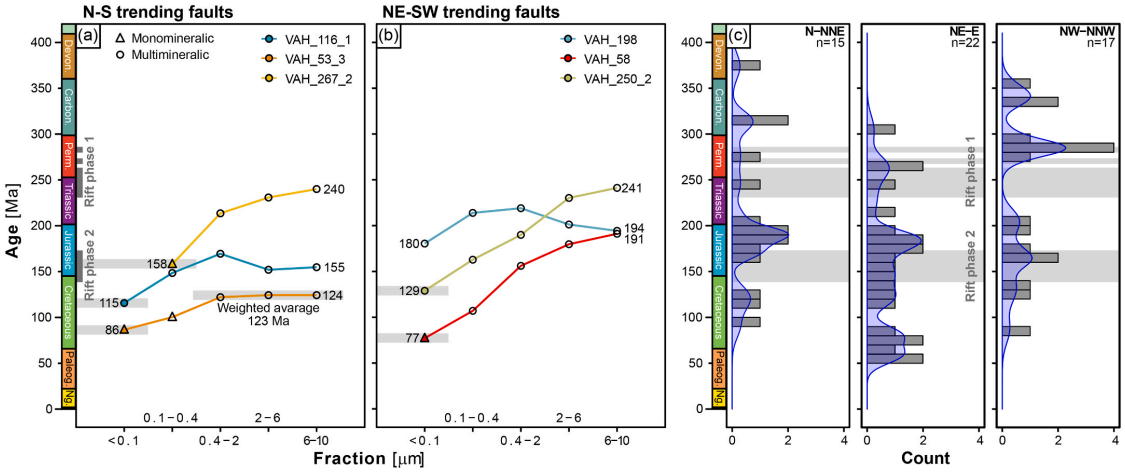

Fig. 8. K–Ar fault gouge data from (a) N–S striking faults and (b) NE-SW striking faults. Circles indicate fractions containing more than one K-bearing mineral phase while triangles indicate monomineralic fractions. Filled shapes and grey bars show interpreted ages of faulting events and maximum ages of faulting (see text for details). (c) Previously published K–Ar fault gouge ages from Western Norway containing both faulting events and maximum ages of faulting grouped by fault strike orientation (bin width 10 and Kernel distribution (bandwidth 10), modified from Fossen et al., 2021).

conditions during faulting (Brockamp and Clauer, 2013; Torgersen et al., 2015b). In this case, euhedral crystal growth might be expected. From BSE images, we see that the K-feldspars (at least in the coarsest fractions) in our samples do not show crystal faces, but are rather replaced by smectite or fractured and decomposed along edges, indicating that they might represent inherited grains. Finally, inherited K-feldspar might have isotopically re-equilibrated during faulting (Zwingmann et al., 2010), and might even show younger cooling ages than the actual timing of faulting if the faulting temperature was higher than the closure temperature of K-feldspar (Koehl et al., 2018).

Biotite is another candidate for inheritance and is abundant in sample VAH_198. Biotite is abundant in the host rock of this fault gouge, and it is therefore probable that at least some of the biotite is inherited. Earlier K–Ar biotite dating from within the study area showed cooling of biotite through 300 °C at about 340 Ma (Lux, 1985). K–Ar dating of biotite is, however, complicated (Kelley, 2002) and the interpretation of this age should be done with caution. If the biotite is inherited, we would expect to see the 340 Ma cooling age reflected in the K–Ar gouge data from the coarsest fraction. Authigenic formation of biotite in fault gouge has not been documented in the literature so far, but cannot be excluded depending on fluid chemistry and PT conditions during faulting.

Illite is commonly interpreted to represent an authigenic phase in fault gouges if located in crystalline and high-grade metamorphic rocks. Out of all the studied samples, VAH 267_2 appears to be the only one whose two coarsest fractions comprise 2M1 illite (Supplementary 6). Thus, we cannot rule out inheritance of host-rock muscovite. Muscovite is usually assumed to have an Ar closure temperature of ~350 °C (Harrison et al., 2009) and within the study area, muscovite ^{40}Ar–^{39}Ar ages are about 380–400 Ma (Chauvet and Dallmeyer, 1992; Walsh et al., 2013). If some inherited muscovite is present, we would expect to see the dates of the coarsest fractions to converge towards the muscovite cooling ages, potentially making the dates older than the actual faulting age. However, depending on the PT conditions of faulting, inherited muscovite might become isotopically reset during faulting (Zwingmann et al., 2010).

Smectite, like illite, is generally assumed to represent an authigenic phase in a gouge in magmatic or high-grade metamorphic host rocks, since it is a low-T mineral formed under diagenetic or hydrothermal processes (Reid-Soukup and Ulery, 2018).

Zeolite is a common product of low temperature (<250 °C) interaction between fluids and crustal rocks (Weisenberger and Bucher, 2010), and is therefore generally interpreted to represent an authigenic growth phase during low-temperature faulting. Zeolite has earlier been documented in fault zones in Norway (Tartaglia et al., 2020). Zeolites do commonly contain very little K, and we therefore assume the influence of zeolite on the K–Ar gouge dates to be minor.

5.1.3. *Fault reactivation*

Reactivation of a fault can potentially lead to several generations of authigenic illite/smectite growth, adding additional complexity to the already complex mixing between inherited and authigenic phases. Unravelling the contribution from inherited or partly re-equilibrated phases versus potentially several generations of authigenic phases is in many cases not unequivocally possible, and many K–Ar dates potentially represent mixed dates not representing any faulting event. We therefore in the following use a conservative approach, and state that some mixing cannot be ruled out even for the finest fractions.

5.1.4. *N–S striking faults*

5.1.4.1. VAH_116_1. In this sample, smectite, K-feldspar and illite/muscovite contribute to the K–Ar dates. The cracked and irregular K-feldspars partly replaced by smectite are interpreted to represent inherited grains from the host rock. The three coarser fractions that contain K-feldspar have similar mineralogical compositions and yield dates of 155 ± 2 Ma (6–10 μm), 152 ± 2 Ma (2–6 μm) and 169 ± 2 Ma (0.4–2 μm). These dates correspond mainly to K-feldspar and illite/muscovite in the samples, since those have a much higher K-content than smectite. Both K-feldspar and illite/muscovite might be either inherited from the host rock, (partially) reset or authigenic. We choose therefore not to attribute much significance to these dates. The two finer fractions contain smectite and illite/muscovite with dates of 148 ± 2 Ma (0.1–0.4 μm) and 115 ± 2 Ma (<0.1 μm). We interpret the date from the 0.1–0.4 μm fraction to result from mixed generations of authigenic illite and smectite, and the <0.1 μm fraction to reflect authigenic smectite with interlayered illite grown during faulting at 115 ± 2 Ma (Fig. 8a). Due to possible traces of illite/muscovite in this fraction, we consider this a maximum age of faulting.

5.1.4.2. VAH_53_3. In this sample, smectite and K-feldspar contribute to the K-content. Dates for the three coarser fractions are similar and plot around 123 ± 2 Ma. Earlier studies (e.g. Torgersen et al. 2015a, 2015b; Scheiber et al., 2019; Fossen et al., 2021) interpreted similar overlapping dates among fractions to represent an extensive faulting event. The K-content from smectite is minor compared to K-feldspar, indicating that the K-feldspar should have an important control on the resulting dates. BSE imaging (Fig. 7b) shows that K-feldspar in the 6–10 μm fraction gets replaced by smectite and does not show euhedral crystal shapes as expected if authigenic. That all three grain size fractions yielded identical ages within the age uncertainties, despite variable K-content, suggests that the K-feldspar was isotopically reset at c. 123 Ma, which we tentatively interpret as an earlier period of activity along this fault (Fig. 8a). Similar ages have been detected elsewhere in Western Norway (Fig. 8c, Supplementary 8) and it is also similar to the ca. 115 Ma faulting age from VAH_116 (see above). The two finer fractions contain only smectite, where we interpret the 0.1–0.4 μm fraction to be a mixed date rather than an individual faulting event and the youngest age of 86 ± 2 Ma (<0.1 μm) to represent an age of faulting (Fig. 8a).

5.1.4.3. VAH_267_2. VAH_267_2 did not yield an <0.1 μm fraction. The coarser fractions contain illite/muscovite, plagioclase and zeolite, whereas smectite is the only K-bearing mineral in the 0.1–0.4 μm fraction. The decreasing content of illite/muscovite with fraction size indicates that this might be an inherited muscovite component, which is further supported by the 2M1 illite in the coarsest fractions (Supplementary 6). We assume the K-contribution from plagioclase to be minor. The inherited muscovite, together with the inclined age spectrum indicates that the dates of the three coarser fractions represent mixed ages. We interpret the monomineralic finest fraction (0.1–0.4 μm) to represent authigenic smectite/illite growth during a faulting event at 158 ± 4 Ma (Fig. 8a).

5.1.5. NE–SW striking faults

5.1.5.1. VAH_198. In this sample, K-feldspar, biotite, zeolite and smectite are the K-bearing minerals contributing to the K–Ar dates. This sample has an unusual composition since it contains biotite in all fractions, with biotite content increasing towards smaller grain fractions. Biotite Ar cooling ages in the area are typically 400-380 Ma (Lux, 1985), which suggests that the biotite has to be at least partially reset or authigenic. K-feldspar is assumed to be inherited, as indicated by its fractured and craked appearance in BSE images of the 6–10 μm fraction (Fig. 6g). Based on the concave-up age spectrum and unusual mineralogy with uncertain proportions of inheritend and reset or authigenic biotite, the significance of any of the dates from this sample is uncertain (Fig. 8b).

5.1.5.2. VAH_58. In this sample, K-feldspar, smectite and potentially plagioclase are the only K-bearing minerals contributing to the K–Ar dates (Fig. 7e). From BSE images we see that the K-feldspar of the coarsest fraction is fractured, indicating an inherited origin. XRD analysis of VAH_58 shows that all fractions except the <0.1 μm fractions contain K-feldspar, and we assume these fractions to show mixed dates. The finest fraction (<0.1 μm), however, only contains smectite and we interpret the date of this fraction to represent authigenic smectite/illite growth during faulting at 77 ± 1 Ma (Fig. 8b).

5.1.5.3. VAH_250_2. In this sample, smectite, K-feldspar, potentially plagioclase and zeolite contribute to the K–Ar dates, where the amount of smectite increases and K-feldspar decreases with decreasing grain size (Fig. 7f). Together with BSE images showing K-feldspar replaced by smectite, this indicates that K-feldspar, at least partly, is inherited from the host rock. This indicates that all fractions containing both K-feldspar and smectite represent mixed dates, and even the finest fraction, which still contains ca. 6% K-feldspar, would be older than the main smectite growth event. However, assuming an inherited K-feldspar age of >240 Ma, and a minor K-contribution from smectite, the age of the authigenic smectite component would need to be unrealistically low to pull down the age of the finest fraction to 129 Ma. Therefore, we suspect that some of the K-feldspar in the finest fraction might be authigenic or reset, as also interpreted for a gouge sample of the Lærdal fault by Tartaglia et al. (2020). The presence of zeolite in the gouge indicates that temperatures during faulting could have been up to 250 °C, a temperature where K-feldspar can grow (e.g. Mark et al. 2008; Brockamp and Clauer 2013). The date of the finest fraction of 129 ± 3 Ma still needs to be regarded as a maximum age of faulting (Fig. 8b). The age overlaps with the 123 Ma age of sample VAH_53_3 (Fig. 8a) and with similar ages interpreted from other faults in the study area (Fig. 8c, Fossen et al., 2021).

5.2. Paleostress analysis

In an attempt to model the stress field(s) which led to the observed fault and fracture pattern in our study area, we performed paleostress analysis using the software WinTensor by Delvaux and Sperner (2003). To highlight different aspects of our data set, we applied two different approaches to sort and treat the structural data during paleostress analysis: 1) a station approach, and 2) a fault mineralization approach.

5.2.1. Station approach

The station approach is suited to show local variations and the potential effect of inheritance of trends from ductile precursor structures. We assigned our field measurements to 24 stations (Fig. 9). The measurements assigned to each station are located within less than 100 m distance from each other. The stations are colour-coded based on the relationship between brittle fracture and fault measurements and the main ductile foliation at that station (Fig. 9g): 1) if the measured fractures are mainly parallel to the foliation, the station is blue, 2) if the measured fractures mainly cut the foliation, the station is orange, and 3) if fractures are both parallel to and cutting the foliation, the station is red. In addition, grey stereoplot background indicates stations where faults and fractures are dominated by mica mineralizations and strained host rock (Fig. 9b–f). For each station, we conducted individual paleostress analyses (Fig. 9a–f). The resulting paleostress analyses show filled arrows (Fig. 9) for stress tensors derived from seven or more faults and fracture measurements, and for stress tensors with an average misfit angle (alpha) of 5° or less. Hollow arrows in Fig. 9 represent stress tensors derived from 5 to 6 fracture and fault measurements and an average misfit angle (alpha) higher than 5°, and are therefore considered less reliable. Details on these analyses and the mineralizations on fracture surfaces are found in the supplementary material (Supplementary 7).

A total of 24 local stress tensors with R' classification were inferred, whereof seven are extensional, seven are transtensional, five are transpressional, four are strike-slip, and one is compressional (Fig. 9). Of the six transpressional and compressional local stress tensors, all except one (station 11) include fractures and faults parallel to the foliation, and five local stress tensors are from stations with mica/stretched host rock mineralizations indicating the formation of these local stress tensors under relatively high temperatures. Subarea B is dominated by extension (Fig. 9b), subarea F is dominated by transpression (Fig. 9f), whereas the other subareas are not dominated by a spesific stress tensor (Fig. 9a, c-e). From the 22 local stress tensors where the extension direction (σ_3) is (sub)horizontal (excluding station 17 and 18), 14 have σ_3 plotting in the NW–SE sector and 7 have σ_3 plotting more or less E–W, whereas 3 have σ_3 plotting in the SW–NE sector.

5.2.2. Fault mineralization approach

The fault mineralization approach is suited to potentially unravel the relative timing of different paleostress fields, by modelling the local

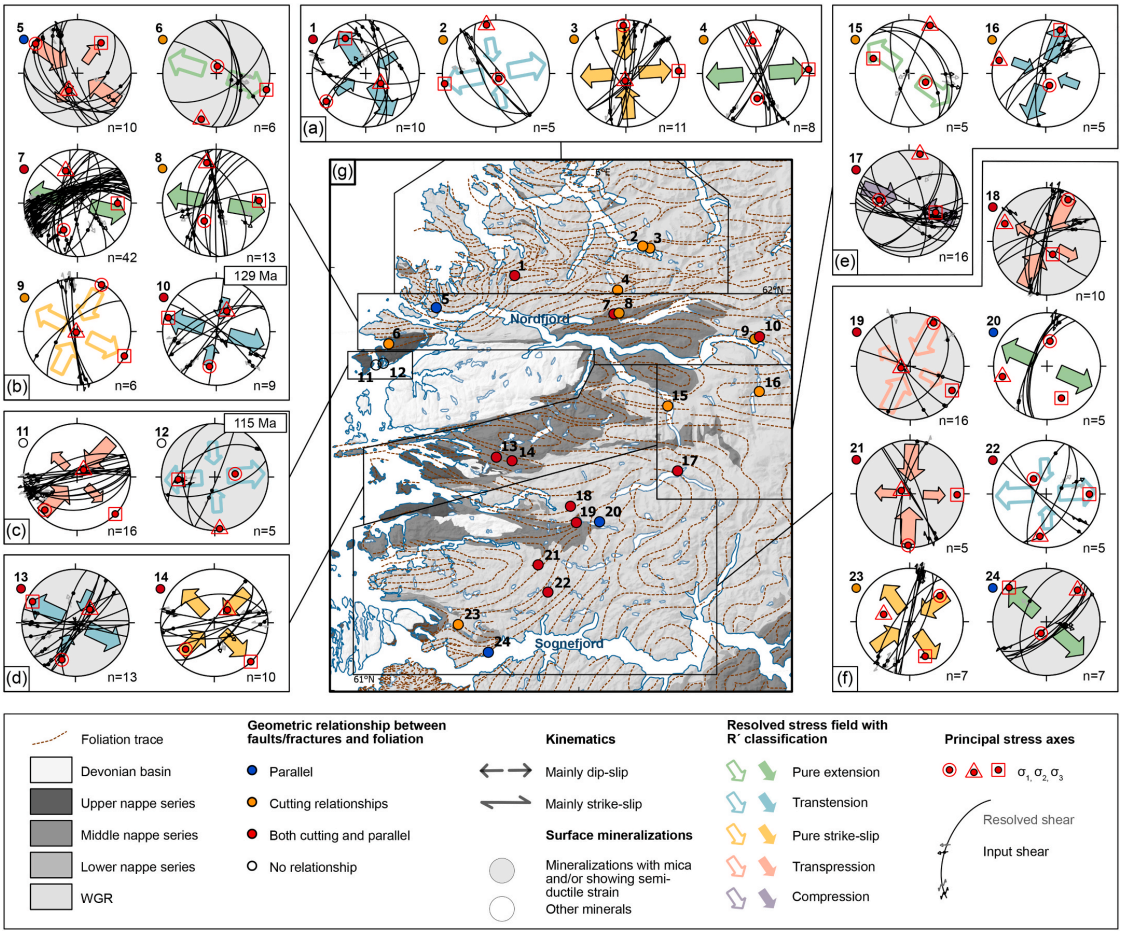

Fig. 9. (a–f) Results from paleostress analysis based on dividing the study area into 24 stations (station approach). (g) Tectonic map with foliation traces. Points mark the location of the station and colours indicate the relationship between foliation and fractures. Background arrows in stereoplots indicate the type of resolved stress field based on R′ classification (hollow arrows indicate local stress tensors with 5 to 6 surfaces included; filled arrows represent local stress tensors with 7 or more surfaces included, or local stress tensors with average misfit angle of 2–5° (supplementary 7)). (For interpretation of the references to colour in this figure legend, the reader is referred to the Web version of this article.)

stress tensors based on fault and fracture mineralization (Fig. 10). In this approach, it is assumed that higher temperature mineralizations such as mica and semi-ductile strained fracture surfaces formed earlier than lower-temperature mineralizations such as zeolite and calcite. This relationship is confirmed by the observation of zeolite and calcite mineralizations having crystallized on top of higher temperature epidote, chlorite and quartz mineralization. Slip lines are often not observed on zeolite and calcite, but rather on epidote, chlorite or quartz. The general absence of slip lines implies that zeolite and calcite mostly crystallized on fractures formed during earlier faulting, and kinematic indicators associated with these faults and fractures are derived from the earlier mineralizations. Therefore, the resulting local stress tensors do not indicate the stress field for the time of calcite formation, but rather indicate what surfaces were reactivated during the time of mineralization. Details on the resulting stress tensors can be found in the supplementary material (Supplementary 7).

Similar to the station approach, we chose local stations with sufficient measurements for each of the mineral groups to obtain a local stress tensor. Note that the measurements included within one station are from a slightly larger area (<2 km, within the same rock types) than for the station approach. Local stations containing high T mineralizations and semi-ductile features, such as SHR, fit into two main local stress tensors: an extensional stress tensor with NW–SE to WNW–ESE extension direction, and a compressional stress tensor with NW–SE compression direction (Fig. 10a). The local stations containing epidote, chlorite and quartz surfaces show three main trends: compressional stress tensor with NW–SE compression direction, transpressional stress tensor with NW-SE compression direction, and strike slip local stress tensors with NW–SE to E–W σ_3 direction (Fig. 10b). The local stations with zeolite measurements show strike-slip and extensional local stress tensors with WNW–ESE σ_3 direction (Fig. 10c).

5.3. Combining paleostress and geochronology

To correlate our fault gouge ages with the modelled paleostress regimes, we identified the local stress tensors to which the fault planes for

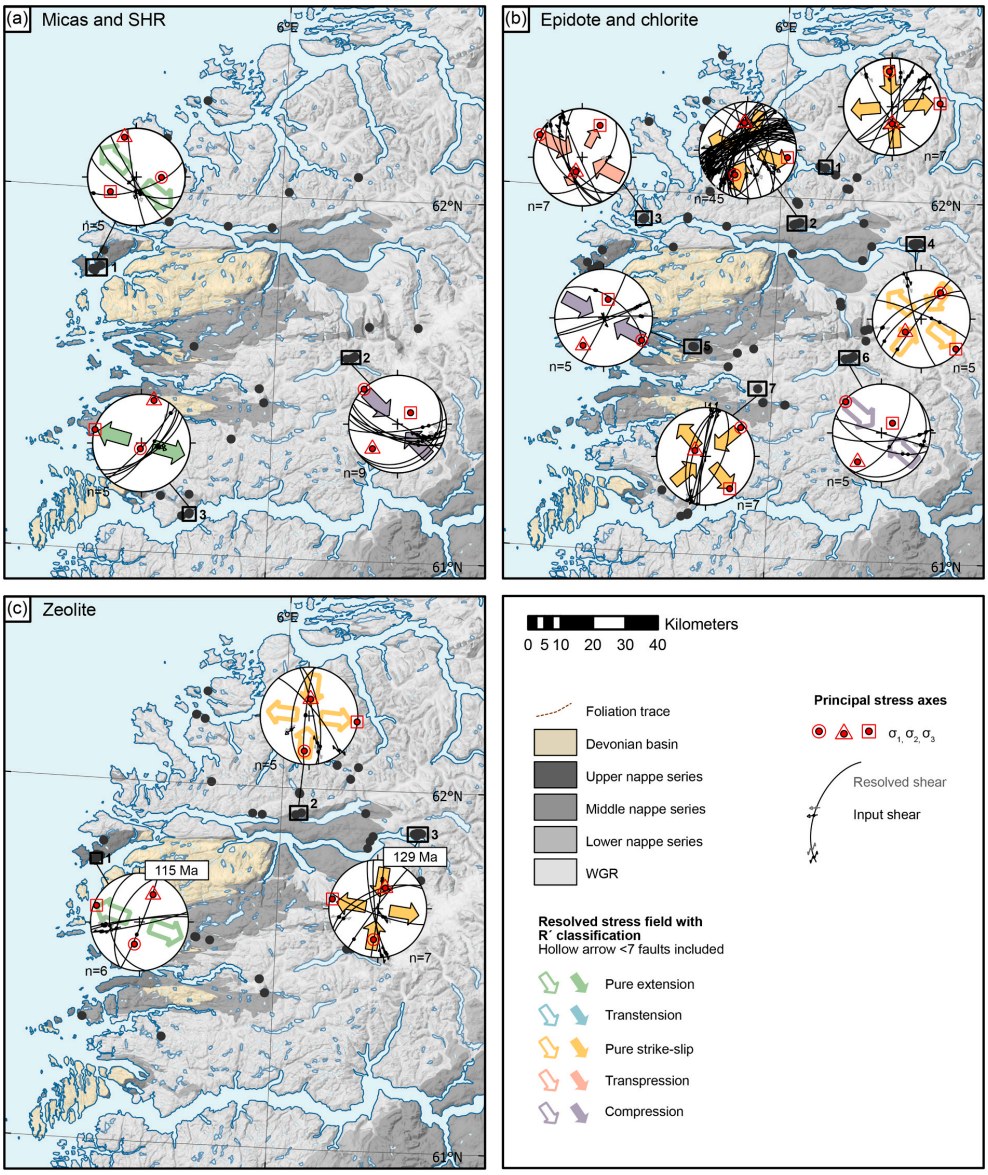

Fig. 10. Paleostress analysis based on fault and fracture mineralizations. Hollow arrows indicate local stress tensors with 5 to 6 surfaces included; filled arrows represent local stress tensors with 7 or more surfaces included, or local stress tensors with average misfit angle of 2–5° (supplementary 7). (a) Analysis of surfaces containing semi-ductile strained fracture and fault surfaces (SHR) and mica mineralization, some also together with chlorite, epidote, and/or quartz. (c) Analysis of surfaces containing chlorite and epidote mineralization, some also together with SHR and mica, zeolite and/or calcite. (d) Analysis of surfaces containing zeolite mineralization, some also together with chlorite, epidote, quartz, and/or calcite.

each dated fault were assigned in the two different paleostress approaches (Figs. 9 and 10). Note that the sense of slip observed on a fault's plane might not be directly related to the event of faulting which caused the authigenesis of the dated mineral phases. Only two of the dated faults fit into a local stress tensor, namely VAH_250_2 (maximum age of faulting 129 Ma) and VAH_116_1 (maximum age of faulting 115 Ma). In the station approach (Fig. 9), VAH_250_2 is represented in station 10, showing transtension with WNW–ESE σ_3 direction, whereas VAH_116 is included in station 12, showing transtension with E–W σ_3 direction. For the fault mineralization approach (Fig. 10) both VAH_250_2 and VAH_116_1 contain striated zeolite on the fault plane surface. VAH_250_2 is included in a stress tensor showing strike-slip with a WNW–ESE σ_3 direction (Fig. 10c), and VAH_116_1 in a local stress tensor showing extension with WNW–ESE σ_3 direction (Fig. 10c).

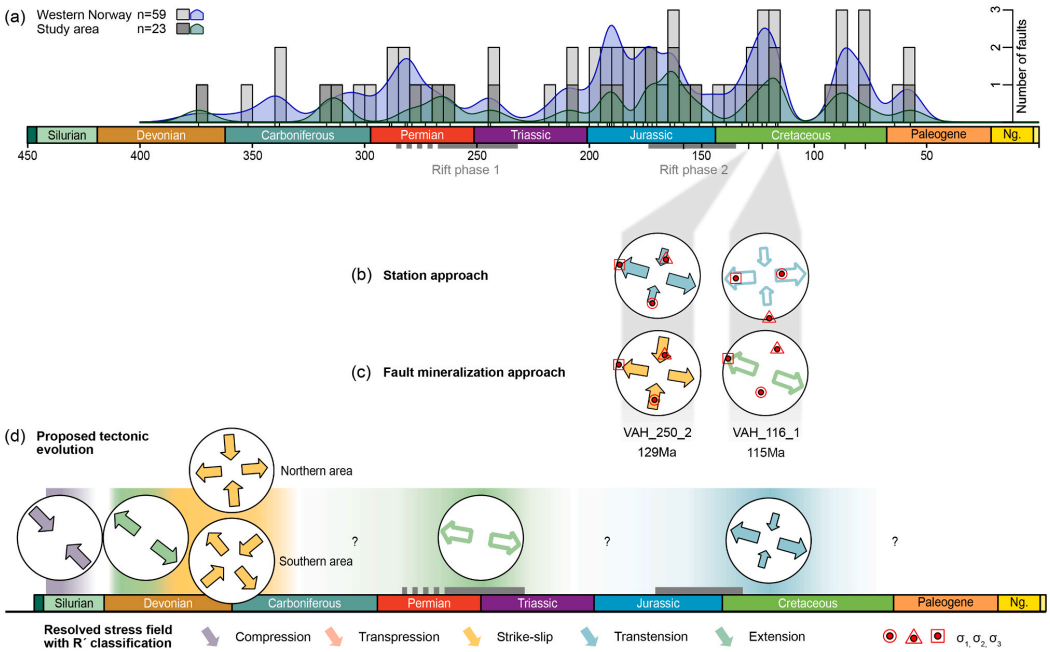

Fig. 11. (a) Histogram (bin width 5 and Kernel distribution (bandwidth 5) of K–Ar fault gouge ages from Western Norway that have been interpreted as constraining fault activity (modified after Fossen et al., 2021, Supplementary 8). Ages from previous studies outside the study area are shown in light grey bars and blue Kernel distributions, whereas ages from within the study area (own and existing data) are shown with dark grey bars and green kernel distribution. The probability density plots include both faulting event and maximum ages of faulting. (b–c) Correlation of fault gouge ages with two different approaches for paleostress analysis. (b) Station approach from Fig. 9 and (c) fault mineralization approach from Fig. 10. (e) Proposed tectonic evolution from Silurian to end-Cretaceous. (For interpretation of the references to colour in this figure legend, the reader is referred to the Web version of this article.)

Comparing these two approaches, it appears that they nicely match and complement each other. The local stress tensor implies that the local stress regime had a WNW–ESE σ_3 direction in the Early Cretaceous (129–115 Ma).

6. Reconstruction of the post-Caledonian brittle evolution

Our data set represents the first systematic investigation of brittle fault mineralizations between Sognefjorden and the Møre Margin (Fig. 1), allowing us to establish relative timing based on formation conditions of the different mineralizations. In the following, we first discuss the relative timing of the lineament and fracture networks, followed by the brittle evolution of the study area from pre-Devonian times to the Cretaceous. Here, we integrate the results from our lineament mapping, fault mineralization mapping, K–Ar dating and paleostress analysis with information from the literature.

6.1. Nature and relative age of fracture networks

From lineament studies and field data of fractures and faults, we detected two major trends in the fracture network striking N–S and NE–SW, and two minor trends striking NW–SE and E–W (Fig. 3b and c). The NE–SW-striking fractures and faults represent a dominating lineament- and fracture set in the study area (Fig. 3b and c) and their strike is in many places parallel or subparallel to the ductile foliation related to the NDSZ, NSZ and MTFC (Figs. 2 and 3). In metamorphic terranes, it is commonly known that brittle structures often develop by geometrically following planar ductile discontinuities in the bedrock (e.g. Butler et al. 2008; Massironi et al. 2011; Williams et al. 2019). We do, however, also observe extensive NE–SW-striking fractures and faults in the Bremanger granodioritic complex (Fig. 3, subarea C). Since the Bremanger granodiorite lacks any ductile deformation features, these faults must have either formed as a continuation of the (inherited) structures outside the granodiorite or they formed according to the given stress field affecting the isotropic granodiorite body. Similarly to the NE–SW fractures and faults discussed above, the E–W trending fractures and faults follow ductile precursors in several subareas (Figs. 2 and 3).

The N–S trending fractures and faults in contrast seem to represent a newly formed conjugate set, without any ductile precursor (Figs. 2 and 3). These N–S fractures and faults are dominant in most subareas (Fig. 3b), and N–S striking lineaments are often related to large-scale valleys, particularly in the inner Nordfjord area (Fig. 2, subarea E). These N–S striking lineaments have earlier been shown to be the most dominant lineament feature, both mainland and offshore Norway (e.g. Gabrielsen et al. 2002). The origin of this important fracture and fault trend has been debated. It has been speculated that these features follow long-lived Proterozoic zones of weakness (Gabrielsen et al., 2018). However, most of the N–S features cut the earlier ductile Caledonian foliation, and do not seem to follow any older shear belts. Several of the main N–S striking fault zones (e.g., Votedalen) formed within late Sveconorwegian intrusions (980–930 Ma; Wang et al., 2021) with only weak ductile Caledonian overprint, supporting a post-Caledonian origin for these N–S trending brittle features.

Our K–Ar fault gouge geochronology from the N–S trending faults indicates faulting activity during the Jurassic to Cretaceous ca. 158, 123–115 and 86 Ma (Fig. 8a). Other K–Ar gouge ages from Western Norway indicate that some of these N–S striking faults were also active earlier, in Devonian, Carboniferous and Permian-Triassic times, but

mostly during the Jurassic (Fig. 8c, Ksienzyk et al., 2016; Scheiber and Viola, 2018; Fossen et al., 2021). These studies often relate the N–S structural trend to rift structures formed during E–W extension (e.g. Fossen et al., 2017; Gabrielsen et al., 2018). Offshore, similar observations have been made, where N–S striking extensional structures formed during the rifting in the northern North Sea (e.g. Bartholomew et al. 1993; Doré et al. 1997; Reeve et al. 2015).

Interestingly, the majority of N–S striking faults and fractures in our data set does not show dip-slip movement as inferred from onshore and offshore interpretations but is rather dominated by strike-slip kinematics (Fig. 2). If these N–S striking fractures and faults originally formed during E–W extension as inferred during earlier studies, the faults must have been reactivated at a later stage creating the strike-slip kinematics. We interpret this as rather unlikely for the following reasons: very few fractures and faults having this orientation show dip-slip kinematics, the strike-slip kinematics are found throughout the region, and the faults and fractures have mostly subvertical dips, which is atypical for dip-slip faults. The N–S fractures and faults are therefore interpreted to have mostly been formed well before the Jurassic rifting episode, possibly as early as the Late Devonian-early Carboniferous (Fig. 11d). In the following, we will attempt to reconstruct the post-Caledonian brittle evolution based on previous work, the fault mineralization approach and the dated K–Ar fault gouges.

6.2. Silurian to Early-Devonian (Caledonian) compression

The probably oldest mineralizations are represented by stretched micas and/or semi-ductile strained host rock minerals, often together with epidote/chlorite/quartz, indicating relatively high temperature during formation. From the station approach, five out of six stations with compressional or transpressional local stress tensors contain such surfaces (Fig. 9), indicating that at least some of these structures might have formed during Caledonian compression/transpression (Fig. 11d). Similar compressional local stress tensors are found in the fault mineralization approach (Fig. 10a and b). Compressional stress fields have been recorded from the ca. 460 Ma Rolvsnes granodiorite on Bømlo further south (Scheiber et al., 2016). There, stretched mica revealed ^{40}Ar–^{39}Ar-dates of ca. 450 Ma formed under a NNW–SSE transpressional stress field, whereas faults related to dykes intruding at 435 Ma formed under WNW–ESE shortening. Caledonian compression was probably ongoing in our region until a switch to syn- and post-collisional extension occurred at around 400 Ma (Fossen, 2010).

6.3. Middle to Late Devonian NW–SE extension in an overall transtensional system

Apart from the compressional local stress tensors, high-T mineralizations also fit into ENE–WSW to NW–SE extensional/transtensional local stress tensors (Figs. 9 and 10a). These features could be early post-Caledonian structures formed in the Middle to Late Devonian, around 400–370 Ma, when rocks passed through the muscovite closure temperature in the region, as interpreted by Walsh et al. (2013). NW–SE extension and brittle faulting in Early to Middle Devonian has been described from the Bergen area (Fossen and Dunlap, 1998; Larsen et al., 2003) and further south (Scheiber and Viola, 2018). The NW–SE extensional stress field is in accordance with early post-Caledonian penetrative ductile extension which was generally oriented towards the NW (mode I back-sliding, Fossen, 1992, 2010). The penetrative ductile extension was followed by a more localized (mode II) extension focused on large-scale shear zones, equally with top-NW shear sense in the south (Hardangerfjord shear zone, Jotun Detachment, Fossen, 1992; 2010). However, in our study area, the ductile extension direction is oriented towards the W along the NSD and top-to-the-WSW along the sinistral MTFZ (Fossen, 1992, 2010; Seranne, 1992; Osmundsen and Andersen, 2001), interpreted to be the result of a large-scale transtensional system in the Middle to Late Devonian (Krabbendam and Dewey, 1998). In such a transtensional system, our derived NW–SE extensional stress field could be explained as representing the orthogonal stretching direction in a strain-partitioned system, with the strike-slip component taken up along strands of the MTFZ (Krabbendam and Dewey, 1998).

6.4. Late Devonian to early Carboniferous strike-slip

Fractures and faults coated with epidote, chlorite, and quartz are the most common in the region (Fig. 4). These minerals form under a wide range of temperatures of ca. 400–100 °C (e.g. Bird and Spieler 2004; Inoue et al. 2009). Given the relatively slow cooling of the entire region (Dunlap and Fossen, 1998; Ksienzyk et al., 2014; Scheiber et al., 2016), the area stayed at temperatures of ca. 400–100 °C from the Devonian until at least the beginning of the Mesozoic, and fractures and faults containing these mineralizations could therefore have formed and/or could have been reactivated during a long time span. In Western Norway, faults containing similar mineralizations have been interpreted to have formed and been reactivated from the Late Devonian-early Carboniferous to the Permian, with possible Mesozoic reactivation (e.g. Braathen, 1999; Larsen et al., 2003; Walsh et al., 2013).

The most prominent local stress tensors obtained from the fault mineralization approach represent strike-slip regimes (R' = 1.43–1.75) with a E–W to NW–SE σ_3 direction and a N–S to NE–SW σ_1 direction (Fig. 10b). Based on paleocurrent and structural analysis of the Devonian Kvamshesten basin, Osmundsen et al. (1998) proposed a model where NW–SE extension and perpendicular NE–SW shortening was overprinted by younger W–E extension and perpendicular N–S shortening from the Middle Devonian to the early Carboniferous, indicating two independent stress fields through time, with the σ_3 direction rotating anticlockwise from NW to W through time. Alternatively, Osmundsen and Andersen (2001) proposed a model where the change in orientation of the extension and shortening directions mainly depends on the distance from the MTFZ, similar to the strain-partitioned transtensional model proposed by Krabbendam and Dewey (1998). From the fault mineralization approach (Fig. 10b), we see that the σ_3 orientation turns into an E–W trend when approaching the MTFC, whereas the stations towards Sognefjorden in the south show a tendency to a NW–SE trending σ_3. The same trends are partially reflected in the station approach (Fig. 9), which indicates a changing stressfield depending on the distance from the MTFC in Late Devonian and early Carboniferous, as proposed by Osmundsen and Andersen (2001) (Fig. 11d).

6.5. Permian E–W extension (rift phase 1)

A few E–W pure extensional local stress tensors are present in the station approach. These local stress tensors are dominated by fractures striking N–S and NE–SW showing normal dip-slip to oblique-slip kinematics. Similar approximately E–W to ENE–WSW extensional stress fields are well known from SW Norway and along the Møre margin, and have earlier been interpreted to first initiate in the Permian and Early Triassic during rift phase 1 (e.g. Torsvik et al., 1997; Fossen and Dunlap, 1998; Walsh et al., 2013; Fossen et al., 2017; Theissen-Krah et al., 2017; Scheiber and Viola, 2018). The W-plunging Dalsfjord fault (Eide et al., 1994) shows Permian ages from palaeomagnetic and ^{40}Ar–^{39}Ar dating, and K–Ar fault gouge ages from Western Norway show a peak of activity in the early to mid Permian (Ksienzyk et al., 2016; Viola et al., 2016; Scheiber et al., 2019; Fossen et al., 2021) (Figs. 8c and 12a). Interestingly, this elsewhere important phase does not seem to be very prominent in our data set. Only few measurements fit into such purely extensional E–W stress fields in the station approach, none in the fault mineralization approach (Figs. 9 and 10), and none of our K–Ar gouge dates are present from this time span (Fig. 8).

6.6. Late Jurassic to Late Cretaceous WNW–ESE transtension

All our four monomineralic K–Ar fault gouge ages, the tentative

faulting age of 123 Ma and the two maximum ages of faulting fall into the Late Jurassic to Late Cretaceous (Figs. 8 and 11). Five of the six ages post-date the well-known Middle Jurassic to Early Cretaceous rift phase 2 (Fig. 11a; Gabrielsen et al., 1999; Viola et al., 2016; Fossen et al., 2017). Rift phase 2 probably represents crustal stretching, but the orientation of the stress field during this phase is debated, from NW–SE or E–W extension (e.g. Bartholomew et al., 1993; Færseth, 1996; Færseth et al., 1997; Reeve et al., 2015), or rotation from E–W extension to NW–SE extension to NE–SW extension (e.g. Doré et al., 1997; Davies et al., 2001). Our oldest sample VAH_267_2 (158 Ma), associated with zeolite mineralization, does not fit into any of the local stress tensors from the fault mineralization approach (Fig. 10). However, the clear strike-slip kinematics of the fault (subhorizontal slip lines) indicates that this fault is not a typical dip-slip rift-related structure.

The five younger ages overlap with what seems to be two regional faulting events when combined with K–Ar fault gouge ages documented onshore by others at around 130–110 Ma (Ksienzyk et al., 2016; Viola et al., 2016; Scheiber and Viola, 2018; Tartaglia et al., 2020; Fossen et al., 2021) and 90–70 Ma (Scheiber et al., 2019; Tartaglia et al., 2020; Fossen et al., 2021) (Fig. 11a). These Cretaceous faulting events have been interpreted as a response to hyperextension along the Mid-Norwegian margin, resulting in cooling and exhumation of the onshore area (Fossen et al., 2017; Ksienzyk et al., 2016; Viola et al., 2016; Scheiber and Viola, 2018; Tartaglia et al., 2020) and coincide with two periods of suggested tectonic activity in the Norwegian Sea (Færseth and Trond, 2002; Theissen-Krah et al., 2017). Two of the dated gouges, VAH_250_2 and VAH_116_1, show kinematics with a E–W to WNW–ESE trending σ_3 and extensional to strike-slip stress tensors. The kinematics and resulting stress tensor could be partly inherited from the previous strike-slip stress tensor derived from epidote-chlorite-quartz mineralizations, but since some of the dated faults also contain striated zeolite and calcite, we interpret the derived local stress tensor to represent the prevailing stress condition during the Cretaceous (Fig. 11d).

The VAH_267_2 (158 Ma) and VAH_116_1 (115 Ma) faults contain synkinematic zeolites, indicating that the widespread low-T zeolite mineralizations could be primarily of Late Jurassic to Cretaceous age. Similarly, the VAH_53_3 fault (123 and 86 Ma) contains striated calcite, supporting the field observation that calcite mineralizations generally are younger than the zeolite mineralizations, possibly being of mainly Cretaceous age, in accordance with the interpretation of Watts (2001).

7. Summary and conclusions

Our interpretation of brittle fault mineralizations, K–Ar fault gouge data and paleostress analyses reveal the following brittle evolution for the area between Sognefjorden and the Møre Margin (Fig. 12e):

(1) High-T fault surface minerals indicate NW–SE compression in the Late Silurian to Early Devonian, followed by NW–SE extension under semi-ductile conditions.
(2) Epidote-, chlorite- and quartz-bearing fractures and faults are interpreted to have initiated mainly in the Middle Devonian to early Carboniferous, representing two distinct paleostress fields: (1) NW–SE compression and, (2) strike-slip stress regimes with a changing σ_3 direction from NW–SE in the southern part of the region to E–W in the northern part of the region. The changing stress tensor is interpreted to be due to increasing strain partitioning closer to the MTFC.
(3) Only a limited number of epidote-, chlorite- and quartz-bearing fractures and faults fit into purely E–W extensional local stress regimes, and these could probably be related to rift phase 1 in the Permian to Early Triassic in the North Sea, though this phase seems not to be very prominent in our study area.
(4) All four K–Ar fault gouge ages and the two maximum ages of faulting fall into the Late Jurassic to Cretaceous, with only one age overlapping with the well-known Late Jurassic offshore rift phase 2. The other five ages constrain two younger extensive faulting events under a WNW–ESE transtensional stress regime with related fluid flow and precipitation of zeolite and calcite in Middle (123–115 Ma) and Late (86–77 Ma) Cretaceous times. These two faulting events can be related to periods of increased tectonic activity in the Norwegian Sea.

Our results show that the brittle architecture of the northern section of the passive margin of Western Norway is controlled by two dominant brittle precursor directions (NE–SW and E–W striking shear zones) as well as two newly formed, mainly strike-slip fault sets with conjugate orientations to the brittle precursors (N–S and NW–SE striking). The interpreted Late Devonian to early Carboniferous age of the N–S trending lineaments is different from previous models where the important N–S lineament population in Western Norway was interpreted to have mainly originated during Permo-Triassic or Jurassic E–W rifting. The domination of strike-slip fault sets is different from the mainly dip-slip controlled brittle architecture of the southern section of the passive margin south of Sognefjorden, indicating a more prominent transtensional/strike-slip regime from the Late Devonian onwards at the transition to the Møre margin. Our multi-method approach shows that detailed fault mineralization mapping is crucial for unravelling both kinematics and relative timing of brittle faulting, giving, combined with paleostress analysis, a more complete picture of the brittle evolution of the area than K–Ar fault gouge geochronology alone.

Author statement

Åse Hestnes: Conceptualization, Writing - Original Draft, Visualization, Formal analysis, Investigation. **Deta Gasser:** Conceptualization, Funding acquisition, Writing - Original Draft, Supervision, Investigation. **Thomas Scheiber:** Conceptualization, Funding acquisition, Writing - Review & Editing, Supervision, Investigation. **Joachim Jacobs:** Conceptualization, Funding acquisition, Writing - Review & Editing, Supervision, Investigation, Project administration. **Roelant van der Lelij:** Writing - Review & Editing, Formal analysis, Resources. **Jasmin Schönenberger:** Writing - Review & Editing, Formal analysis. **Anna Ksienzyk:** Writing - Review & Editing.

Funding

This work was funded by VISTA, a basic research programme in collaboration between The Norwegian Academy of Science and Letters and Equinor (grant number 6274).

Declaration of competing interest

The authors declare the following financial interests/personal relationships which may be considered as potential competing interests:
Åse Hestnes reports financial support was provided by VISTA.

Acknowledgements/Funding

We are grateful for thorough reviews by José L. Simón and Sam Haines, which improved the manuscript greatly. We thank Espen Torgersen and Tim Redfield for providing us with vertical derivative maps based on DTMs for lineament analysis. Irene Heggstad at UiB helped with imaging.

Appendix A. Supplementary data

Supplementary data to this article can be found online at https://doi.org/10.1016/j.jsg.2022.104621.

References

Altaner, S.P., Ylagan, R.F., 1997. Comparison of structural models of mixed-layer illite/smectite and reaction mechanisms of smectite illitization. Clay Clay Miner. 45, 517–533. https://doi.org/10.1346/CCMN.1997.0450404.

Andersen, T.B., Torsvik, T.H., Eide, E.A., Osmundsen, P.T., Faleide, J.I., 1999. Permian and Mesozoic extensional faulting within the Caledonides of central south Norway. J. Geol. Soc. 156, 1073–1080. London.

Angelier, J., 1984. Tectonic analysis of fault slip data sets. J. Geophys. Res. Solid Earth 89, 5835–5848. https://doi.org/10.1029/JB089iB07p05835.

Angelier, J., 1979. Determination of the mean principal directions of stresses for a given fault population. Tectonophysics 56. https://doi.org/10.1016/0040-1951(79)90081-7.

Barthelmy, D., 2014. Webmineral [WWW document]. http://webmineral.com/ accessed 12.17.21.

Bartholomew, I.D., Peters, J.M., Powell, C.M., 1993. Regional structural evolution of the North Sea: oblique slip and the reactivation of basement lineaments. In: Petroleum Geology Conference Proceedings, 4, pp. 1109–1122. https://doi.org/10.1144/0041109.

Bense, F.A., Wemmer, K., Löbens, S., Siegesmund, S., 2014. Fault gouge analyses: K-Ar illite dating, clay mineralogy and tectonic significance-a study from the Sierras Pampeanas, Argentina. Int. J. Earth Sci. 103, 189–218. https://doi.org/10.1007/s00531-013-0956-7.

Bird, D.K., Spieler, A.R., 2004. Epidote in geothermal systems. Rev. Mineral. Geochem. 56, 235–300. https://doi.org/10.2138/gsrmg.56.1.235.

Braathen, A., 1999. Kinematics of post-Caledonian polyphase brittle faulting in the Sunnfjord region, western Norway. Tectonophysics 302, 99–121. https://doi.org/10.1016/S0040-1951(98)00281-9.

Braathen, A., Osmundsen, P.T., Gabrielsen, R.H., 2004. Dynamic development of fault rocks in a crustal-scale detachment: an example from western Norway. Tectonics 23, 1–21. https://doi.org/10.1029/2003TC001558.

Brockamp, O., Clauer, N., 2013. Hydrothermal and unexpected diagenetic alteration in Permian shales of the Lodève epigenetic U-deposit of southern France, traced by K-Ar illite and K-feldspar dating. Chem. Geol. 357, 18–28. https://doi.org/10.1016/j.chemgeo.2013.08.009.

Butler, R.W.H., Bond, C.E., Shipton, Z.K., Jones, R.R., Casey, M., 2008. Fabric anisotropy controls faulting in the continental crust. J. Geol. Soc. 165, 449–452. https://doi.org/10.1144/0016-76492007-129.

Chauvet, A., Dallmeyer, R.D., 1992. 40Ar/39Ar mineral dates related to Devonian extension in the southwestern Scandinavian Caledonides. Tectonophysics 210, 155–177. https://doi.org/10.1016/0040-1951(92)90133-Q.

Corfu, F., Andersen, T.B., 2002. U–Pb ages of the Dalsfjord Complex, SW Norway, and their bearing on the correlation of allochthonous crystalline segments of the Scandinavian Caledonides. Int. J. Earth Sci. 91, 955–963. https://doi.org/10.1007/s00531-002-0298-3.

Corfu, F., Andersen, T.B., Gasser, D., 2014. The Scandinavian Caledonides: main features, conceptual advances and critical questions, 390. Geological Society, London, Special Publications, pp. 9–43. https://doi.org/10.1144/SP390.25.

Davies, R.J., Turner, J.D., Underhill, J.R., 2001. Sequential dip-slip fault movement during rifting: a new model for the evolution of the Jurassic trilete North sea rift system. Petrol. Geosci. 7, 371–388. https://doi.org/10.1144/petgeo.7.4.371.

Delvaux, D., Sperner, B., 2003. New Aspects of Tectonic Stress Inversion with Reference to the TENSOR Program, 212. Geological Society Special Publication, pp. 75–100. https://doi.org/10.1144/GSL.SP.2003.212.01.06.

Doré, A.G., Lundin, E.R., Fichler, C., Olesen, O., 1997. Patterns of basement structure and reactivation along the NE Atlantic margin. J. Geol. Soc. 154, 85–92. https://doi.org/10.1144/gsjgs.154.1.0085.

Dunlap, W.J., Fossen, H., 1998. Early Paleozoic orogenic collapse, tectonic stability, and late Paleozoic continental rifting revealed through thermochronology of K-felsdspars, souther Norway. Tectonics 17, 604–620.

Eide, E.A., Torsvik, T.H., Andersen, T.B., 1994. Absolute dating of brittle fault movements: late Permian and late Jurassic extensional fault breccias in western Norway. Terra 9, 135–139. https://doi.org/10.1046/j.1365-3121.1997.d01-21.x.

Færseth, R.B., 1996. Interaction of permo-triassic and jurassic extensional fault-blocks during the development of the northern North Sea. J. Geol. Soc. 153, 931–944. https://doi.org/10.1144/gsjgs.153.6.0931.

Færseth, R.B., Knudsen, B.E., Liljedahl, T., Midbøe, P.S., Søderstrøm, B., 1997. Oblique rifting and sequential faulting in the Jurassic development of the northern North Sea. J. Struct. Geol. 19, 1285–1302. https://doi.org/10.1016/s0191-8141(97)00045-x.

Færseth, R.B., Trond, L., 2002. Cretaceous evolution in the Norwegian Sea - a period characterized by tectonic quiescence. Mar. Petrol. Geol. 19, 1005–1027. https://doi.org/10.1016/S0264-8172(02)00112-5.

Fossen, H., 2010. Extensional Tectonics in the North Atlantic Caledonides: a Regional View, 335. Geological Society Special Publication, pp. 767–793. https://doi.org/10.1144/SP335.31.

Fossen, H., 1992. The role of extensional tectonics in the Caledonides of south Norway. J. Struct. Geol. 14, 1033–1046. https://doi.org/10.1016/0191-8141(92)90034-T.

Fossen, H., Dunlap, W.J., 1998. Timing and kinematics of Caledonian thrusting and extensional collapse, southern Norway: evidence from 40Ar/39Ar thermochronology. J. Struct. Geol. 20, 765–781. https://doi.org/10.1016/S0191-8141(98)00007-8.

Fossen, H., Khani, H.F., Faleide, J.I., Ksienzyk, A.K., Dunlap, W.J., 2017. Post-Caledonian extension in the West Norway–northern North Sea region: the role of structural inheritance. Geological Society, London, Special Publications 439, 465–486. https://doi.org/10.1144/SP439.6.

Fossen, H., Ksienzyk, A.K., Rotevatn, A., Bauck, M.S., Wemmer, K., 2021. From widespread faulting to localised rifting: evidence from K-Ar fault gouge dates from the Norwegian North Sea rift shoulder. Basin Research bre 12541. https://doi.org/10.1111/bre.12541.

Furnes, H., Skjerlie, K.P., Pedersen, R.B., Andersen, T.B., Stillman, C.J., Suthren, R.J., Tysseland, M., Garmann, L.B., 1990. The Solund—Stavfjord Ophiolite Complex and associated rocks, west Norwegian Caledonides: geology, geochemistry and tectonic environment. Geol. Mag. 127, 209–224. https://doi.org/10.1017/S0016756800014497.

Gabrielsen, R.H., Braathen, A., Dehis, J., Roberts, D., 2002. Tectonic lineaments of Norway. Nor. Geol. Tidsskr. 82, 153–174.

Gabrielsen, R.H., Nystuen, J.P., Olesen, O., 2018. Fault distribution in the precambrian basement of south Norway. J. Struct. Geol. 108, 269–289. https://doi.org/10.1016/j.jsg.2017.06.006.

Gabrielsen, R.H., Odinsen, T., Grunnaleite, I., 1999. Structuring of the northern Viking Graben and the Møre basin; the influence of basement structural grain, and the particular role of the Møre-Trøndelag Fault complex. Mar. Petrol. Geol. 16, 443–465. https://doi.org/10.1016/S0264-8172(99)00006-9.

Gómez, M., Vergés, J., Fernàndez, M., Torne, M., Ayala, C., Wheeler, W., Karpuz, R., 2004. Extensional geometry of the mid Norwegian margin before early tertiary continental breakup. Mar. Petrol. Geol. 21, 177–194. https://doi.org/10.1016/j.marpetgeo.2003.11.017.

Grathoff, G.H., Moore, D.M., 1996. Illite polytype quantification using WILDFIRE© Calculated X-ray diffraction patterns. Clay Clay Miner. 44, 835–842. https://doi.org/10.1346/CCMN.1996.0440615.

Grunnaleite, I., Gabrielsen, R.H., 1995. Structure of the Møre basin, mid-Norway continental margin. Tectonophysics 252, 221–251. https://doi.org/10.1016/0040-1951(95)00095-X.

Hacker, B.R., Andersen, T.B., Johnston, S., Kylander-Clark, A.R.C.C., Peterman, E.M., Walsh, E.O., Young, D., 2010. High-temperature deformation during continental-margin subduction & exhumation: the ultrahigh-pressure Western Gneiss Region of Norway. Tectonophysics 480, 149–171. https://doi.org/10.1016/j.tecto.2009.08.012.

Hacker, B.R., Andersen, T.B., Root, D.B., Mehl, L., Mattinson, J.M., Wooden, J.L., 2003. Exhumation of high-pressure rocks beneath the Solund basin, western gneiss region of Norway. J. Metamorph. Geol. 21, 613–629. https://doi.org/10.1046/j.1525-1314.2003.00468.x.

Hacker, B.R., Gans, P.B., 2005. Continental collisions and the creation of ultrahigh-pressure terranes: petrology and thermochronology of nappes in the central Scandinavian Caledonides. Bull. Geol. Soc. Am. 117, 117–134. https://doi.org/10.1130/B25549.1.

Hansen, J., Skjerlie, K.P., Pedersen, R.B., De La Rosa, J., 2002. Crustal melting in the lower parts of island acrs: an example from the Bremanger Granitoid Complex, West Norwegian Caledonides. Contrib. Mineral. Petrol. 143, 316–335. https://doi.org/10.1007/s00410-001-0342-5.

Harrison, T.M., Célérier, J., Aikman, A.B., Hermann, J., Heizler, M.T., 2009. Diffusion of 40Ar in muscovite. Geochem. Cosmochim. Acta 73, 1039–1051. https://doi.org/10.1016/j.gca.2008.09.038.

Howie, R.A., Zussman, J., Deer, W., 1992. An Introduction to the Rock-Forming Minerals. Longman London, UK.

Inoue, A., Meunier, A., Patrier-Mas, P., Rigault, C., Beaufort, D., Vieillard, P., 2009. Application of chemical geothermometry to low-temperature trioctahedral chlorites. Clay Clay Miner. 57, 371–382. https://doi.org/10.1346/CCMN.2009.0570309.

Kelley, S., 2002. Excess argon in K-Ar and Ar-Ar geochronology. Chem. Geol. 188, 1–22. https://doi.org/10.1016/S0009-2541(02)00064-5.

Koehl, J.P., Bergh, S.G., Wemmer, K., 2018. Neoproterozoic and Post-caledonian Exhumation and Shallow Faulting in NW Finnmark from K – Ar Dating and P/T Analysis of Fault Rocks, pp. 923–951.

Krabbendam, M., Dewey, J.F., 1998. Exhumation of UHP Rocks by Transtension in the Western Gneiss Region, Scandinavian Caledonides, 135. Geological Society Special Publication, pp. 159–181. https://doi.org/10.1144/GSL.SP.1998.135.01.11.

Ksienzyk, A.K., Dunkl, I., Jacobs, J., Fossen, H., Kohlmann, F., 2014. From orogen to passive margin: constraints from fission track and (U–Th)/He analyses on Mesozoic uplift and fault reactivation in SW Norway. Geological Society, London, Special Publications 390, 679–702. https://doi.org/10.1144/SP390.27.

Ksienzyk, A.K., Wemmer, K., Jacobs, J., Fossen, H., Schomberg, A.C., Süssenberger, A., Lünsdorf, N.K., Bastesen, E., 2016. Post-caledonian brittle deformation in the Bergen area, West Norway: results from K–Ar illite fault gouge dating. Nor. Geol. Tidsskr. 96, 275–299. https://doi.org/10.17850/njg96-3-06.

Kylander-Clark, A.R.C.C., Hacker, B.R., Johnson, C.M., Beard, B.L., Mahlen, N.J., Lapen, T.J., 2007. Coupled Lu-Hf and Sm-Nd geochronology constrains prograde and exhumation histories of high- and ultrahigh-pressure eclogites from western Norway. Chem. Geol. 242, 137–154. https://doi.org/10.1016/j.chemgeo.2007.03.006.

Labrousse, L., Jolivet, L., Andersen, T.B., et al., 2004. Pressure-temperature-time deformation history of the exhumation of ultra-high pressure rocks in the Western Gneiss Region, Norway. In: Special Paper of the Geological Society of America, 380, pp. 155–183. https://doi.org/10.1130/0-8137-2380-9.155.

Lacombe, O., 2012. Do fault slip data inversions actually yield " paleostresses" that can be compared with contemporary stresses? A critical discussion. Compt. Rendus Geosci. 344, 159–173. https://doi.org/10.1016/j.crte.2012.01.006.

Larsen, Ø., Fossen, H., Langeland, K., Pedersen, R.B., 2003. Kinematics and timing of polyphase post-Caledonian deformation in the Bergen area, SW Norway. Nor. Geol. Tidsskr. 83, 149–165. https://doi.org/10.1016/j.ajodo.2008.06.033.

Lux, D.R., 1985. K/Ar ages from the Basal Gneiss region, Stadlandet area, western Norway. Nor. Geol. Tidsskr. 65, 277–286.

Mark, D.F., Kelley, S.P., Lee, M.R., Parnell, J., Sherlock, S.C., Brown, D.J., 2008. Ar-Ar dating of authigenic K-feldspar: quantitative modelling of radiogenic argon-loss through subgrain boundary networks. Geochem. Cosmochim. Acta 72, 2695–2710. https://doi.org/10.1016/j.gca.2008.03.018.

Massironi, M., Bistacchi, A., Menegon, L., 2011. Misoriented faults in exhumed metamorphic complexes: rule or exception? Earth Planet Sci. Lett. 307, 233–239. https://doi.org/10.1016/j.epsl.2011.04.041.

Mattila, J., Viola, G., 2014. New constraints on 1.7Gyr of brittle tectonic evolution in southwestern Finland derived from a structural study at the site of a potential nuclear waste repository (Olkiluoto Island). J. Struct. Geol. 67, 50–74. https://doi.org/10.1016/j.jsg.2014.07.003.

Orife, T., Lisle, R.J., 2006. Assessing the statistical significance of palaeostress estimates: simulations using random fault-slips. J. Struct. Geol. 28, 952–956. https://doi.org/10.1016/j.jsg.2006.03.005.

Osmundsen, P.T., Andersen, T.B., 2001. The middle Devonian basins of western Norway: sedimentary response to large-scale transtensional tectonics? Tectonophysics 332, 51–68. https://doi.org/10.1016/S0040-1951(00)00249-3.

Osmundsen, P.T., Andersen, T.B., Markussen, S., Svendby, A.K., 1998. Tectonics and sedimentation in the hangingwall of a major extensional detachment: the Devonian Kvamshesten Basin, western Norway. Basin Res. 10, 213–234. https://doi.org/10.1046/j.1365-2117.1998.00064.x.

Osmundsen, P.T.T., Eide, E.A.A., Haabesland, N.E.E., Roberts, D., Andersen, T.B.B., Kendrick, M., Bingen, B., Braathen, A., Redfield, T.F.F., 2006. Kinematics of the Høybakken detachment zone and the Møre–Trøndelag Fault complex, central Norway. J. Geol. Soc. 163, 303–318. https://doi.org/10.1144/0016-764904-129.

Redfield, T.F., Torsvik, T.H., Andriessen, P.A.M.M., Gabrielsen, R.H., 2004. Mesozoic and Cenozoic tectonics of the Møre Trøndelag Fault Complex, central Norway: constraints from new apatite fission track data. Phys. Chem. Earth 29, 673–682. https://doi.org/10.1016/j.pce.2004.03.005.

Redfield, T.F.F., Osmundsen, P.T.T., Hendriks, B.W.H.W.H., 2005. The role of fault reactivation and growth in the uplift of western Fennoscandia. J. Geol. Soc. 162, 1013–1030. https://doi.org/10.1144/0016-764904-149.

Reeve, M.T., Bell, R.E., Duffy, O.B., Jackson, C.A.L., Sansom, E., 2015. The growth of non-colinear normal fault systems; what can we learn from 3D seismic reflection data? J. Struct. Geol. 70, 141–155. https://doi.org/10.1016/j.jsg.2014.11.007.

Reid-Soukup, D.A., Ulery, A.L., 2018. Smectites. In: Dixon, J.B., Schulze, D.G. (Eds.), Soil Mineralogy with Environmental Applications, pp. 467–499. https://doi.org/10.2136/sssabookser7.c15.

Reiners, P.W., Carlson, R.W., Renne, P.R., Cooper, K.M., Granger, D.E., McLean, N.M., Schoene, B., 2017. Geochronology and Thermochronology. John Wiley & Sons, 2017.

Roberts, A.M., Yielding, G., Kusznir, N.J., Walker, I.M., Dorn- Lopez, D., 1995. Quantitative analysis of triassic extension in the northern Viking Graben. J. Geol. Soc. (Lond.) 152, 15–26. https://doi.org/10.1144/gsjgs.152.1.0015.

Roberts, D., Sturt, B.A., 1980. Caledonian deformation in Norway. J. Geol. Soc. 137, 241–250. https://doi.org/10.1144/gsjgs.137.3.0241.

Røhr, T.S., Bingen, B., Robinson, P., Reddy, S.M., 2013. Geochronology of paleoproterozoic augen gneisses in the western gneiss region, Norway: evidence for Sveconorwegian zircon Neocrystallization and caledonian zircon deformation. J. Geol. 121, 105–128. https://doi.org/10.1086/669229.

Røhr, T.S., Corfu, F., Austrheim, H., Andersen, T.B., 2004. Sveconorwegian U-Pb zircon and monazite ages of granulite-facies rocks, Hisarøya, Gulen, western gneiss region, Norway. Nor. Geol. Tidsskr. 84, 251–256.

Scheiber, T., Fredin, O., Viola, G., Jarna, A., Gasser, D., Łapińska-Viola, R., 2015. Manual extraction of bedrock lineaments from high-resolution LiDAR data: methodological bias and human perception. GFF 137, 362–372. https://doi.org/10.1080/11035897.2015.1085434.

Scheiber, T., Viola, G., 2018. Complex bedrock fracture patterns: a multipronged approach to resolve their evolution in space and time. Tectonics 37, 1030–1062. https://doi.org/10.1002/2017TC004763.

Scheiber, T., Viola, G., Lelij, R. Van Der, Margreth, A., Schönenberger, J., 2019. Microstructurally-constrained versus bulk fault gouge K - Ar dating. J. Struct. Geol. 127, 103868. https://doi.org/10.1016/j.jsg.2019.103868.

Scheiber, T., Viola, G., Wilkinson, C.M., Ganerød, M., Skår, Ø., Gasser, D., 2016. Direct40Ar/39Ar dating of late ordovician and Silurian brittle faulting in the southwestern Norwegian Caledonides. Terra. Nova 28, 374–382. https://doi.org/10.1111/ter.12230.

Seranne, M., 1992. Late Palaeozoic kinematics of the More-Trondelag fault zone and adjacent areas, central Norway. Nor. Geol. Tidsskr. 72, 141–158.

Seranne, M., Seguret, M., 1987. The Devonian basins of western Norway: tectonics and kinematics of an extending crust. Geological Society, London, Special Publications 28, 537–548. https://doi.org/10.1144/GSL.SP.1987.028.01.35.

Simón, J.L., 2019. Forty years of paleostress analysis: has it attained maturity? J. Struct. Geol. 125, 124–133. https://doi.org/10.1016/j.jsg.2018.02.011.

Skyttä, P., Torvela, T., 2018. Brittle reactivation of ductile precursor structures: The role of incomplete structural transposition at a nuclear waste disposal site, Olkiluoto. Finland: J. Struct. Geol. 116, 253–259. https://doi.org/10.1016/j.jsg.2018.06.009.

Steel, R., Ryseth, A., 1990. The Triassic — early Jurassic succession in the northern North Sea: megasequence stratigraphy and intra-Triassic tectonics. Geological Society, London, Special Publications 55, 139–168. https://doi.org/10.1144/GSL.SP.1990.055.01.07.

Talwani, M., Eldholm, O., 1972. Continental margin off Norway: a geophysical study. Geol. Soc. Am. Bull. 83, 3575–3606.

Tartaglia, G., Viola, G., van der Lelij, R., Scheiber, T., Ceccato, A., Schönenberger, J., 2020. Brittle structural facies" analysis: a diagnostic method to unravel and date multiple slip events of long-lived faults. Earth Planet Sci. Lett. 545, 116420. https://doi.org/10.1016/j.epsl.2020.116420.

Theissen-Krah, S., Zastrozhnov, D., Abdelmalak, M.M., Schmid, D.W., Faleide, J.I., Gernigon, L., 2017. Tectonic evolution and extension at the Møre Margin – offshore mid-Norway. Tectonophysics 721, 227–238. https://doi.org/10.1016/j.tecto.2017.09.009.

Torgersen, E., Viola, G., Zwingmann, H., Harris, C., 2015a. Structural and temporal evolution of a reactivated brittle–ductile fault – Part II: timing of fault initiation and reactivation by K–Ar dating of synkinematic illite/muscovite. Earth Planet Sci. Lett. 410, 212–224. https://doi.org/10.1016/j.epsl.2014.09.051.

Torgersen, E., Viola, G., Zwingmann, H., Henderson, I.H.C.C., 2015b. Inclined K-Ar illite age spectra in brittle fault gouges: effects of fault reactivation and wall-rock contamination. Terra. Nova 27, 106–113. https://doi.org/10.1111/ter.12136.

Torsvik, T.H., Andersen, T.B., Eide, E.A., Walderhaug, H.J., 1997. The age and tectonic significance of dolerite dykes in western Norway. J. Geol. Soc. 154, 961–973. https://doi.org/10.1144/gsjgs.154.6.0961.

Torsvik, T.H., Sturt, B.A., Swensson, E., Andersen, T.B., Dewey, J.F., 1992. Palaeomagnetic dating of fault rocks: evidence for Permian and Mesozoic movements and brittle deformation along the extensional Dalsfjord Fault, western Norway. Geophys. J. Int. 109, 565–580. https://doi.org/10.1111/j.1365-246X.1992.tb00118.x.

Viola, G., Scheiber, T., Fredin, O., Zwingmann, H., Margreth, A., Knies, J., 2016. Deconvoluting complex structural histories archived in brittle fault zones. Nat. Commun. 7, 1–10. https://doi.org/10.1038/ncomms13448.

Walsh, E.O., Hacker, B.R., Gans, P.B., Wong, M.S., Andersen, T.B., 2013. Crustal exhumation of the Western Gneiss Region UHP terrane, Norway: 40Ar/39Ar thermochronology and fault-slip analysis. Tectonophysics 608, 1159–1179. https://doi.org/10.1016/j.tecto.2013.06.030.

Wang, C.-C., Wiest, J.D., Jacobs, J., et al., 2021. Tracing the Sveconorwegian orogen into the Caledonides of West Norway: Geochronological and isotopic studies on magmatism and migmatization. Precambrian Res. 362 https://doi.org/10.1016/j.precamres.2021.106301.

Watts, L.M., 2001. The Walls Boundary Fault Zone and the Møre Trøndelag Fault Complex: A Case Study of Two Reactivated Fault Zones. Durham University. http://etheses.dur.ac.uk/3878/.

Weisenberger, T., Bucher, K., 2010. Zeolites in fissures of granites and gneisses of the Central Alps. J. Metamorph. Geol. 28, 825–847. https://doi.org/10.1111/j.1525-1314.2010.00895.x.

Wennberg, O.P., 1996. Superimposed fabrics due to reversal of shear sense: an example from the Bergen Arc Shear Zone, western Norway. J. Struct. Geol. 18, 871–879. https://doi.org/10.1016/0191-8141(96)00014-4.

Wiest, J.D., Jacobs, J., Fossen, H., Ganerød, M., Osmundsen, P.T., 2021. Segmentation of the Caledonian orogenic infrastructure and exhumation of the Western Gneiss Region during transtensional collapse. J. Geol. Soc. 178, jgs2020–j2199. https://doi.org/10.1144/jgs2020-199.

Williams, J.N., Fagereng, Å., Wedmore, L.N.J., Biggs, J., Mphepo, F., Dulanya, Z., Mdala, H., Blenkinsop, T., 2019. How do variably striking faults reactivate during rifting? Insights from southern Malawi. G-cubed 20, 3588–3607. https://doi.org/10.1029/2019GC008219.

Young, D., 2018. Structure of the (ultra)high-pressure Western Gneiss Region, Norway: Imbrication during Caledonian continental margin subduction. Bull. Geol. Soc. Am. 130 (5–6), 926–940. https://doi.org/10.1130/B31764.1.

Zwingmann, H., Mancktelow, N., Antognini, M., Lucchini, R., 2010. Dating of shallow faults: new constraints from the AlpTransit tunnel site (Switzerland). Geology 38, 487–490. https://doi.org/10.1130/G30785.1.

Graphic design: Communication Division, UiB / Print: Skipnes Kommunikasjon AS

uib.no

ISBN: 9788230869482 (print)
9788230853344 (PDF)